Integrating Compressed Air Energy Storage with Borehole Thermal Energy Storage: A Feasibility Study

by

Wayne Sunghyun Park

A thesis

presented to the University of Waterloo

in fulfilment of the

thesis requirement for the degree of

Master of Applied Science

in

Civil Engineering

Waterloo, Ontario, Canada, 2020

Author's Declaration

I hereby declare that I am the sole author of this thesis. This is a true copy of the thesis, including any required final revisions, as accepted by my examiners.

I understand that my thesis may be made electronically available to the public.

Abstract

There is an increasing demand for an Energy Storage System (ESS) mainly driven by the growing applications of intermittent renewable energy. The ESS technologies allow storing electrical energy into a different form of energy such as chemical, electrical, mechanical, and thermal energy for future usages. This thesis focuses on integrating existing ESS technologies, Compressed Air Energy Storage (CAES) and Borehole Thermal Energy Storage (BTES). In this thesis, a study conducted to evaluate the feasibility of integrating CAES and BTES is presented. The integrated ESS system referred to as an integrated CAES-BTES system, excess electrical energy in the form of compressed air. The heat of compression is stored in soil or rock, which is a storage medium of the BTES. When there is an energy demand, the stored compressed air is used to operate a series of expanders to generate electricity. The thermal energy captured by the BTES system can be transferred to the expansion side of the CAES or supplied to end-users outside of the system.

This thesis aims to conduct a feasibility study on the design of the integrated CAES-BTES system. For the study, several existing configurations of CAES and BTES and their design methods outlined in the literature are reviewed first. A conceptual design of the integrated system is proposed, based on the literature review. From the literature review, key parameters that affect the overall performance of the ESS technologies are also identified. The integrated system's computer model is then constructed with the MATLAB®, which allows prompt thermodynamics simulation and sizing of the system, based on user-defined parameters, such as the energy demand and operational/physical constraints. A parametric study is conducted using the model to analyze the system's performance under different operating conditions. The integrated system's economic feasibility is determined relatively by comparing its Levelized Cost of Energy Storage (LCOS) with the other ESS technologies. A financial model is created using Microsoft Excel/VBA, which calculates the LCOS based on the technical and financial input parameters from the MATLAB® model and existing literature.

With the computer model, a hypothetical integrated CAES-BTES with a power output of 1.5 MW that operates in a continuous daily cycle of 8 hours of discharge is considered in the parametric study. Based on the scenarios considered for the parametric study, the CAES system can achieve up to 60% and 40% round-trip efficiency for Adiabatic CAES (aCAES) and Diabatic CAES (dCAES) configurations. The results have demonstrated the more notable influence of the expander inlet temperature and the number of compression-expansion stages on the system's efficiency. For instance, the round-trip efficiency improved by 25% for increasing compression-expansion stages from one to six. A similar improvement was

observed for increasing the inlet temperature for the first stage of expansion considered in this study, from 373.15 K to 873.15 K. The parametric study results suggest that minimizing heat loss from the system's compression side, adding more thermal energy for air expansion, and lowering air mass flow rate on the expansions ide greatly influence the round-trip efficiency of the system. It is also economical to operate the system with high storage pressure to reduce its storage volume requirement. For the BTES side of the integrated system, the storage medium and grout materials' thermal conductivities have shown significant impacts on the design. For instance, it is strategic to choose a storage medium and grout material with greater thermal conductivities as it enhances the thermal energy storage capacity. However, a storage medium with high thermal diffusivity is less desired as the thermal energy can dissipate away to the far-field quicker.

The method proposed by Jülch (2016) is used to calculate the LCOS of the integrated CAES-BTES system and compared to conventional dCAES and aCAES systems. A rated storage capacity of 2.5 GWh is assumed for all of the considered CAES systems. The LCOS analysis result shows that when electricity cost is not accounted for, the integrated CAES-BTES has similar LCOS as the aCAES system. For instance, their LCOS can be lower than dCAES, when more than 1800 yearly full load hours are considered. The LCOS of the integrated system presents better cost-competitiveness than both conventional systems when electricity cost is higher than 0.03€/kWh. The integrated system also possesses environmental advantages over other ESS technologies, such as batteries. Compared to the batteries, the CAES system emits approximately 1.5 times less greenhouse gases per MWh of storage capacity. Also, as the integrated system requires less raw materials for its construction, its environmental impacts throughout its life cycle are considerably lower than batteries as less disruptive mining and disposal activities are required.

This study concludes that integrated CAES-BTES can be a technically and economically feasible energy storage option. It also demonstrates a potential design approach and determines critical parameters for the system's performance, which can be valuable for designers and decision-makers.

Acknowledgements

I would like to express sincere gratitude to my supervisors, Professor Maurice Dusseault and Professor Yuri Leonenko, for their guidance and support. They have provided me with great learning opportunities that broadened my perspectives on the energy issues and beyond.

I would like to thank my family for their unconditional support throughout the journey.

Table of Contents

List of Figures

List of Tables

Chapter 1: Introduction

1.1 Energy Transition and Renewable Energy

Global energy consumption is projected to rise continuously in the foreseeable future, mainly because of the continued expansion of the population and the global economy. According to BP's Energy Outlook (2019), the global energy demand will increase by approximately 30% by 2035, with an average growth rate of 1.3% per year. As shown in Figure 1-1, more demand for renewable energy sources is forecast for the near future, including wind, solar, geothermal, biomass, and biofuels. The increased demand is driven by the environmental benefits, such as lowered greenhouse gas (GHG) emission and reduced environmental footprint (Oreskes, 2004 & World Nuclear Association, 2011), as well as the declining cost of renewable power generation (IRENA, 2019).

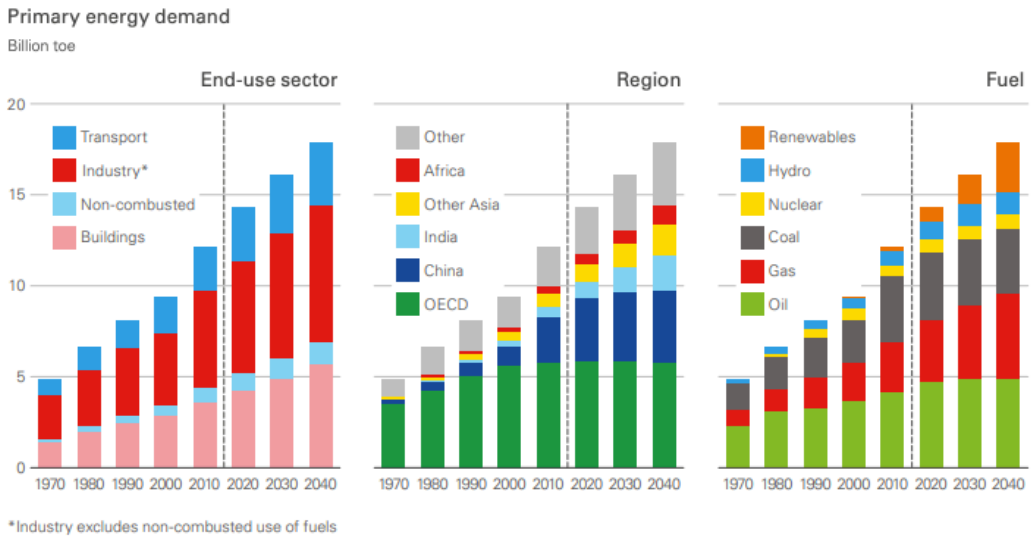

Figure 1-1 Primary energy consumption outlook (BP, 2019)

Despite the advantages, renewable power generation faces many challenges, especially because of intermittent availability of the resources in the case of wind, solar and tidal energy. The intermittency can cause a supply-demand imbalance, which consequently increases the difficulty of stabilizing the power network (Ibrahim *et al.*, 2008). The imbalance issue can be overcome by integrating appropriate Energy

Storage Systems (ESS) into electrical grids that have substantial amounts of intermittent renewable energy.

1.2 Background - Energy Storage Systems (ESS)

Energy Storage Systems (ESS) support the stable and continuous supply of energy at all times for the consumer. ESS allows storing energy produced during low demand periods for later consumption. ESS is typically integrated with renewable power generation systems, storing electrical energy produced during peak production hours by converting it into a form of storable energy. Based on the approach, ESS technologies are classified as chemical, electrochemical, electrical, mechanical, and thermal energy storage (Wagner, 2007), as shown in Table 1-1.

Table 1-1 Classifications of ESS technologies (Guney and Tepe, 2017)

Storage Type				
Chemical	**Electrochemical**	**Electrical**	**Mechanical**	**Thermal**
Hydrogen	Primary cell or battery	Capacitor	Flywheel system	Sensible heat system
Synthetic natural gas (SNG)	Secondary cell or battery	Supercapacitor	Pumped hydro storage (PHS)	Latent heat system
Biofuels	Reserve cell	Superconducting magnetic energy storage	Compressed air energy storage (CAES)	Absorption and adsorption system
Thermo-chemical energy storage (TCES)	Fuel cell			

Couffin & Perrin (2004) conducted a comparative study of different ESS based on the suitability to the specified application. The study considered costs, the density of energy, specific power, recyclability, durability, and energy efficiency. The authors classified the ESS technologies into four categories:

- Category 1: Low-power applications in isolated areas, to feed transducers and meet emergencies
- Category 2: Medium-power applications in isolated areas (i.e., individual electrical systems)
- Category 3: Network connection applications with peak levelling
- Category 4: Power-quality control applications

As shown in Figure 1-2, mechanical ESS technologies with a storage capacity greater than several MWh, such as large-scale compressed air energy storage (CAES) and flywheel storage, are more suitable for peak-hour load-levelling applications (Category 3). For power-quality control applications (Category 4),

energy release capacity and cycling capacity are the most important criteria. Flywheel storage and supercapacitors are more applicable for these purposes. For low-power application or emergency responses requiring modest amounts of energy (Category 1), the lithium-ion battery is the most suitable, as it has the lowest self-discharge possibility, but for larger storage needs with estimated energy storage needs ranging from a few kWh to 1 MWh (Category 2), the lead-acid battery may be more applicable. For Category 2, autonomy is the critical criterion, and the maximum amount of time the system can continuously release energy at a constant rate is the important metric (Ibrahim *et al.*, 2008).

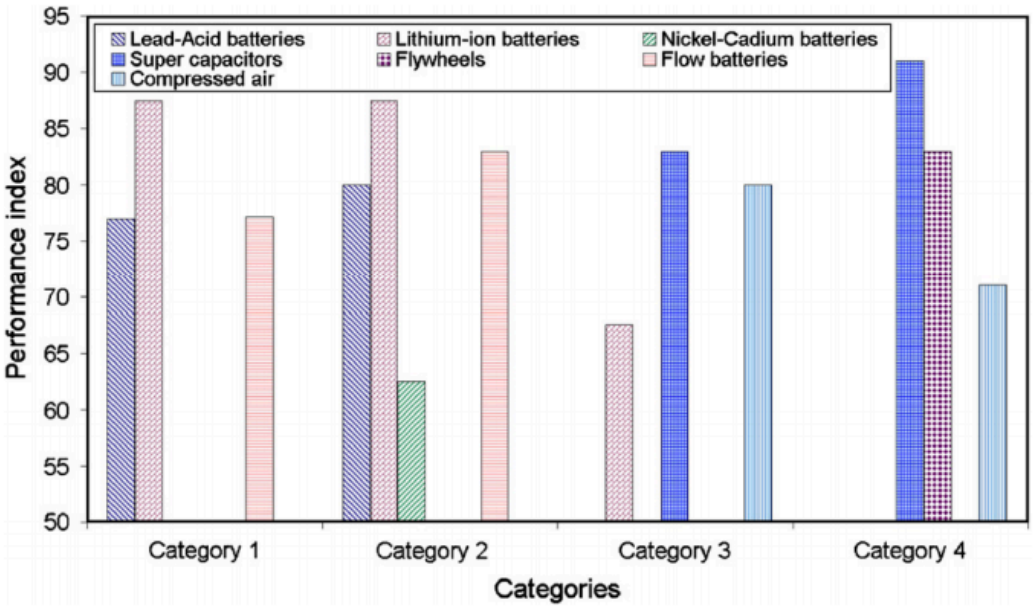

Figure 1-2 Performance index for the nine storage technologies for the four categories of application (Couffin & Perrin, 2004)

Carnegie *et al.* (2013) assessed the applications of ESS technologies according to storage time and power requirements, and created the storage application and technology map shown in Figure 1-3. In total, six applications are identified, including small-scale power supply, primary frequency regulation, end-user peak shaving, load leveling for T & D postponement, renewable integration, and load leveling for large-scale power generation and utilization.

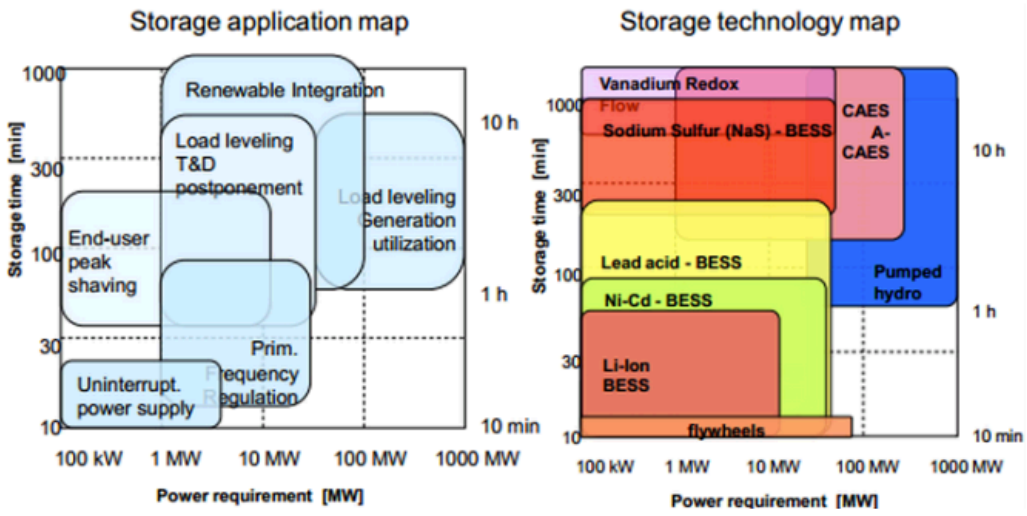

Figure 1-3 Storage applications and technologies maps (Carnegie *et al.*, 2013)

1.3 Background - Compressed Air Energy Storage (CAES)

CAES is highly compatible with renewable energy sources and integrated power grids because of its comparatively low capacity cost per cycle, long discharge time with relatively high power output, long life expectancy, and start-up times on the order of minutes (Carnegie *et al.*, 2013). Also, as a long-term and large-scale ESS, subsurface CAES systems have relatively low environmental footprints (Guney & Tepe, 2017). In this Section, the fundamental principles, types, current status, and challenges of CAES are discussed.

1.3.1 Principles of CAES

A CAES system operates in two modes: charging and discharging modes. For the charging mode, electrical energy is provided to a motor attached to a compressor. As the compressor operates, the air is compressed to high pressure and stored in a storage vessel (Ibrahim *et al.*, 2008). More than one compression stage with intercoolers is preferred to avoid overheating problems. The heat of compression is either disposed into the atmosphere or stored in thermal energy storage (TES) system. The compressed air would typically be stored in large underground caverns dissolved in salt, porous and permeable aquifers or pinnacle reefs, abandoned salt mines, abandoned mines with water level management, or within pressure vessels installed in underground mines. These subsurface storage options are considered viable as the surrounding earth material can withstand the high pressure exerted by the compressed air on the wall of the vessel of chamber, and have impervious walls, minimizing air leakage and self-discharging

risks (Bardshaw, 2000). Different proposed types of compressed air storage reservoirs are shown in Figure 1-4. Several projects have also attempted to use above-ground storage vessels (e.g., SustainX, 2015) such as shallow underground piping made of carbon-fibre structures (Bardshaw, 2000). Others propose a subsurface approach based on a high-pressure steel-cased wellbore (CleanTech Geomechanics, 2019).

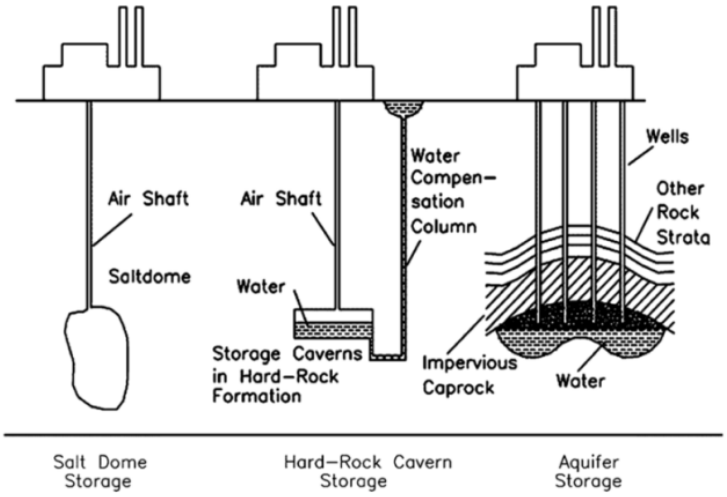

Figure 1-4 Different types of compressed air storage reservoirs (Bardshaw, 2000)

For the discharging mode, air under pressure is released from storage and transported to the expansion-generation side of the system. Additional thermal energy may be introduced for air expansion as the compressed air enters the power engines to produce electricity. Staged-expansion of the air is also preferred to avoid overcooling issues (icing) and over-reduction in pressure (turbine or reciprocating engine efficiency loss).

1.3.2 Types of CAES

CAES systems can be classified as diabatic, adiabatic and isothermal (Budt *et al.*, 2016), as shown in Figure 1-5.

Diabatic CAES (dCAES) is the most mature type of CAES. For dCAES, the heat of compression is removed through intercoolers and disposed to the environment. When the compressed air is released from the storage for power generation, a fuel, such as natural gas, is used to heat the air before it enters the power units. Currently, there are two commercial grid-scale CAES plants in the world, both adjacent to

nuclear power plants, and both of them are dCAES type. The first CAES plant was constructed in 1978 in Huntorf, Germany. The Huntorf plant has an electrical power output of 321 MW with discharging time of 3 hours and a round-trip efficiency of 42% (Budt *et al.*, 2016). The other CAES plant is located in Alabama, USA, and was constructed in 1991. The CAES plant, called McIntosh plant, has an electrical power output of 110 MW with discharging time of 24 hours and a round-trip efficiency of 54%. Figure 1-6 summarizes the processes involved in a dCAES plant (Kaldemeyer *et al.*, 2016).

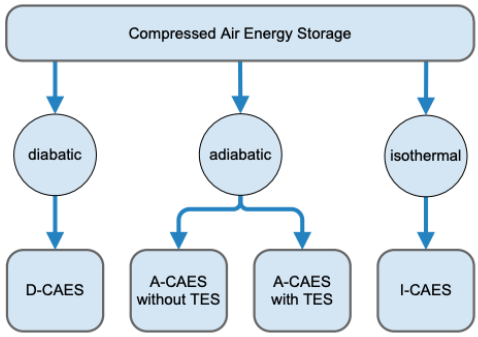

Figure 1-5 Compressed air energy storage concepts classified by their idealized change of state: (D(diabatic)-, A(adiabatic)-, I(isothermal)-CAES) (Budt *et al.*, 2016)

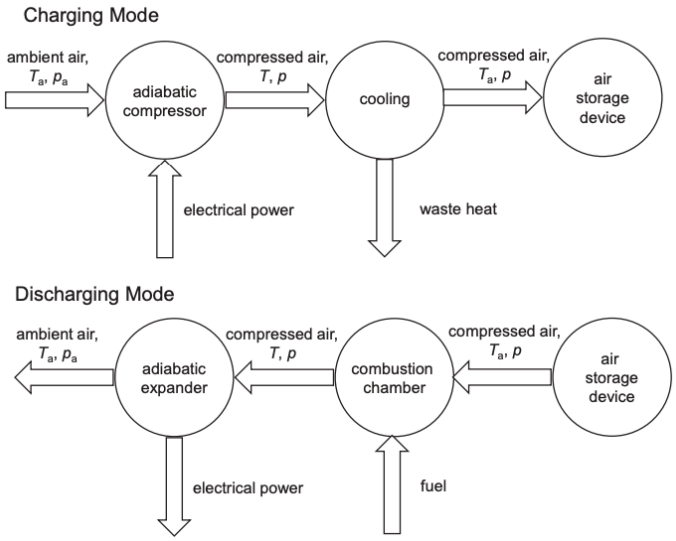

Figure 1-6 Simplified system of a dCAES plant (Budt *et al.*, 2016)

In contrast to dCAES, adiabatic CAES (aCAES) captures the heat of compression and stores it in Thermal Energy Storage (TES) system. The heat of compression is used for heating the compressed air instead of using an additional fuel or heat source. aCAES without TES has been proposed, but it has demonstrated problems associated with designing thermally durable storage with the low energy density of hot

compressed air (Abd-el Fattah, 2006). Because aCAES systems do not require fuel, the round-trip efficiency can be up to 70% (Budt *et al.*, 2016). A simplified process diagram of an aCAES plant is shown in Figure 1-7.

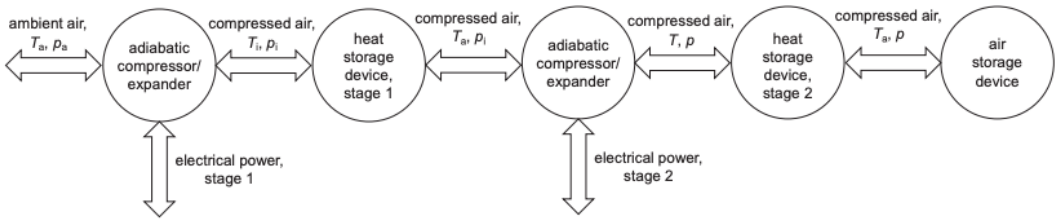

Figure 1-7 Simplified system of an aCAES plant with multiple stages (Budt *et al.*, 2016)

For Isothermal CAES (I-CAES), the compressed air temperature is kept constant throughout the charging and discharging cycles. Relatively slow compression and expansion processes are desired to provide enough time for heat exchange processes inside the machinery (Budt *et al.*, 2016). Hence, it is more advantageous to use piston machinery over rotary machinery for this application, as it can perform compression and expansion processes more slowly. A few methods are proposed to maintain a low temperature including spraying liquids on the machinery and compressing pre-mixed foam instead of atmospheric air (McBride *et al.*, 2013). An American start-up company called SustainX (2015) developed an I-CAES system with an electrical power output of 1.5 MW and up to 54% round-trip efficiency.

1.4 Background - Borehole Thermal Energy Storage (BTES)

A significant portion of the energy produced globally is consumed for heating and cooling purposes. For instance, space heating accounts for approximately 32% and 33 % of the total energy consumed in residential and commercial buildings, respectively (IEA, 2012). Currently, the majority of space and water heating demand is supplied by hydrocarbon-based resources. Concerns relating to climate change and increasing energy demand are also motivating the deployment and development of more sustainable alternatives for heating and cooling.

Of many options, the district heating system, coupled with renewable sources, is frequently considered an attractive option. The integration of combined heat and power plants with a district heating system can further enhance economic and environmental benefits (Rezaie & Rosen, 2012). One technology that is readily available for the purpose of energy storage as heat is Borehole Thermal Energy Storage (BTES). In this chapter, brief backgrounds on TES and BTES technologies are presented.

1.4.1 Thermal Energy Storage (TES)

TES stores thermal energy in a storage medium for further usages, such as space heating or cooling, process heating and cooling, hot water production, or electricity generation (Cabeza *et al.*, 2015). They are typically categorized depending on the storage period of thermal energy and the form of the energy storage medium (Cao, 2010). The storage period may vary from diurnal, weekly, or seasonal, depending on the application. Some of the TES design constraints include the storage period, economic viability compared to current alternatives, and operating conditions (Gao *et al.*, 2009). The main design goal of the TES system is to minimize thermal energy losses and achieve high energy recovery during the extraction of stored thermal energy (Lee, 2013).

Generally, TES technologies are classified into latent, sensible, or thermochemical types (Socaciu, 2012). The latent heat system stores thermal energy by changing the phase of materials. The materials used as storage media in the latent heat system are known as phase change materials (PCMs). The sensible heat system stores thermal energy by directly changing the medium's temperature, such as water, salt, or rock (Pfleger *et al.*, 2016). Thermochemical TES stores thermal energy based on physio-chemical processes such as absorption and adsorption (Bales *et al.*, 2005).

1.4.2 Principles and Applications of BTES

Borehole Thermal Energy Storage (BTES) is a sensible TES technology that uses the heat capacity of subsurface rock or soil as a storage medium. For charging mode, a warm heat-exchange fluid circulates inside the heat exchanging pipe loop, called a ground loop. The ground loop is installed to pass through multiple boreholes for heat exchange with the surrounding ground, and this configuration is referred to as borehole heat exchangers (BHEs). As the circulating fluid flows through the ground loop into the ground, the thermal energy from the heated fluid is transferred to the surrounding ground. The field of BHEs in the BTES systems, where the boreholes are positioned within confined boundaries and arranged in a systematic geometry, is called a borefield (Gao *et al.*, 2018; Bar *et al.*, 2015). A short-term TES such as a water tank is often included in the system to meet peak demand (Bar *et al.*, 2015).

For the discharging mode, the stored thermal energy from the storage medium is recovered by injecting cold fluid into the ground. BTES systems generally consist of BHEs, a heat pump, a storage medium, a circulation pump, and short-term TES capacity. Each of these components in the system is linked with a

pipe loop conveying heat exchange fluid (Lee, 2013). Figure 1-8 is a schematic of a solar seasonal BTES district heating system used at a community called Drake Landing in Okotoks, Alberta, Canada.

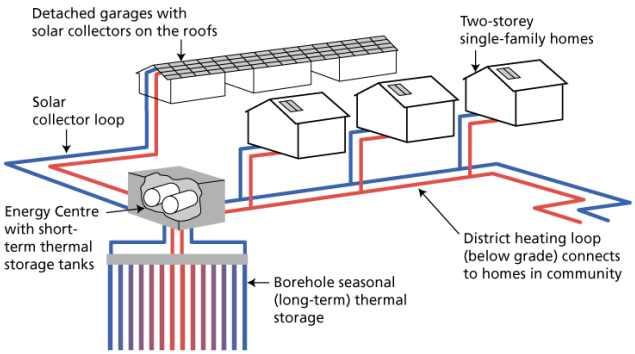

Figure 1-8 Solar seasonal borehole thermal energy storage and district loop in Drake Landing (Mesquita *et al.*, 2018)

BTES is highly suitable as a seasonal TES because of its scalability (Nordell, 2000); a large-scale BTES system is applicable as a seasonal TES at a community-scale. At this scale, BTES can be used in conjunction with solar power plants, industrial waste heat sources, and combined heating and power (CHP) plants. Another common option for a seasonal TES is an Aquifer Thermal Energy Storage (ATES) system (Dincer & Rosen, 2002). The main difference between the BTES and ATES systems is that the former is a closed-loop system, and the latter is an open-loop system. For BTES systems, the circulating fluid is not released into the subsurface environment; in contrast, the fluid for ATES systems is released into the aquifer as this approach mainly relies on the convective heat transfer mode within the aquifer. Because of the difference, BTES systems have several advantages over ATES systems, as listed below:

- BTES systems have minimal effects on groundwater's physical and chemical conditions in the shallow aquifer;
- The presence of groundwater is not required. Hence, BTES systems are less geographically limited than ATES systems (Lanahan & Tabares-Velasco, 2017).

A simplified schematic of ATES and BTES systems is shown in Figure 1-9.

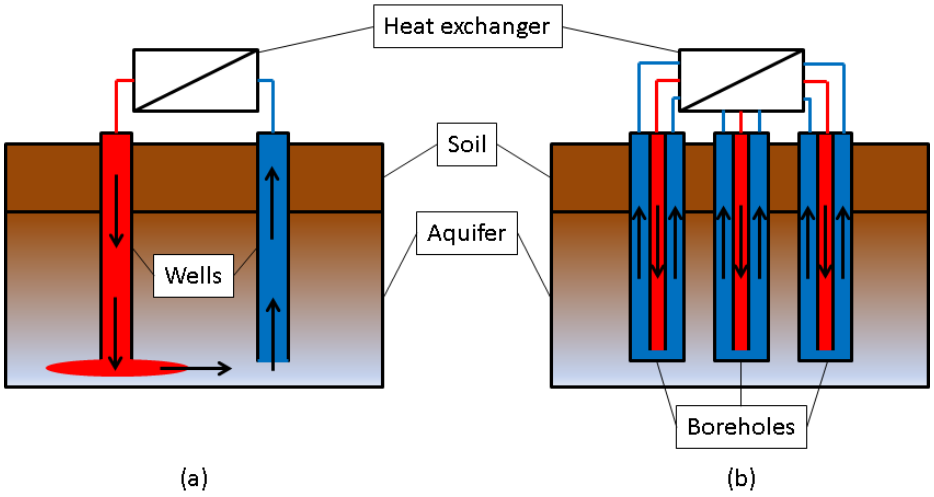

Figure 1-9 Simplified schematic of (a) ATES and (b) BTES system

A small-scale BTES system can also be deployed for a single home. However, the BTES system is often referred to as a seasonal TES system capable of providing heating and cooling at a community scale, with a storage volume higher than 10,000 m^3 (Lanahan & Tabares-Velasco, 2017; Ruess *et al.*, 2015).

Since the 1970s, seasonal BTES systems have been integrated with several heating plants, mainly in Europe (Nordell, 2000; Reuss, 2015). The first BTES systems for seasonal storage for solar district heating systems were constructed in Sweden and the Netherlands in the 1980s. These systems also utilized waste heat from industrial sources (Malmberg *et al.*, 2018; Ruess, 2015). Figure 1-10 presents a simplified schematic of a typical borehole seasonal solar thermal storage system (Gao *et al.*, 2015).

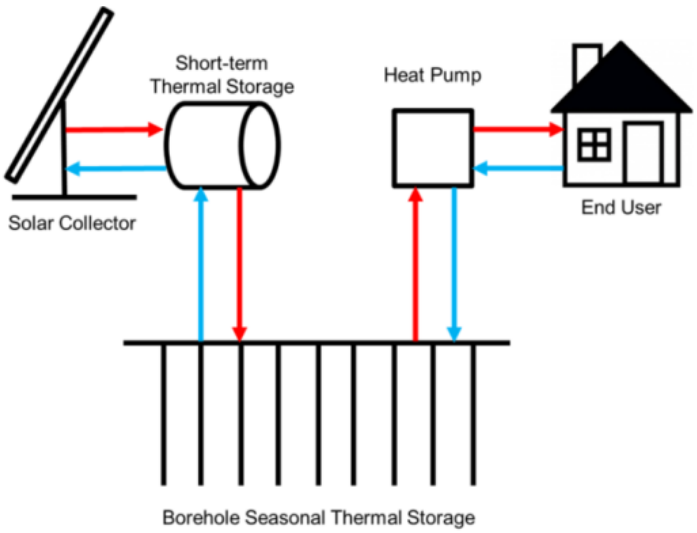

Figure 1-10 A schematic of borehole seasonal solar thermal storage system (Gao *et al.*, 2015)

In 1993, an R&D program called “Solarthermie 2000” was launched from Germany to demonstrate the feasibility of solar thermal heating systems in buildings and solar-driven district heating systems (Lottner *et al.*, 2000). As a part of this program, BTES was compared with different types of seasonal TES for solar district heating systems in Germany and Denmark. As suggested in Figure 1-11, the investment costs of BTES were the lowest when the storage volume was in the range of 5,000 - 20,000 m^3 water equivalents (Mangold *et al.*, 2012). The trend suggests that the larger storage capacity generally leads to greater efficiency and economic feasibility of the BTES systems.

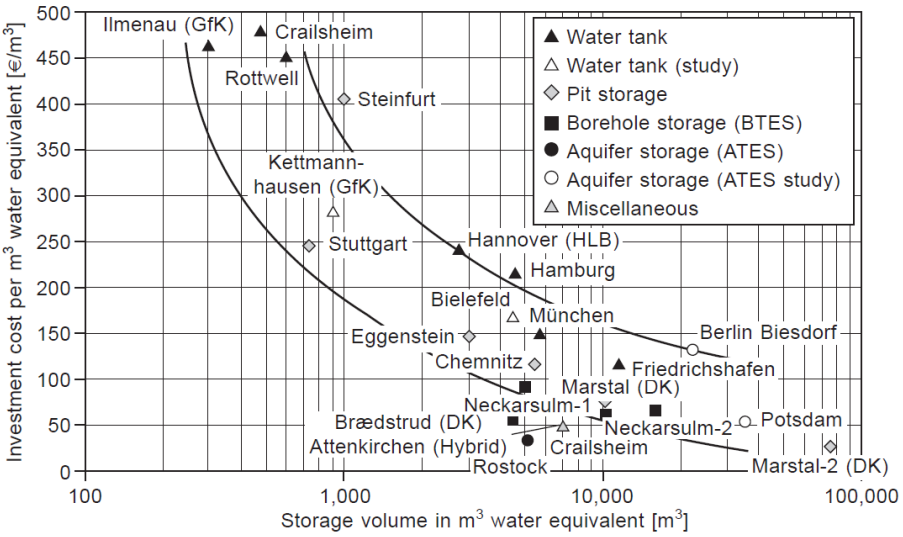

Figure 1-11 Specific investment costs of different seasonal storage types in realized solar district heating systems (without planning and VAT) (Mangold *et al.*, 2012)

BHEs are generally installed to a depth between 20 - 300 m below the surface (Florides & Kalogirou, 2007). One of the challenges of the conventional BTES is the temperature increase of the aquifer during operation, which can lead to an alteration of chemical (Brons *et al.*, 1991; Griffioen & Appelo, 1993) and biological (Brielmann *et al.*, 2009; Hall *et al.*, 2008) properties of the groundwater. However, operating the system at a low temperature can limit performance and efficiency (Welsch *et al.*, 2016). In order to overcome the challenge, deep or medium-deep BTES systems, consisting of BHEs installed to depths of up to 1,000 m or below, are proposed (Holmberg *et al.*, 2015 & Welsch, 2019). An illustration of the medium-deep BTES system is shown in Figure 1-12.

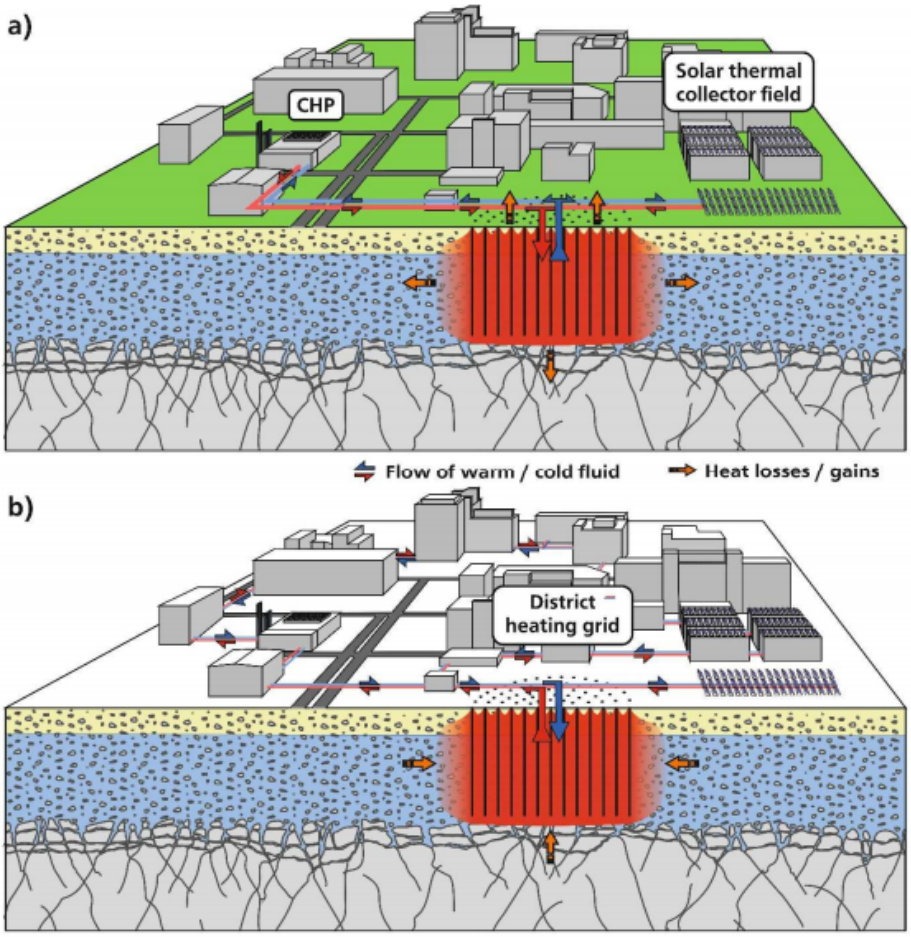

Figure 1-12 Schematic illustration of (a) summer and (b) winter operation of an exemplary BTES system (Welsch, 2019)

1.5 Objectives

The goal of this thesis is to conduct a feasibility study on integrating CAES and BTES systems, hereafter referred to as an integrated CAES-BTES system. The feasibility of the system is assessed based on the overall efficiency and the cost-effectiveness compared to other technologies. The system's configuration and the simulation model are proposed based on the background information on CAES and BTES outlined in Chapter 1, with review of existing configurations and design approaches presented in Chapter 2. In Chapter 3 of this thesis, details on the integrated CAES-BTES system and the simulation model are provided. As part of the feasibility study, the performance of the integrated CAES-BTES system is evaluated with the model, and it is used to conduct a parametric study to assess the performance under different operating scenarios, as presented in Chapter 4. The proposed system's economic feasibility is

assessed with a Levelized Cost of Energy Storage (LCOS) analysis. The explanations of the LCOS method and the results of the analysis are demonstrated in Chapter 5. The conclusions and the limitations of the thesis are addressed in Chapter 6, along with suggestions for potential future research for the integrated CAES-BTES system.

Chapter 2: Literature Review

2.1 CAES Configurations and Design Methodologies

Giramonti *et al.* (1978) have proposed a conceptual design of diabatic compressed air energy storage (dCAES) and estimated its performance. The design maximizes the usage of commercial or nearly developed components, such as a modified steam turbine and gas turbines, to reduce engineering and development costs. The proposed dCAES is comprised of three-stage compressor and four-stage expander trains, as shown in Figure 2-1. For this design, the air is compressed with a pressure ratio of 16:1 in the low-pressure section (LC and HC in Figure 2-1), and further compressed to the desired level with a booster compressor (BC in Figure 2-1). For air expansion, the air from storage is released to the high-pressure turbine (ET in Figure 2-1) first, then to the low-pressure turbine sections (HT, LT and FT in Figure 2-1). The base design had a power output of 253 MW and 20 hours of storage capacity. A parametric study has shown that reducing the pressure ratio from 66.3:1 to 20:1 resulted in an approximately 25% reduction in the power output. However, the heat transfer rate is increased by less than 5%. This study has suggested incorporating thermal energy storage (TES) as one of the cost reduction strategies, but TES is not further discussed.

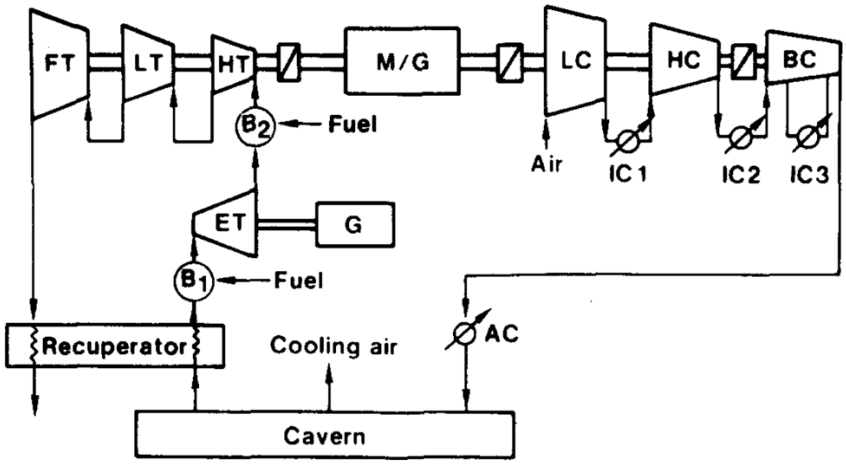

Figure 2-1 - CAES configuration proposed by Giramonti *et al.* (1978)

A CAES system for a small-scale solar PV power plant for a radio base is proposed by Jannelli *et al.* (2014). As shown in Figure 2-2, the system is composed of a PV power unit, and an adiabatic CAES (aCAES) using a diathermic oil tank that acts as a TES. A steady-state model with a series of analytical equations is used to design the system through iterative processes. The size requirement of the PV power unit is determined based on the existing weather data. Based on the size of the PV power unit and the projected energy demand of the radio base, the size of the turbines, storage tank, and compressors are determined. Lastly, the TES unit's size is calculated based on the thermodynamics of the compression and expansion processes. The storage system efficiency (SSE) and storage polygeneration efficiency (SPE) are selected as performance criteria. Note that the SPE accounts for a scenario where cold exhaust gas from the expansion side provides an additional cooling load needed for the equipment. The optimized design is composed of three stages of compression and two stages of expansion. The study concludes that a peak power output of 33 kW and SSE of 57% can be achieved for the small-scale power generation-storage system. The SPE of the system can be increased by up to 2% by utilizing the exhaust gas.

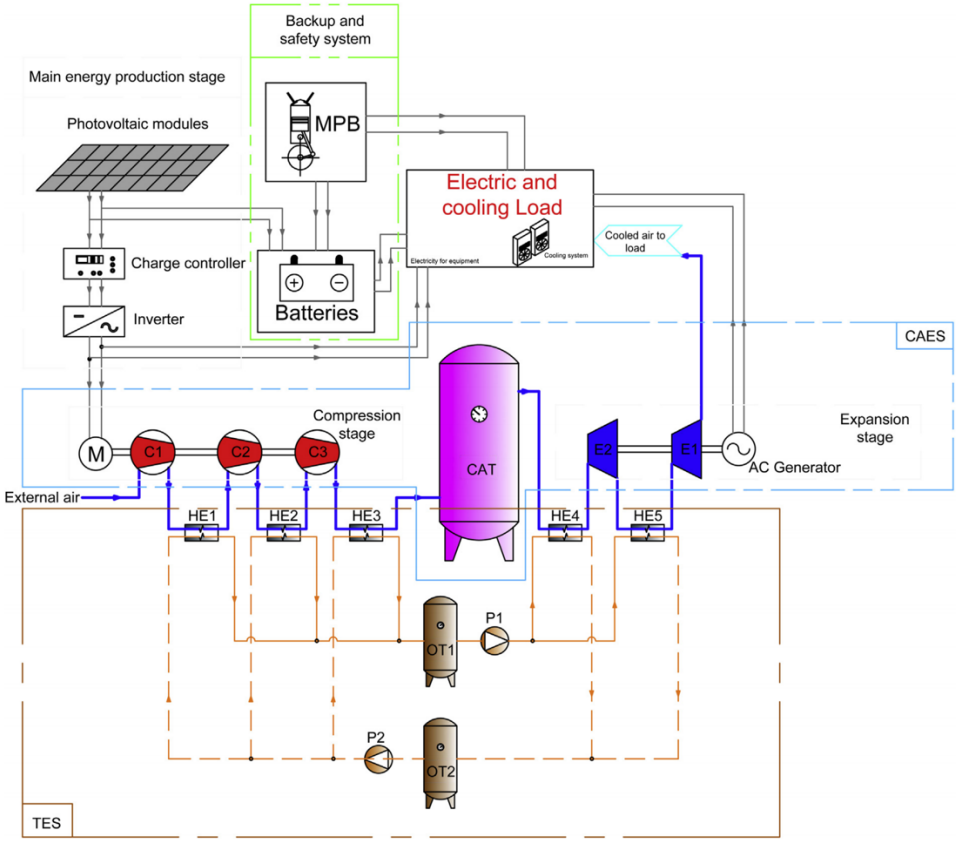

Figure 2-2 - A small-scale CAES system for stand-alone renewable energy power plant for radio base station (Jannelli *et al.*, 2014)

Ibrahim *et al.* (2010) proposed a unique hybrid power generation system for remote communities, called wind-diesel hybrid systems (WDCAS). The proposed system combines a diesel generator and a small-scale wind power plant with CAES, as shown in Figure 2-3. This system generates power with a diesel engine-generator, and the compressed air is used for turbocharging the diesel engine. For instance, when wind turbines are halted, the compressed air is released to operate air turbines, connected to the compressor by a turbocharger shaft. As the air passes through the turbines, the compressor also rotates synchronously with them. The compressor withdraws the air from the atmosphere to turbocharge the diesel engine, increasing the power output. A case study is conducted with the hybrid system for a remote village with the maximum and average electric loads of 851 kW and 506 kW, respectively. Two diesel generators of 544 kW of maximum power output and four wind turbines with nominal power equal to 335 kW are considered. The case study shows that utilizing the hybrid system with CAES resulted in a 51% reduction of the annual maintenance and operations costs and an annual fuel saving of 27%, compared to the base scenario without the CAES. The study mainly focuses on the performance of the hybrid system, but the thermodynamic constraints and conditions during operations are not discussed in detail.

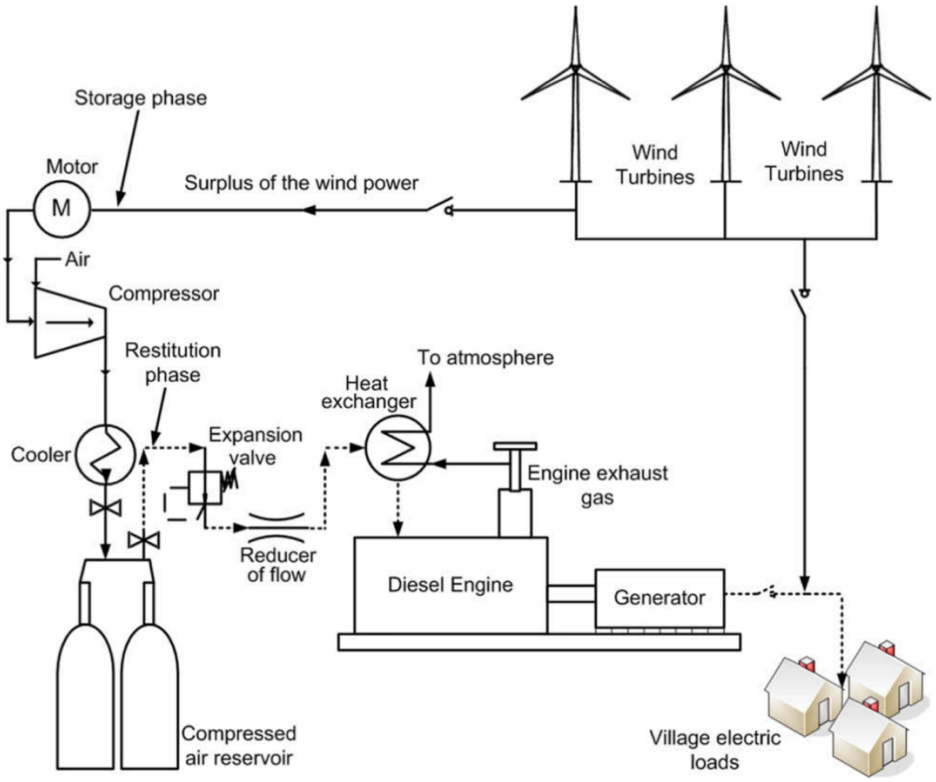

Figure 2-3 Illustration of wind–diesel hybrid systems (WDCAS) combined with CAES (Ibrahim *et al.*, 2010)

The hybrid system proposed by Yan *et al.* (2018) combines an internal combustion engine, wind turbines, and solar PVs. The system is equipped with an aCAES (Figure 2-4), which stores thermal energy from the power generation units and the heat of compression. A tri-level collaborative optimization strategy is selected as a design approach for the integrated system. At the first level of the optimization, the CAES's key parameters affecting the energy conversion efficiency and exergy efficiency are studied. The critical parameters for the system's performance are concluded to be output temperature, expansion ratio, and inlet flow rate of the turbine. The design is optimized in terms of economic and environmental costs at the second level. The OPEX of the CAES is considered in the third stage. The design methodology is applied in a case study to prove its effectiveness. The case study shows that using the CAES can result in a cost reduction compared to battery storage technologies.

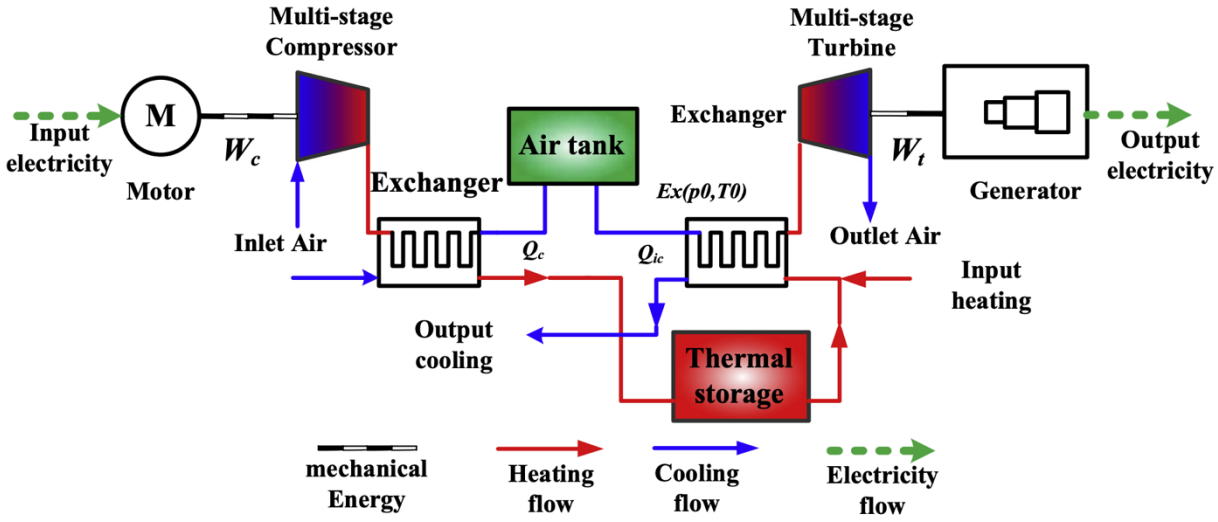

Figure 2-4 Structure and energy flow of CAES proposed by Yan *et al.* (2018)

A multi-level underwater CAES (UWCAES) system that stores energy generated from offshore wind turbines or solar PV is proposed by Wang *et al.* (2016). The configuration of the UWCAES system is shown in Figure 2-5. UWCAES stores the compressed air in an air accumulator located underwater to benefit from hydrostatic pressure. For the proposed UWCAES, the compression and expansion of the air can be performed in two modes by having two separate sets of compressors and expanders. Depending on the electricity supply-demand condition, the system can either operate in low-pressure or high-pressure mode. A case study suggests that the proposed system can achieve efficiencies from 62% to 81%, depending on the different working modes. A thermodynamics model is presented for the analysis, but the sizing of the components is not discussed.

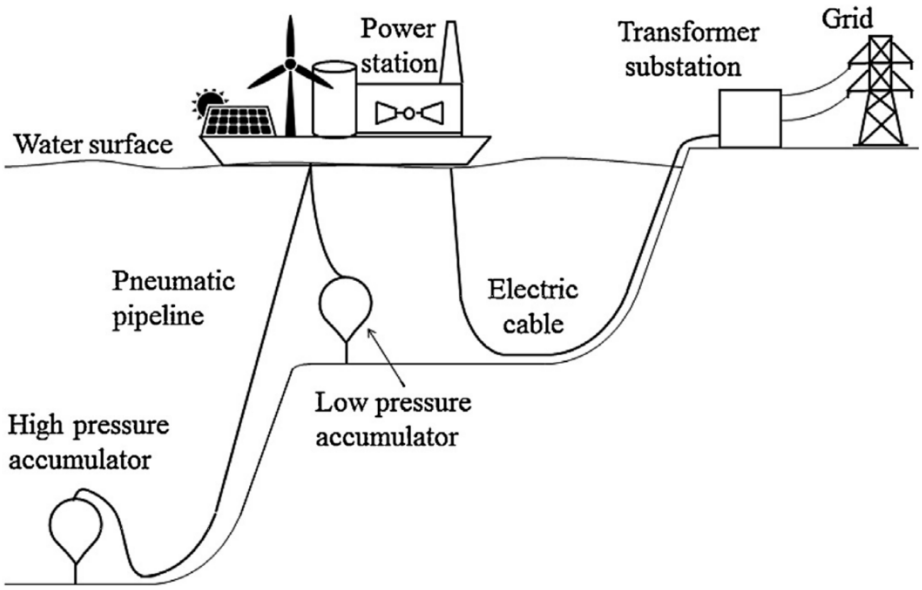

Figure 2-5 A fixed offshore 2-level UWCAES system (Wang *et al.*, 2016)

Safaei & Aziz (2017) proposed a conceptual aCAES design where the heat of compression is captured for electrolysis of steam and water to produce hydrogen. As shown in Figure 2-6, this configuration allows chemical storage of the compression heat in the form of hydrogen, instead of conventional TES. The produced hydrogen is then used as fuel for the heating of the compressed air instead of natural gas. The economics of the hydrogen-fuelled CAES is not covered in the study.

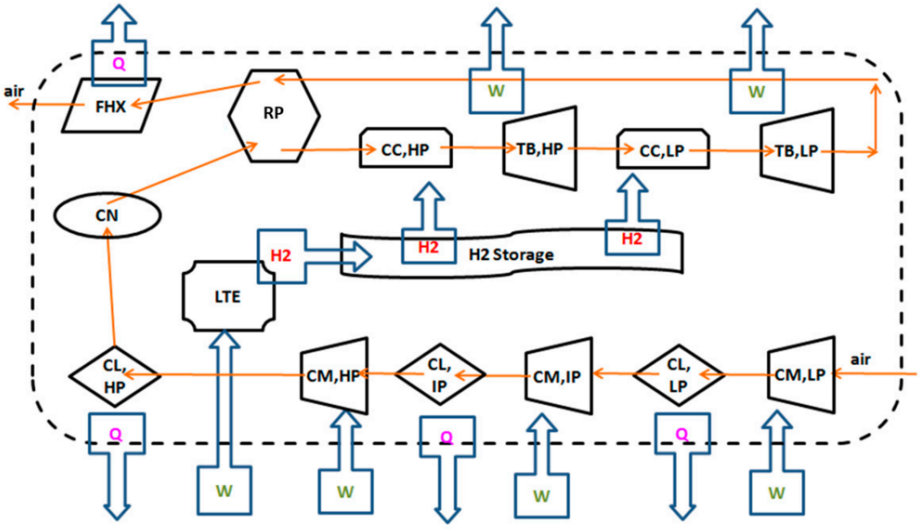

Figure 2-6 Schematic of the CAES system integrated with hydrogen storage (Safaei & Aziz, 2017)

Barbour *et al.* (2015) conducted a preliminary study on an aCAES system using packed bed regenerators as its supplementary TES. The application of packed bed regenerators is less common than indirect-contact heat exchangers, but they have several advantages, including very high heat transfer rates, good pressure and temperature tolerances, and relatively inexpensive construction costs. The packed bed eliminates the needs for many components required for the indirect-contact heat exchange process, such as circulating fluid and fluid storage tanks. A case study presented in the study shows that the maximum temperature of the packed bed storage can be up to 440°C, and it can contribute to achieving a cycle efficiency greater than 70%. As the compressed air directly passes through vertically-packed gravels, the pressure threshold for the packed bed container should be considered. According to the study, the packed bed container can withstand pressure up to 8 MPa, which may be insufficient for an process that requires compressing air to greater than 8 MPa. The first underground aCAES pilot plant has implemented the packed bed TES approach (Geissbühler *et al.*, 2018).

Mazloum *et al.* (2017) considered insulated hot and cold oil tanks filled with synthetic oil, Therminol 55, for their CAES system. The oil has an operating range between -28°C to 315°C (Naresh *et al.,* 2012). The cold oil passes through heat exchangers in the CAES system to absorb the heat of compression, transported to the hot oil tank, and stored for future air expansion. Pressurized water or other glycol-based synthetic fluids may also be used for CAES applications.

2.2 Equipment Selections for CAES

2.2.1 Selection of Compressors

Selecting appropriate turbomachinery is critical for CAES systems, as they influence the overall performance (He & Wang, 2018). As presented in the handbook by the Gas Processors Suppliers Association (GPSA, 2004), there are three types of compressors: positive-displacement, dynamic, and thermal types.

As shown in Figure 2-7, reciprocating and rotary compressors are considered as positive-displacement compressors. Reciprocating compressors are suitable for a system that requires a high pressure ratio and a low inlet flow. Other advantages of reciprocating compressors include higher compressor efficiency, lower power cost, and less sensitivity to changes in gas composition and density. However, reciprocating compressors are rate limited ($<10^3$ acfm) and thus most suitable for small-scale CAES applications. A

rotary type of compressor is not recommended for CAES application, as it often suffers from internal leakage issues and is more challenging to manufacture (He & Wang, 2018).

For large-scale CAES applications, where a high inlet flow rate (~10^2 – 10^4 acfm) must be achieved, centrifugal compressors are more suitable (GPSA, 2004). Also, centrifugal compressors have lower installation and maintenance costs compared to reciprocating compressors. Axial flow compressors may be considered for applications with very fast inlet flow (>10^5 acfm). Hence, the axial compressors are more appropriate for a very large system (~10 MW). Figures 2-8 and 2-9 are compressor coverage charts based on the desired pressure ratio and discharge pressure, respectively.

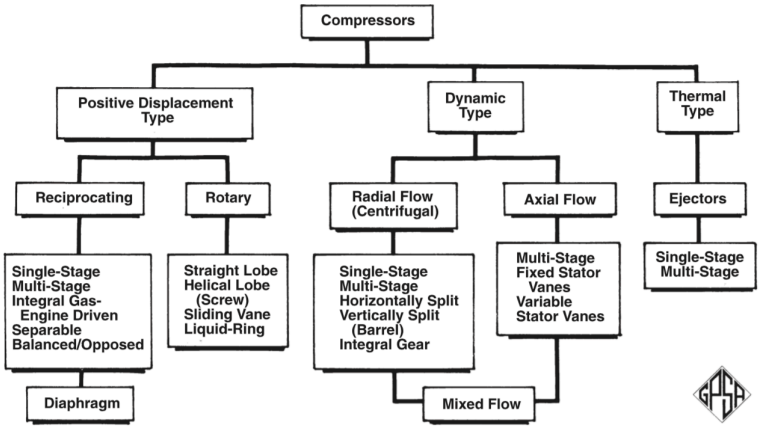

Figure 2-7 Types of compressors (GSPA, 2004)

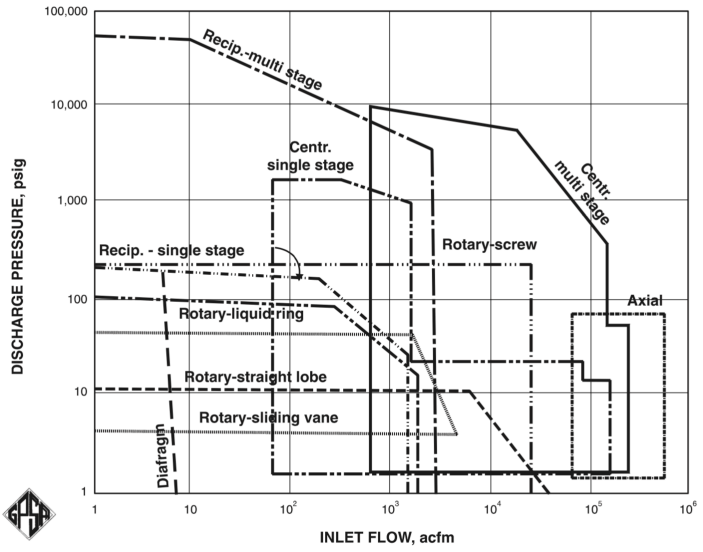

Figure 2-8 Compressor coverage chart based on inlet flow and discharge pressure (GPSA, 2004)

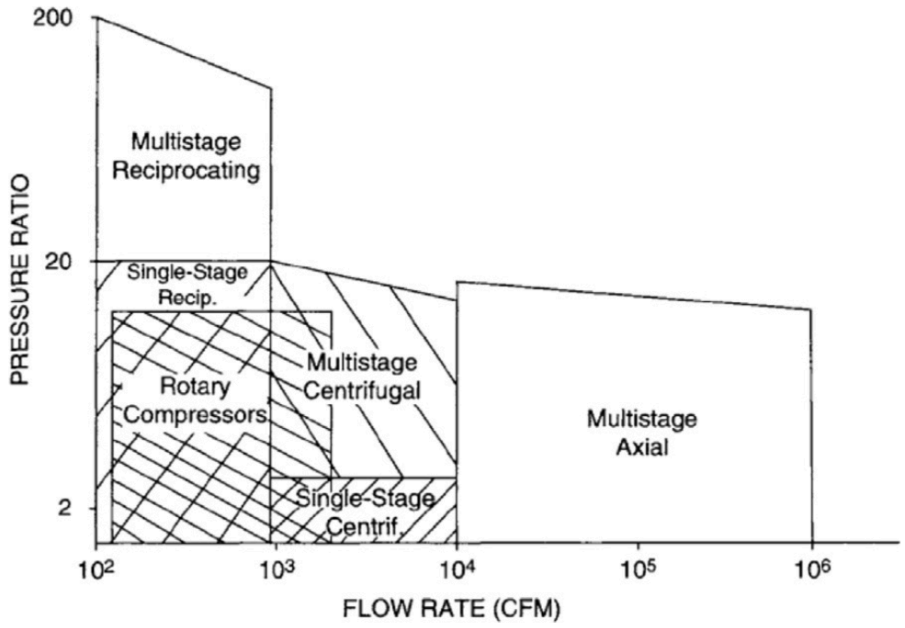

Figure 2-9 Compressor coverage chart based on inlet flow and pressure ratio (Brown, 2011)

2.2.2 Selection of Expanders

Expanders are classified as positive-displacement, dynamic, and thermal types. For CAES applications, the air expansion machine selection process is less developed than the compressor selection process. The review paper by He & Wang (2018) outlines an optimal selection of air expansion machines based on numerous cases presented in the literature. For desing, the authors suggest first defining the number of air expansion stages and inter-stage heating units required for the air expansion process. Detailed operational parameters such as air properties, input and output pressures, input temperature, and airflow rate should be estimated to identify the most suitable expander type and its specifications. The specific speed, N_s, and the specific diameter, D_s, are introduced as expander selection parameters in the study. These two parameters are expressed as:

$$N_s = \frac{N V_{ex}^{1/2}}{\Delta h_s^{3/4}} \tag{2-1}$$

$$D_s = \frac{D \Delta h_s^{1/2}}{V_{ex}^{1/2}} \tag{2-2}$$

where Δh_s is the specific enthalpy drop of the expansion stage, V_{ex} is the volumetric flow rate of fluid at the exhaust port, N is the rotational speed, and D is the characteristic diameter.

With the calculated N_s and D_s, the performance chart, shown in Figure 2-10, can be used to select an expansion machine for CAES. After reviewing the operating conditions and configurations of numerous CAES systems from the literature, He and Wang (2018) have made a general recommendation for selecting expansion machines in CAES systems, as summarized in Table 2-1.

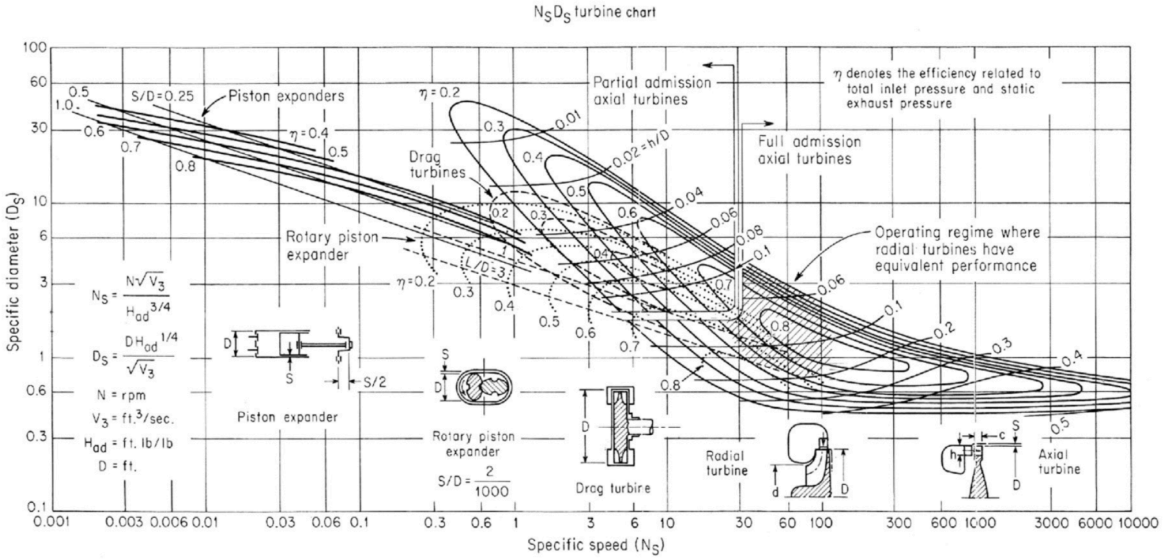

Figure 2-10 Performance chart of expansion machines subject to specific speed N_s and specific diameter D_s (Baljé, 1962)

Table 2-1 Recommendation for selecting expansion machines in CAES systems (He & Wang, 2018)

Machine type		CAES system scale	Operational condition	CAES system types
Reciprocating		Micro- & small-scale CAES	High pressure ratio, low rotation speed	I-CAES & aCAES
Rotary positive displacement	Scroll	Micro-scale CAES	Medium pressure ratio and low rotation speed	I-CAES & aCAES
	Screw	Small-scale CAES	Medium pressure ratio and low rotation speed	I-CAES & aCAES
Turbo-machine	Radial	Small- and large-scale CAES	High rotation speed and low-pressure ratio of single-stage	aCAES
	Axial	Large-scale CAES	High rotation speed and low-pressure ratio of single-stage	aCAES & dCAES

2.3 Design of BTES

Correct sizing and design are essential for the economical operation of a borehole thermal energy storage (BTES) system. Numerous analytical and numerical models have been developed over the past few decades as design tools. These models can estimate the performance of a BTES system by considering critical parameters of its components, including borehole heat exchangers (BHEs), heat pump, storage medium, and circulation pump. This chapter reviews the key components of BTES, the design models, and the key parameters for the system's performance.

2.3.1 Key Components of BTES

Four types of BHEs are the most common for BTES application, including a single U-tube type (1U), a double U-tube type (2U), a coaxial type with an annular inlet (CXA) and coaxial type with the centred inlet. The 1U type consists of a single U-shaped pipe for fluid circulation, where the 2U type has two U-shaped pipes. In practice, the 1U type is the most widely used, mainly because of its low upfront construction cost (Zizzo, 2009). One study (Florides *et al.*, 2013) suggests that the building BHEs with the 2U type instead of the 1U type is 22 - 29% more expensive. However, it is noted that the 2U type can provide 26 - 29% greater efficiency than the parallel 1U configuration and 42 - 59% greater efficiencies than the series configuration of the 1U system. A cross-section of the 1U and 2U BHEs are shown in Figure 2-11.

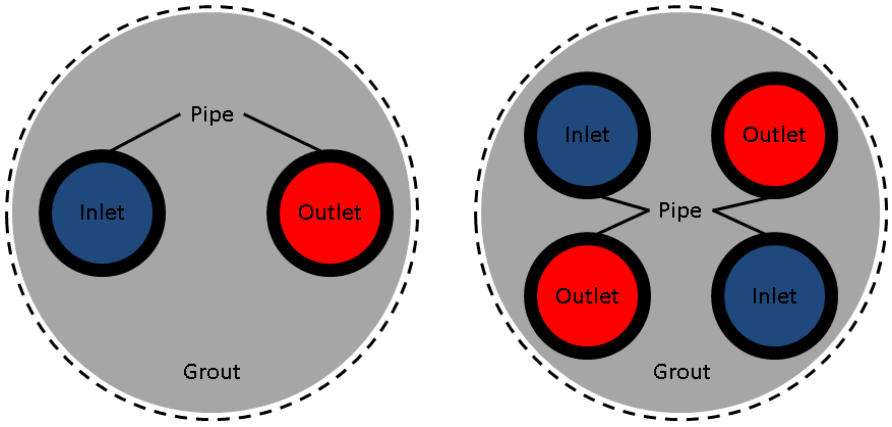

Figure 2-11 Cross-section of single U-tube BHE (left) and double U-tube BHE (right)

CXA and CXC systems have one centre pipe with a smaller diameter, one annulus pipe with a larger diameter, and a grout that fills the gap between the borehole wall and the outer pipe (shown in Figure 2-12). For the CXA system, the fluid is injected through the annulus pipe and retrieved from the centre pipe. For the CXC system, the fluid is injected via the centre pipe and recovered from the annulus pipe. Bär *et al.* (2015) suggest that the CXC configuration can be used for the charging phase of seasonal high-temperature heat storage, as heat loss of the hot fluid injected into the inner pipe to the surrounding ground can be minimized. In contrast, for the extraction phase, it is recommended to inject cold fluid into the outer pipe to maximize the heat extraction from the surrounding ground and to minimize its heat loss as it flows upward to the surface. For this configuration, it is essential to consider a material with low thermal conductivity for the inner pipe.

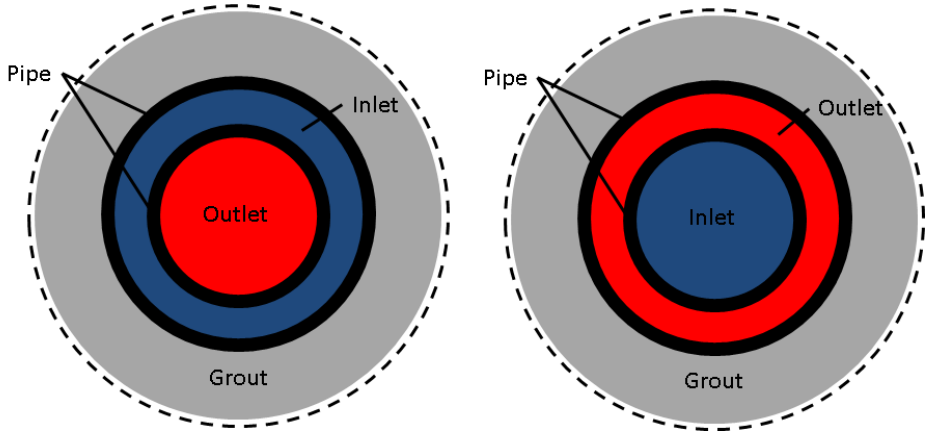

Figure 2-12 Cross-section of CXA BHE (left) and CXC BHE (right)

CXA and CXC BHEs can be advantageous for deep BHEs with length greater than 200 m. For instance, the injected fluid's flow rate has to increase with borehole length to reduce the thermal contact between the fluids traveling in opposite directions. Since the flow area for coaxial BHEs is relatively large, they can accommodate a higher mass flow rate without experiencing significant pressure drops for deep BHEs. These systems are most practical if the available surface area is small, and large heating loads are required (Holmberg *et al.*, 2016). Also, this type allows the centre pipe and annular pipe to have different thermal properties to improve the heat exchange process. For instance, it is possible to have a centre pipe with lower thermal conductivity material to minimize the thermal shunt between the downward and upward flows. For the annulus pipe, a high conductivity material is recommended for the annular pipe to enhance heat exchange between the injected fluid and the rock mass. Thermal conductivities of BHE pipes and grout materials are shown in Table 2-2 and Table 2-3, respectively.

Table 2-2 Thermal conductivity of BHE pipes (VDI, 2001)

Material	k (W/m·K)
PE100	0.42
PE100-RC	0.42
PE-RT	0.42
PA	0.24
PB	0.22
PE-X	0.41

Table 2-3 Average thermal conductivity of cementitious grouts with different fillers (w/c = water/cement ratio; f/c = filler/cement ratio) (Allan and Kavanaugh, 1999)

Grout Type	Filler Material	w/c	f/c	k (W/m·K)
Neat cement + superplasticizer	-	0.4	-	0.71
Neat cement	-	0.6	-	0.59
Neat cement	-	0.8	-	0.46
Neat cement	Silica sand	0.45	1.2	1.61
Neat cement	Silica sand	0.45	2	2.27
Neat cement	Silica sand	0.75	2	1.49
Neat cement	Coarse alumina	0.45	1.9	2.13
Neat cement	Fine alumina	0.45	1.3	1.79
Neat cement	Coarse silicon carbide	0.45	1.4	2.49
Neat cement	Fine silicon carbide	0.45	1.1	2.15
Neat cement	Steel grit	0.45	3.8	1.92

It is a common practice to arrange BHEs in a square, hexagonal, or cylindrical array for a large-scale application. The geometrical arrangements control heat loss from BHEs to the undisturbed ground by overlapping the heat storage field of a borehole to the adjacent one. In this regard, the most optimized arrangement would have the lowest surface-area-to-volume ratio. It leads to a more efficient accumulation of thermal energy within the storage medium (Skarphagen *et al.*, 2019).

For BTES, an antifreeze solution such as ethanol, ethylene, or propylene glycol is typically used as a working fluid. However, for high-temperature BTES, where the fluid temperature is always greater than 0°C, water with some additives such as biocides and corrosion inhibitors can be used. (Skarphagen *et al.*, 2019).

The circulation pump is another essential component of the BTES. According to the study by Kerme and Fung (2020), increasing the fluid mass flow rate results in increase in the temperature of the fluid temperature, grout material, and the surface of the borehole wall. The increased mass flow rate raises the heat transfer rate into the borehole as more cooling fluid is supplied to the BHEs. Also, when the fluid

circulates at a higher mass flow rate, there is less heat exchange between the upward and the downward flow. For an optimized BTES system design, an energy-efficient circulation pump capable of maintaining an adequate mass flow rate is mandatory.

2.3.2 Geological Conditions

For a closed-loop BTES system, thermal energy is conveyed by thermal conduction to the surrounding ground from BHEs. Therefore, thermal conductivity and thermal capacity are the two most critical parameters for the storage medium (Lee, 2013). Although BTES can be theoretically constructed anywhere, the storage efficiency can vary dependent on the two parameters. Generally, the preferred storage medium is saturated sediments for shallow applications, and rocks for deep BTES applications. They are preferred as a greater moisture content in the storage medium leads to higher volumetric heat capacity. The worst-case scenario would be an unconsolidated and unsaturated formation with high porosity, as it has both low thermal conductivity and capacity. Table 2-4 outlines the thermal conductivity of common rocks. Note that the variations in the thermal conductivity for each rock are due to water content in fractures and primary porosity, structure, mineral content, and size of crystals (Lee, 2013).

Table 2-4 Thermal conductivities of rocks (EU Commission SAVE Programme and Nordic Energy Research, 2004)

Type or rock	Thermal conductivity (W/m K)
Quartzite	4.0–6.0
Light granites	3.5–4.0
Light gneisses	3.0–3.5
Dark granites	2.5–3.0
Limestones	2.5–3.0
Sandstones	2.5–4.0
Shales	2.0–3.0

Another critical parameter is the geothermal gradient. The global average geothermal gradient is approximately 25 K/km. One study (Holmberg *et al.*, 2016) states that the BTES system installed at a site with the geothermal gradient of 25 K/km can result in a 55% higher heating load at 1000 m depth than for the BTES at a site with 15 K/km.

2.3.3 Review of BTES Models

There are numerous simulation models for designing a BTES system. Yang *et al.* (2010) have conducted a review of various heat transfer models often used to analyze BHEs. The models compared in their study are summarized in Table 2-5. The heat transfer process in BHEs is often analyzed in two separate regions because of its complexity. The first region is the solid outside the borehole, and the second region is inside the borehole. Depending on design objectives, either an analytical or numerical method is selected for the simulation.

The earliest analytical model for calculating the heat transfer between the ground and the BHEs is an infinite line source (ILS) model (Ingersoll & Plass, 1948). The ILS model assumes BHE as an infinitely long line source transferring heat to the surrounding ground. For this model, the surrounding ground is treated as an infinite medium with a uniform temperature. Heat transfer along the axial direction, parallel to the BHE, is neglected. The solution is limited for simulation times from a few hours to months.

Table 2-5 Comparison of the BHE models (Yang *et al.*, 2010)

Model		**Method**	**Thermal interference between boreholes**	**Boundary effects**
Outside borehole	Kelvin's line source	Infinite line source	Yes	No
	Cylindrical source	Infinite cylindrical source	Yes	No
	Eskilson's model	Combination of numerical and analytical methods	Yes	Yes
	Finite line-source solution	Analytical method	Yes	Yes
	Short time-step model	Numerical methods	Yes	Yes
Model		**Method**	**Thermal interference between U-tube pipes**	**Heat flux along depth**
Inside borehole	One-dimensional model		No	No
	Two-dimensional model		Yes	No
	Quasi-three-dimensional model		Yes	Yes

The infinite cylindrical source (ICS) model is also one of the earlier analytical models developed for BHE application (Carslaw & Jaeger, 1959). This model assumes a BHE as an infinitely long cylindrical source in direct contact with a homogeneous medium with constant properties. The surface temperature and the heat transfer rate are assumed to be constant for the ICS model. The solution to the analytical transient

heat conduction equation between the BHE and the ground is expressed with pre-defined G-function, a function of time and distance from the centre of BHE.

Eskilson's model (Eskilson & Claesson, 1988) or Finite Line Source (FLS) model was developed to incorporate the axial heat flow along the BHE in the earlier two analytical models. For the FLS model, the BHE has a finite length, and the surrounding ground is assumed to be homogenous with constant initial and boundary temperatures. The thermal resistance between the pipe and grout materials is still neglected. This model is particularly useful for modelling multiple BHEs, where there is significant thermal interaction between them. The thermal interaction between the BHEs is estimated using spatial and temporal superposition approaches. Eskilson & Claesson (1988) have pre-calculated G-functions for numerous potential borefield configurations. The analytical solution is developed by Zeng *et al.* (2002). Since the model does not account for the thermal resistance, it is mainly valid for a long-term simulation, for instance, a period greater than 2 – 6 hours. Yavuzturk & Spitler (1999) proposed a short time-step model valid for an hour and below. This modified model is based on a fully-implicit finite volume method.

Hellström (1991) developed a duct storage (DST) model for designing BTES. The model considers three subprocesses: the thermal interaction between the working fluid and the ground immediately outside the heat exchanger, the heat exchanger interacting with the surrounding ground in a local thermal process, and the global process involving the surrounding ground's storage volume. For this model, a combination of analytical and numerical methods is used for the heat transfer processes. For instance, the analytical method calculates the temperature difference between the fluid and the ground. The local and global heat transfer processes are determined by a finite difference method. The model is currently implemented in transient system simulation software TRNSYS.

Several approaches based on numerical methods, such as finite element, finite volume, and finite difference methods, are later proposed to simulate the heat transfer processes related to the BHEs. These numerical methods based approaches can provide more flexibility compared to the analytical models. However, commercial software tends to adapt analytical models for simplicity and computational efficiency. For using the analytical models, reasonable assumptions have to be made to compensate for simplification.

2.3.4 Applications of BTES

A conceptual BTES system integrated with a copper plant and a solar collector field is discussed by Xu *et al.* (2018). The system accepts the excess thermal energy produced from the copper plant and the solar thermal collectors, as shown in Figure 2-13. For the simulation of the system, constant fluid flow rate and injection temperature are assumed. The borefield is composed of 468 1-U type BHEs installed with 4 m spacing in a hexagonal array. Modelica is selected as a simulation tool, and Picard & Helsen's hybrid step-response model (HSRM) is incorporated into it. The HSRM model is a validated model for both short and long-term simulation capacity (Picard & Helsen, 2014). The integrated system is compared to the district system that operates with natural gas. The study also states that the most sensitive parameter for the performance of the BTES is the thermal conductivity of the surrounding ground.

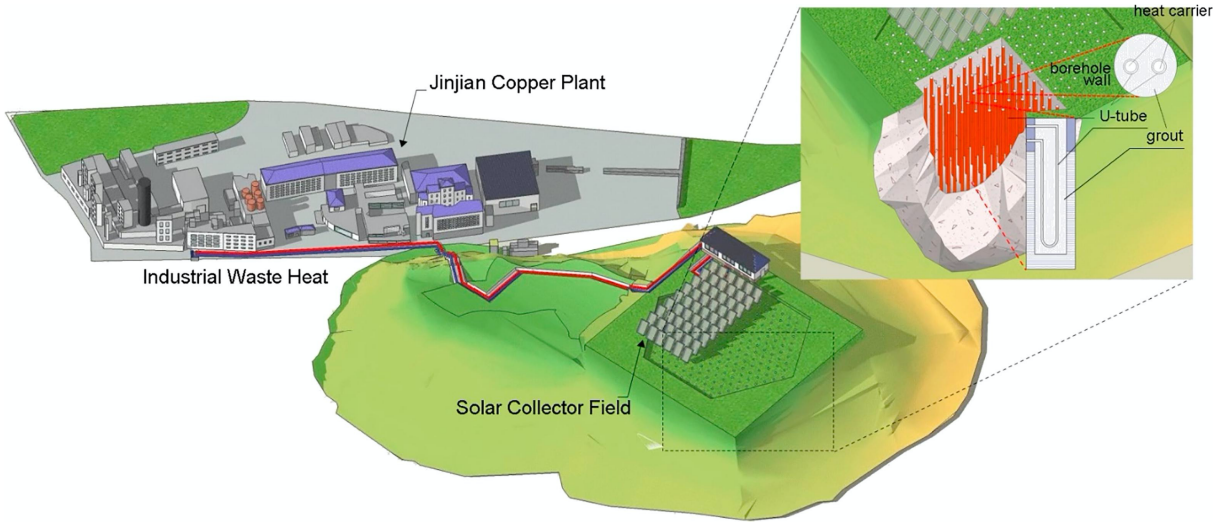

Figure 2-13 A schematic of conceptual BTES system integrated with a copper plant and a solar collector (Xu *et al.*, 2018)

For an application where only a small surface area is available, medium-deep borehole thermal energy storage (MD-BTES) can be desirable. MD-BTES, presented by Bär *et al.* (2015), consists of BHEs with a length between 500 m to 1,500 m. The operating temperature for this system can be up to 90°C, as the top insulated part of the BHEs prevents heat transfer between the circulating fluid and the aquifer. In the study, a conceptual system with the MD-BTES coupled with CHP and solar thermal collectors is analyzed for its feasibility. The first step of designing the MD-BTES is to obtain geological conditions of the site and determining the energy demand of the end-users. With the information, numerical modelling is carried out with simulation software, FEFLOW. The main focus of the analysis is on the transient

behaviour of the subsurface and performance of the system. The performance of the system is measured with parameters such as storage efficiency and outlet temperature.

Madiesh *et al.* (2019) have studied the application of BTES in recovering waste heat from diesel generators in remote cold climate locations. The authors first studied the existing diesel generator in Prince George, British Columbia, Canada, to determine the recoverable thermal energy from its different components. Also, the energy demand of the nearby northern community is obtained. The simulation of the proposed system is conducted using ANSYS and SolidWorks. The long-term performance of the system is evaluated. An economic analysis is conducted to determine the potential savings by implementing the proposed system. The system is composed of 100 m deep BHEs, evenly distributed in the 6 x 6 grid. It is concluded that the BTES system could save up to CAD $48,000 and reduce 90 tons of CO_2 emission annually.

2.4 Summary of Review and Research Opportunities

The literature review shows that various configurations, simulation models, and design approaches are proposed for CAES and BTES systems. In the 1970s, dCAES systems were solely considered, but more recent studies focused on designing an adiabatic system coupled with renewable power systems. For aCAES systems, short-term TES, such as packed TES and fluid tank, are considered. However, there is less emphasis on integrating it with a long-term seasonal TES. Although the operating temperature of the long-term TES is relatively low compared to the short-term TES, it can provide space and water heating or other purposes.

BTES is a long-term TES system that is applicable as a seasonal TES because of its large storage capacity and scalability. Numerous simulation models describing the heat transfer processes involved in the BTES system are published in the literature. Moreover, they are incorporated into commercial design software. Both analytical and numerical models are available for the BTES application. The analytical models such as ILS, ICS, and FLS models are useful as their applications are simpler and more computationally efficient than the numerical models. In contrast, the numerical models, based on finite element, finite difference, and finite volume methods, can provide greater flexibility. Similar to the CAES systems, BTES systems are often integrated with renewable sources.

The design approaches for CAES and BTES systems are also reviewed. In general, the first step is to determine the energy demand of the application. Also, the relevant geological and environmental

conditions have to be defined, as they can substantially affect the performance of the ESS. The collected data are used in a simulation model as input parameters. The simulation model can be created by incorporating one of the analytical and numerical methods depending on design purposes. With the model, the system's performance is evaluated based on metrics, such as round-trip efficiency or thermal efficiency. A case study or a parametric study is often accompanied to assess its conditional feasibility. The parametric study also provides information on the critical design parameters and their degree of impact. The case study is useful for evaluating the opportunities for the real-world implementation. Some studies include comparative economic analysis with other similar energy storage technologies to examine the economic benefits of utilizing CAES and BTES. `

According to the literature review, an ESS system that integrates CAES and BTES is unavailable. Hence, the integrated CAES-BTES system is a novel configuration of ESS-TES, and its feasibility is addressed in this thesis. The description of the system and the models used for the performance analysis are presented in the following chapter.

Chapter 3: System and Model Descriptions

3.1 System Description

The integrated CAES-BTES system is capable of storing both electrical and thermal energy. For instance, the electrical energy is stored as compressed air in a storage vessel. The attached seasonal borehole thermal energy storage (BTES) system can store the heat of compression or thermal energy from other external sources. The integrated system is composed of compressors, expanders, intercoolers, heaters, and thermal storage tanks (i.e. cold and hot oil tanks) for the compressed air energy storage (CAES). The BTES system includes borehole heat exchangers (BHEs), heat exchangers, and a circulation pump. A conceptual diagram of the integrated CAES-BTES system is shown in Figure 3-1.

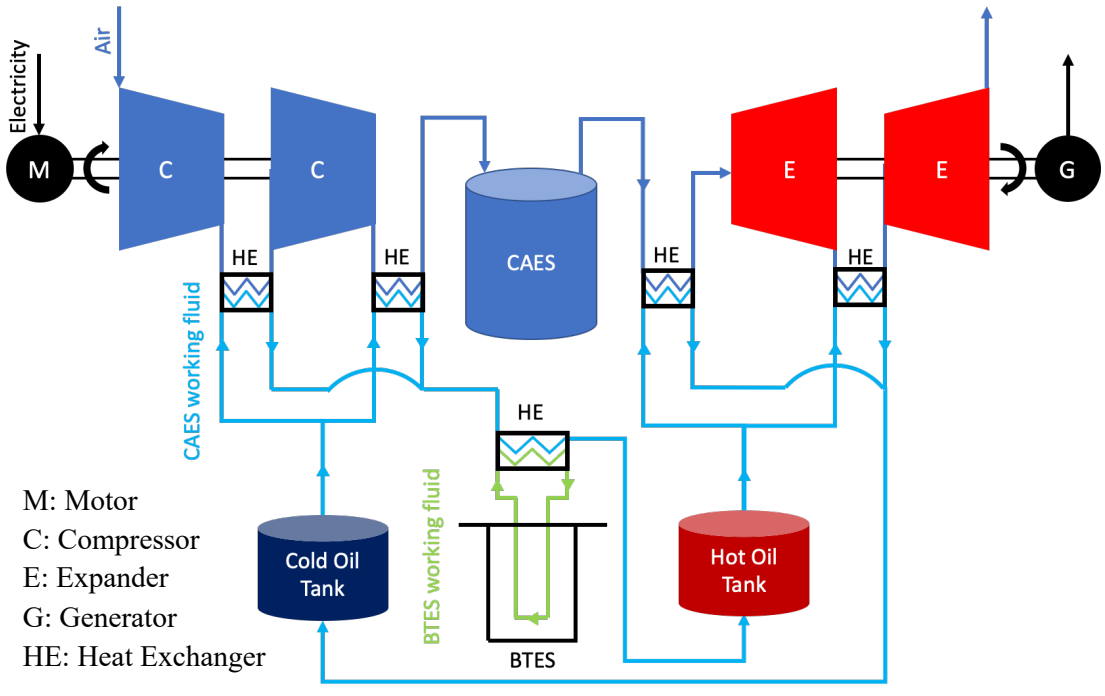

Figure 3-1 A conceptual diagram of the integrated CAES-BTES system

The system operates in a cycle of charging and discharging modes. For the charging mode, electrical energy operates the motor and subsequently the attached compressors. The compressors withdraw the air from the atmosphere and compress it to high pressure. In order to lower the temperature of the compressed air, some thermal energy is removed from it by circulating working fluid from the heat exchangers (i.e., intercoolers). The compressed air is then stored in a storage vessel. The heated working fluid is stored in the hot oil tank. A portion of the thermal energy from the CAES working fluid is transmitted to another working fluid circulating the BTES system before it is conveyed to the hot oil tank. The BTES working fluid stores the thermal energy to the storage medium of the BTES system. For the discharging mode, the compressed air is released from the storage vessel to the expansion side of the CAES system to operate the air expansion turbines and the generator. The hot working fluid stored in the hot fluid tank can be transported to the expansion side of the CAES system and provide the thermal energy for air expansion.

3.2 CAES Thermodynamics Model

This chapter contains the thermodynamics models of each component in the CAES part of the integrated CAES-BTES system. The components considered for the model include the compressor, turbine (expander), TES (hot and cold fluid tanks), and intercoolers/heaters. The model based on the First Law of Thermodynamics is used to determine the temperature, enthalpy, and pressure of the working fluid and the air at different control points. The model can also calculate air mass flow rate, storage volume requirement, and charging and discharge time. The results produced by the model can be used to evaluate the efficiency of the system. As these values depend on the components' design parameters, a parametric study on the system's performance is also feasible using the model presented here. Note that the governing equations presented in this chapter are modified forms of the functions from the work of Guewouo *et al.* (2019). Figure 3-2 presents the design workflow for the CAES part of the integrated system. An elaborated global design workflow for the integrated CAES-BTES system is provided in Chapter 3.4.

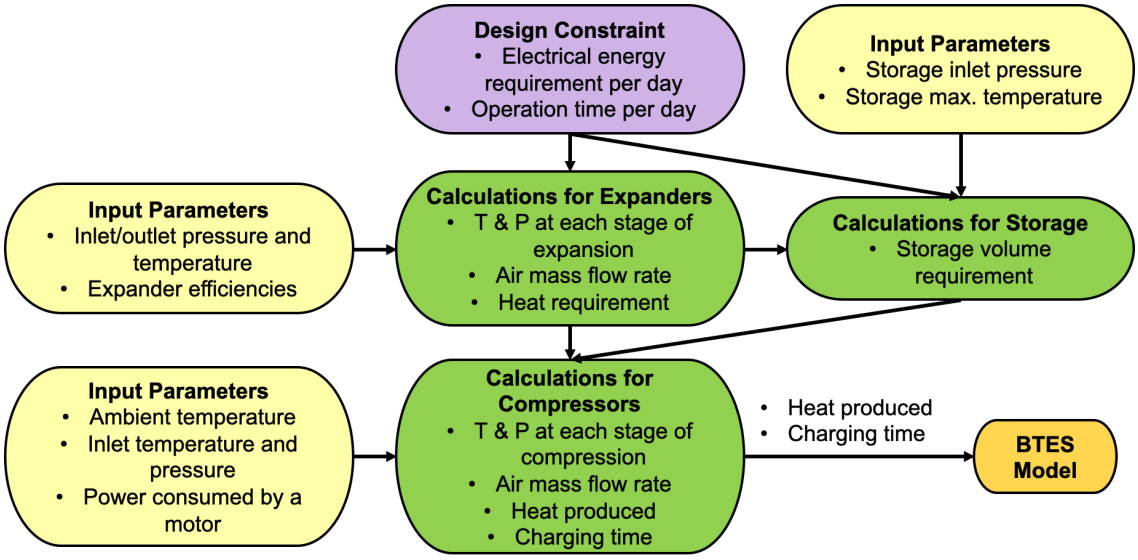

Figure 3-2 Design workflow for the CAES part of the integrated system

3.2.1 General Assumptions

The modified functions introduced by Guewouo *et al.* (2019) are used as a basis for the model constructed for this study. The model is based on the First Law of Thermodynamics and can determine the temperature, enthalpy, and pressure of the working fluid and the air at selected control points. The model also calculates air mass flow rate, required storage volume, and charging/discharging time. For simplifications, the following assumptions are considered (Guewouo *et al.,* 2019):

- A steady-state condition is assumed for all components
- Air behaves as an ideal dry gas
- No energy loss is assumed at the throttle valve of the storage vessel
- An ambient pressure of 100 kPa is assumed
- The thermodynamics properties are interpolated from published engineering tables, as needed (Moran *et al.,* 2010).
- Same inlet temperature for each compression stage equal to atmospheric temperature
- Same inlet temperature for each expansion stage equal to user-defined value
- The following parameters are assumed to be constant:
    - Isentropic electric and mechanical efficiency for the compressors and expanders
    - Air mass flow rate
    - Working fluid mass flow rate
    - Power input and output for the motor and generator

3.2.2 Expander-Generator

The output specific enthalpy of air is determined as:

$$h_{e,i}^{out} = h_{e,i}^{in} - \eta_{e,IS}(h_{e,i}^{out} - h_{e,IS,i}^{in}) \quad (3\text{-}1)$$

where $\eta_{e,IS}$ is the expander isentropic efficiency, $h_{e,i}^{out}$ is the outlet specific enthalpy of the ith expansion stage, $h_{e,IS,i}^{in}$ is the inlet specific enthalpy of the ith stage of isentropic expansion, and $h_{e,i}^{in}$ is the inlet specific enthalpy of the ith expansion stage.

To determine $h_{e,IS,i}^{in}$, the inlet temperature of the ith stage of isentropic expansion, $T_{e,IS,i}^{in}$, should be determined beforehand. The following expression is used to determine $T_{e,IS,i}^{in}$:

$$S^0\left(T_{e,IS,i}^{out}\right) = S^0\left(T_{e,i}^{in}\right) + Rln\ (1/PR_e) \quad (3\text{-}2)$$

where R is the gas constant (287 J/kg·K), S^0 is the specific entropy as a function of temperature $T_{e,IS,i}^{out}$ and the inlet temperature $T_{e,i}^{in}$ of the ith expansion stage. PR_e is expansion pressure ratio at each stage, assuming at each expansion stage PR_e is same, determined as:

$$PR_e = \left(\frac{p_{e,1}^{in}}{p_{e,Ne}^{out}}\right)^{1/N_e} \quad (3\text{-}3)$$

where $p_{e,1}^{in}$ is the inlet pressure for the first expansion stage, N_e is the number of expansion stages in the system, and $p_{e,Ne}^{out}$ is the outlet pressure for the last compression stage which is also equal to the atmospheric pressure.

The average electrical power demand, P_G, is one of the input parameters for the model. The P_G and the inlet and outlet enthalpy of the air are used to determine the air mass low rate on the expansion side of the system, $\dot{m}_e$. $\dot{m}_e$ can be determined from the equation below:

$$\dot{m}_e = \frac{\sum_{i=1}^{Ne}(h_{e,i}^{in} - h_{e,i}^{out})}{P_G} \quad (3\text{-}4)$$

3.2.3 Storage

The mass storage capacity, $m_{air,s}^{max}$, is calculated by rearranging the ideal gas law (PV = mRT) as below:

$$m_{air,s}^{max} = \frac{p_s V_s}{R T_s} \quad (3\text{-}5)$$

where p_s, V_s, and T_s are estimated storage maximum pressure, volume, and temperature, respectively. With $m_{air,s}^{max}$ and the air mass flow rate on the compression side, $\dot{m}_c$, the maximum charge time, t_{charge}^{max}, is calculated as:

$$t_{charge}^{max} = m_{air,s}^{max} / \dot{m}_c \quad (3\text{-}6)$$

Similarly, the maximum discharge time, $t_{discharge}^{max}$, emptying the storage from its full capacity, is determined with the equation below:

$$t_{discharge}^{max} = m_{air,s}^{max} / \dot{m}_e \quad (3\text{-}7)$$

Note that $\dot{m}_e$ is the air mass flow rate in the expansion-generation side of the system.

3.2.4 Compressor

The outlet enthalpy of air is determined as:

$$h_{c,i}^{out} = h_{c,i}^{in} + \frac{h_{c,IS,i}^{out} - h_{c,i}^{in}}{\eta_{c,IS}} \quad (3\text{-}8)$$

where $\eta_{c,\,IS}$ is the compressor isentropic efficiency, $h_{c,i}^{out}$ is the outlet specific enthalpy of the ith compression stage, $h_{c,IS,i}^{out}$ is the outlet specific enthalpy of the ith stage of isentropic compression, and $h_{c,i}^{in}$ is the inlet specific enthalpy of the ith compression stage.

To determine $h_{c,IS,i}^{out}$, the outlet temperature of the ith stage of isentropic compression, $T_{c,IS,i}^{out}$, should be determined beforehand. The following expression is used to determine $T_{c,IS,i}^{out}$:

$$S^0\left(T_{c,IS,i}^{out}\right) = S^0\left(T_{c,i}^{in}\right) + Rln\ (PR_C) \tag{3-9}$$

where S^0 is the specific entropy as a function of the outlet temperature $T_{c,IS,i}^{out}$ and the inlet temperature $T_{c,i}^{in}$ of the ith compression stage. PR_C is compressor pressure ratio at each stage defined as:

$$PR_C = \left(\frac{p_{c,\,Nc}^{out}}{p_{c,\,1}^{in}}\right)^{1/Nc} \tag{3-10}$$

where $p_{c,\,1}^{in}$ is the inlet pressure for the first compression stage, generally equal to atmospheric pressure. N_c is the number of compression stages in the system, and $p_{c,\,Nc}^{out}$ is the outlet pressure for the last compression stage. $p_{c,\,Nc}^{out}$ is also equal to the maximum storage pressure.

By assuming the inlet temperature is constant for each compression stage, $S^0\left(T_{c,IS,i}^{out}\right)$ and $T_{c,IS,i}^{out}$ can be interpolated using a predefined thermodynamics table (Moran *et al.*, 2019). With $T_{c,IS,i}^{out}$, $h_{c,IS,i}^{out}$ is determined using the same interpolation method. $h_{c,IS,i}^{out}$ is then used to estimate $h_{c,i}^{out}$ as well as $T_{c,i}^{out}$, that is the outlet temperature ith compression stage.

Given the average electrical power consumed by the compressor, $P_{elec,c}$, the mass flow rate of air in the compression side of the system, $\dot{m}_c$, can be determined from the equation below:

$$\dot{m}_c = \frac{\sum_{i=1}^{Nc}(h_{c,i}^{out} - h_{c,i}^{in})}{P_{elec,c}} \tag{3-11}$$

3.2.5 Intercoolers

Intercoolers are installed after each compression stage to extract thermal energy from the heated compressed air before it enters either the next compression stage or the storage vessel. The enthalpy of cooling fluid is determined with the following equation:

$$h_{cf,i}^{out} = h_{cf,i}^{in} + \frac{\dot{m}_c}{\dot{m}_{cf}}(h_{c,i}^{out} - h_{c,i+1}^{in}) \quad (3\text{-}12)$$

where $h_{cf,i}^{out}$ is the outlet specific enthalpy of cooling fluid of the ith intercooling stage, $h_{cf,i}^{in}$ is the inlet specific enthalpy of cooling fluid of the ith intercooling stage, and $h_{c,i+1}^{in}$ is the inlet specific enthalpy of the (i+1)th compression stage. The cooling fluid mass flow rate $\dot{m}_{cf}$ is determined iteratively, with a goal of achieving minimal $\dot{m}_{cf}$.

The total heat transfer rate between air and cooling fluid in intercoolers in the compression side of the system, $\dot{Q}_{c,cf}$, can be calculated as:

$$\dot{Q}_{c,cf} = \dot{m}_c \sum_{i=0}^{Nc}(h_{c,i}^{out} - h_{c,i+1}^{in}) \quad (3\text{-}13)$$

To determine the temperature of cooling water entering the hot fluid tank by interpolation, the specific enthalpy of cooling fluid entering the hot water tank, $h_{cf,t}^{in}$, is determined with the equation below:

$$h_{cf,t}^{in} = \dot{m}_c \sum_{i=1}^{Nc}(h_{cf,i}^{out}) \quad (3\text{-}14)$$

With the determined enthalpy, the temperature of the cooling fluid can be determined. The equations (3-12) to (3-14) can be also applied to heaters used on the expansion side of the system.

3.2.6 Heat Exchange between Working Fluid of CAES and BTES

After the cooling fluid absorbs the heat of compression, it passes through another heat exchanger where the CAES fluid provides the thermal energy to BTES working fluid. In this study, the initial temperature

of the BTES working fluid temperature is assumed to be 20°C. Also, it is assumed that the inlet temperature for the BHEs is constant for each charging and discharging mode. Therefore, the inlet and outlet enthalpies of the BTES working fluid, h_{BTES}^{in} and h_{BTES}^{out}, can be determined with the temperature by interpolation. Finally, the enthalpy of CAES working fluid entering the hot oil tank, h_{hf}^{in}, can be calculated as:

$$h_{hf}^{in} = h_{cf,Nc}^{in} + \frac{\dot{m}_{BTES}}{\dot{m}_{cf}}(h_{BTES}^{out} - h_{BTES}^{in}) \quad (3\text{-}15)$$

where $\dot{m}_{BTES}$ is mass flow rate of BTES working fluid. The total heat transfer rate between these two fluids, $\dot{Q}_{BTES,in}$, is equal to the heat being injected to the BHEs. $\dot{Q}_{BTES,in}$ can be calculated as:

$$\dot{Q}_{BTES,in} = \dot{m}_c(h_{h,f}^{in} - h_{cf,Nc}^{in}) \quad (3\text{-}16)$$

3.2.7 Cycle Efficiency of CAES

For the simulation process, the round-trip efficiency (RTE) is considered as a performance criterion for the CAES system. The RTE is defined as the ratio of energy outputs and inputs (Guewouo *et al.*, 2019). The RTE of a diabatic system ($\eta_{RTE,d}$) is calculated as:

$$\eta_{RTE,d} = \frac{W_e}{Q_{req}+W_c} \quad (3\text{-}17)$$

where W_e is the electrical work output from the expanders, W_c is the electrical work input into the compressors, and Q_{req} is the thermal energy required for air expansion.

An adiabatic RTE, $\eta_{RTE,a}$ is defined as:

$$\eta_{RTE,a} = \frac{Q_{req}+W_e}{Q_{req}+W_c},\ Q_{req} > Q_{rel} \quad (3\text{-}18)$$

where Q_{rel} is the amount of thermal energy release from the compression side of the system.

Figure 3-3 is a process flow diagram of the CAES system linked to the equations (3-1) to (3-18).

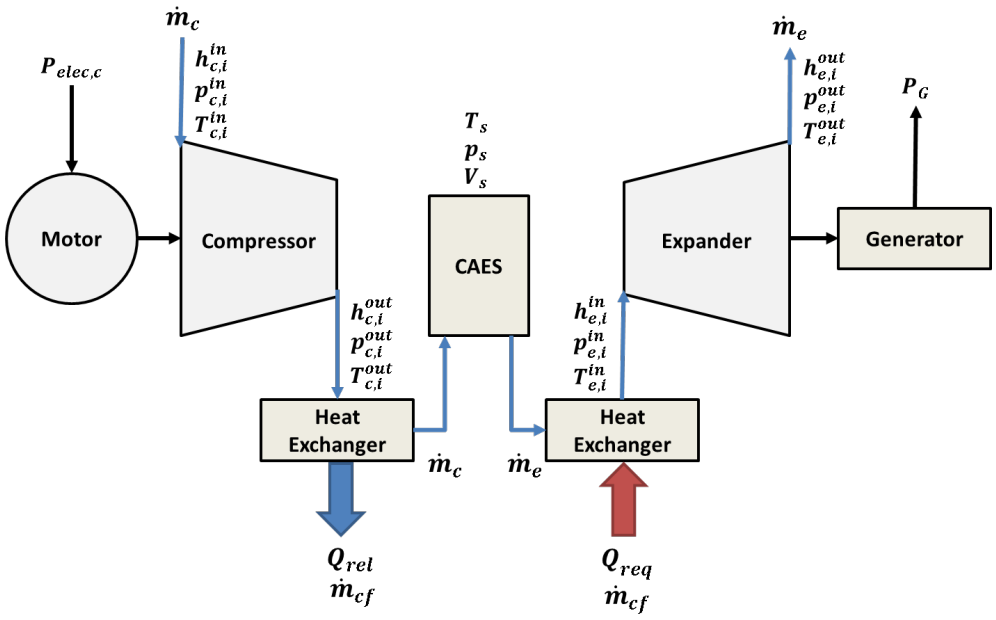

Figure 3-3 CAES Process Flow Diagram

3.3 BTES Model

This chapter discusses the BTES model used to estimate appropriate sizing for the BTES part of the integrated system. As presented in Chapter 2, numerous models are available to simulate the heat transfer processes involved in the BTES. After reviewing the available models and approaches, the writer has selected the method employed by the ASHRAE (Philippe *et al.*, 2010), for its simplicity. The workflow shown in Figure 3-4 is used to design the BTES system.

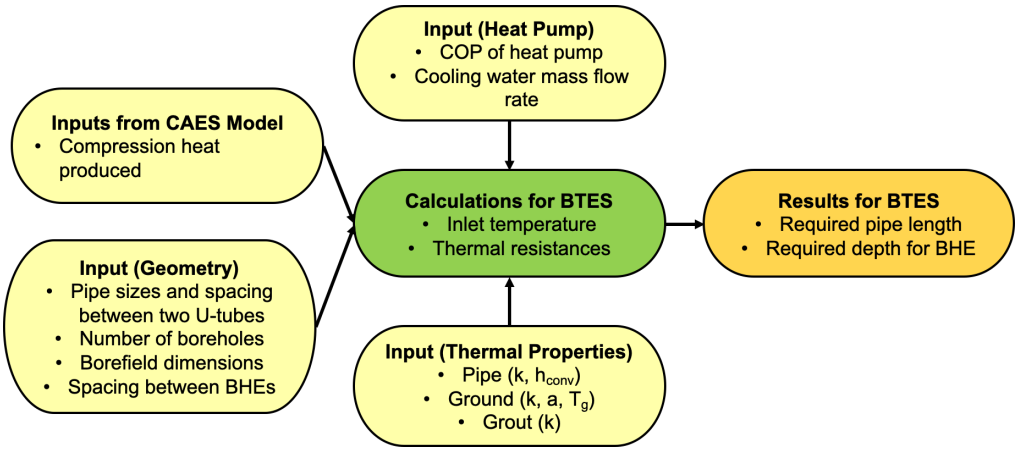

Figure 3-4 Design workflow for the BTES part of the integrated system

The overall approach is based on the work of Kavanaugh & Rafferty (1997), and the effective thermal resistance, R_b, is determined by the method presented in Hellström's duct storage (DST) model (Hellström, 1991). Note that Kavanaugh & Rafferty's model is based on the infinite cylindrical solution (ICS), initially proposed by Carlsaw and Jaeger (1959), combined with the temporal superposition method proposed by Ingersoll and Plass (1948). The overarching equation for this approach, recast by Bernier (2006), is as below:

$$L = \frac{q_h R_b + q_y R_{10y} + q_m R_{1m} + q_h R_{6h}}{T_m - (T_g + T_p)} \tag{3-19}$$

where L is the total borehole length, T_m is the mean fluid temperature in the borehole, T_g is the undisturbed ground temperature, T_p is the temperature penalty due to the thermal interferences between boreholes, q_y, q_m and q_h are the yearly average, the highest monthly ground load, and the peak hourly ground load, respectively. Lastly, R_{10y}, R_{1m} and R_{6h} are effective ground thermal resistances corresponding to 10 years, one month and six hours ground loads, respectively.

According to the case studies presented in the article by Philippe *et al.* (2010), the sizing approach has good agreement with Hellström's duct storage (DST) model (Hellström, 1991), and Eskilson's finite line source (FLS) model (Eskilson & Claesson, 1988). Both models are adapted in numerous BTES simulation software systems for the HVAC industry. The only notable errors occur when calculating R_{10y} and T_p. However, according to Philippe *et al.*, (2009), the error is less than 5%, compared to the more complicated models based on numerical methods. Also, the way T_p is evaluated based on the correlation method proposed by Bernier *et al.* (2008) produces similar results with Eskilson's method (Eskilson & Claesson, 1988), with a difference less than 10% for a BTES with more than or equal to 4 BHEs. For this thesis, these error ranges are acceptable.

3.3.1 Assumptions and Limitations of the BTES Model

The following assumptions are considered for the BTES model developed in this thesis for compensating uncertainties and simplification purposes:

- Only steady-state heat conduction occurs in the ground
- No groundwater movement takes place – convective heat transfer is not considered

- As shown in equation (3-19), three ground heat loads are considered initially. For this thesis, only one average ground load value is considered, as the thermal energy is supplied from the CAES at a relatively consistent rate year-round
- Coefficient of Performance (COP) of the heat pump is assumed to be 5 (NRCan, 2017)
- The BHEs are assumed to be the 1-U type and positioned in an equally spaced rectangular grid
- The BHEs are assumed to be infinitely-long cylindrical heat sources
- The storage medium is homogenous and isotropic
- The heat transfer along the height of the BHE is neglected.
- The average fluid temperature within the borehole, T_m, is constant along the borehole

The validity of the solutions produced by the model is restricted to the following ranges (Bernier *et al.*, 2008):

$$-2 \leq \ln\left(\frac{t}{t_s}\right) \leq 3$$
$$4 \leq NB \leq 144 \qquad (3\text{-}20)$$
$$1 \leq \mathrm{A} \leq 9$$
$$0.05 \leq \mathrm{B/H} \leq 0.1$$

where t is the total simulation time (i.e. 10 years), t_s is a characteristic time, NB is the number of boreholes, A is the geometrical aspect ratio (i.e. number of boreholes in a row over column), B is the spacing between boreholes, and H is the borehole depth. The t_s is defined as below:

$$t_s = H^2/9\alpha \qquad (3\text{-}21)$$

where α is the ground thermal diffusivity.

Figure 3-5 graphically presents the variables used in the equations (3-19) to (3-21).

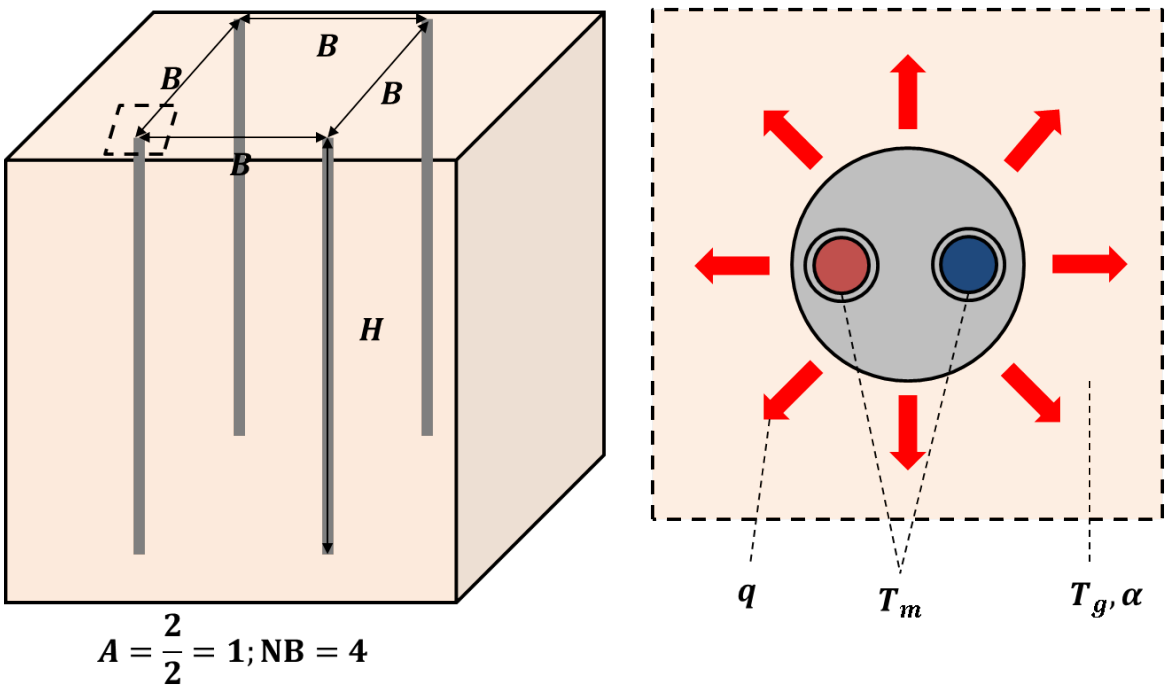

Figure 3-5 Example BTES configuration

3.3.2 Thermal Resistances

In this BTES sizing approach, two different thermal resistances are considered, including the effective ground thermal resistances (R_{10y}, R_{1m} and R_{6h}) and the effective borehole thermal resistance, R_b. R_{10y}, R_{1m} and R_{6h} define the thermal resistance between a BHE and the far-field undisturbed ground temperature due to the transient heat transfer for 10 years, 1 month, and 6 hours time periods (Philippe *et al.*, 2010). R_b accounts for the transient heat transfer between the BHE and the borehole wall (i.e. the contact between the BHE and the surrounding ground).

The effective boreholes resistances are estimated as (Kavanaugh & Rafferty, 1997):

$$R_{6h} = \frac{1}{k} G(\alpha t_{6h}/r_{bore}^2)$$
$$R_{1m} = \frac{1}{k}\left[G\left(\frac{\alpha t_{1m+6h}}{r_{bore}^2}\right) - G\left(\frac{\alpha t_{6h}}{r_{bore}^2}\right)\right] \quad (3\text{-}22)$$
$$R_{10y} = \frac{1}{k}\left[G\left(\frac{\alpha t_{10y+1m+6h}}{r_{bore}^2}\right) - G\left(\frac{\alpha t_{1m+6h}}{r_{bore}^2}\right)\right]$$

where k is the ground thermal conductivity and r_{bore} is the borehole radius. The G-functions are thermal response factors used to model the transient heat transfer, originally proposed by Eskilson (1987). For the

estimation of the G-functions, Baudoin's curve-fitting method (Baudoin, 1988) on the Eskilson's work is employed in this approach. Then, the effective ground thermal resistances can be calculated as below:

$$R_j = \frac{1}{k} f_j(\alpha r_{bore})$$

$$f_j = b_o + b_1 r_{bore} + b_2 r_{bore}^2 + b_3 a + b_4 a^2 + b_5 \ln(a) + b_6 \ln(a)^2 + b_7 r_{bore} a + a_8 r_{bore} \ln(a) + b_9 a \ln(a) \quad (3\text{-}23)$$

where the function *f* is the correlation function, and b_n are correlation coefficients. The subscripts j corresponds to 6h, 1m, and 10y. The correlation coefficients for the function *f* are presented in Appendix A.

R_b for a single 1-U type BHE is calculated with the expression below (Hellström, 1991):

$$R_b = R_g + \frac{R_p + R_{conv}}{2} \quad (3\text{-}24)$$

R_p is the conductive thermal resistance from each tube, and it is calculated as below:

$$R_p = \frac{\ln (r_{p,ext}/r_{p,in})}{2\pi k_{pipe}} \quad (3\text{-}25)$$

where k_{pipe} is the thermal conductivity of the pipe, and $r_{p,ext}$ and $r_{p,in}$ are external and internal radius of the pipe, respectively.

R_g is defined as the conductive thermal resistance imposed by the grout material, and it is calculated as:

$$R_g = \frac{1}{4\pi k_{grout}} \left[\ln \left(\frac{r_{bore}}{r_{p,ext}}\right) + \ln \left(\frac{r_{bore}}{L_u}\right) + \frac{k_{grout} - k_{ground}}{k_{grout} + k_{ground}} \ln \left(\frac{r_{bore}^4}{r_{bore}^4 - \left(\frac{L_u}{2}\right)^4}\right)\right] \quad (3\text{-}26)$$

where k_{grout} is the thermal conductivity of the grout, k_{ground} is the thermal conductivity of the ground, and L_u is the centre-to-centre distance between the two pipes in a single 1U BHE.

Lastly, the convective thermal resistance inside each tube is expressed as below:

$$R_{conv} = \frac{1}{2\pi r_{p,in} k_{pipe}} \tag{3-27}$$

where k_{pipe} is the thermal conductivity of the pipe. Figure 3-6 is a cross-section of a 1U BHE which corresponds to the equations (3-24) to (3-27).

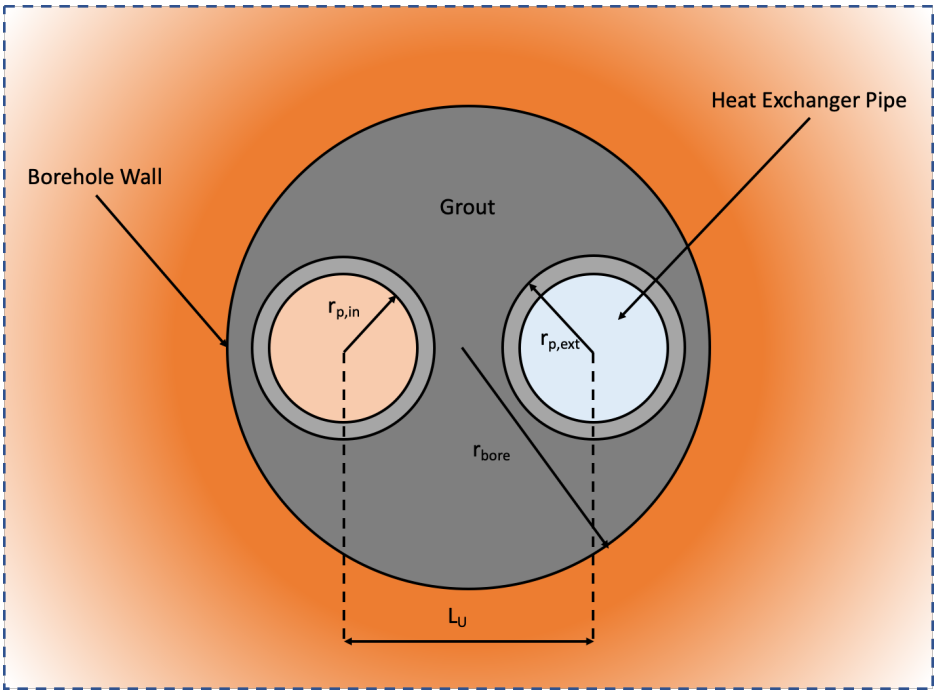

Figure 3-6 Cross-section of a 1U BHE

3.3.3 Thermal Interactions between Adjacent BHEs

Bernier (2008) has proposed an expression to determine the temperature penalty, T_p to accommodate the thermal interference between BHEs based on a correlation function, F, as below:

$$T_p = \frac{q_y}{2\pi kL} F\left(\frac{t}{t_s}, \frac{B}{H}, NB, A\right) \tag{3-28}$$

where F is calculated as below:

$$F = \sum_{i=0}^{36} b_i \times c_i \tag{3-29}$$

When more thermal energy is retrieved than stored from the underground storage medium, a phenomenon called thermal imbalance occurs in the ground. If the imbalance persists for many years, neighbouring BHEs thermally interact with each other. The thermal interaction has to be considered in the design process of a BTES system, as it affects the performance of heat pump. Hence, the $T_{p,}$ which accounts for the long-term temperature changes in the undisturbed ground temperature, is considered in the equation (3-19). As shown in Table 3-1, a greater temperature penalty is considered for a borefield configuration with more BHEs and less spacing between BHEs. Also, a storage medium with greater thermal diffusivity tends to result in a greater temperature penalty value. For calculating the values of T_p shown in Table 3-1, a borehole depth of 100 m and an operation time of 10 years are assumed.

Table 3-1 Values of nondimensional temperature penalty for various borefield configurations (Bernier, 2008)

Borefield Configuration	Borehole spacing (m)	Nondimensional T_p ($T_P=2\pi k/q$)	
		$\alpha = 0.089$ m^2/day	$\alpha = 0.056$ m^2/day
1 x 8	5	5.1	4.2
	6	4.4	3.6
	7	3.8	3.0
3 x 8	5	14.9	12.3
	6	12.8	10.4
	7	10.9	8.7
5 x 5	5	16.7	13.7
	6	14.3	11.6
	7	12.1	9.7
10 x 10	5	30.3	23.3
	6	25.2	19.1
	7	20.7	15.1

3.4 Global Design Flowchart

The computer model is constructed with MATLAB®, based on the equations introduced in Chapters 3-2 and 3-3. Figure 3-7 presents the global design flowchart for the integrated CAES-BTES system that can

be completed with the model presented in this thesis. Note that the design flowchart can be followed iteratively for the design optimization.

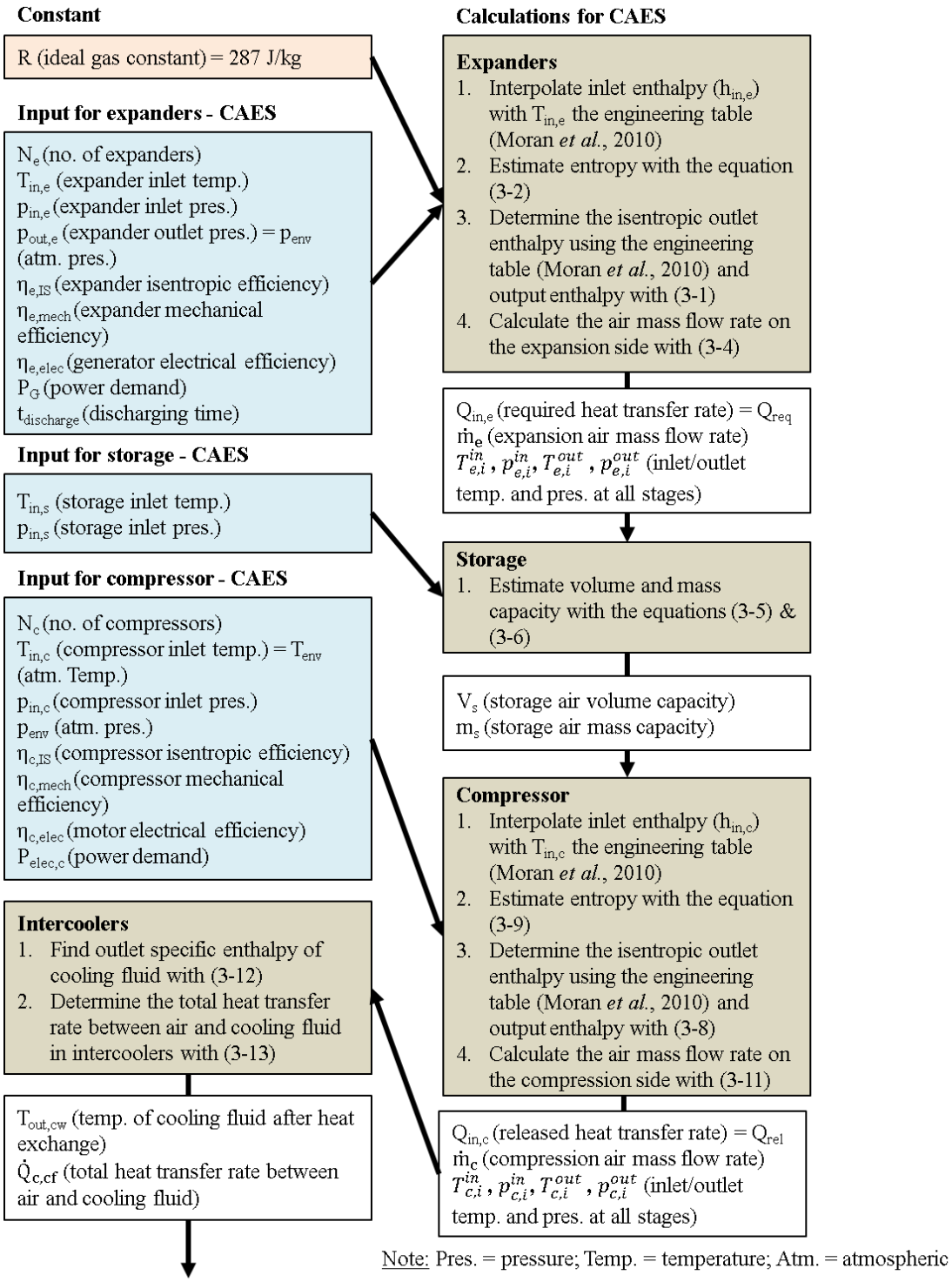

Figure 3-7a Global design flowchart of the integrated CAES-BTES system

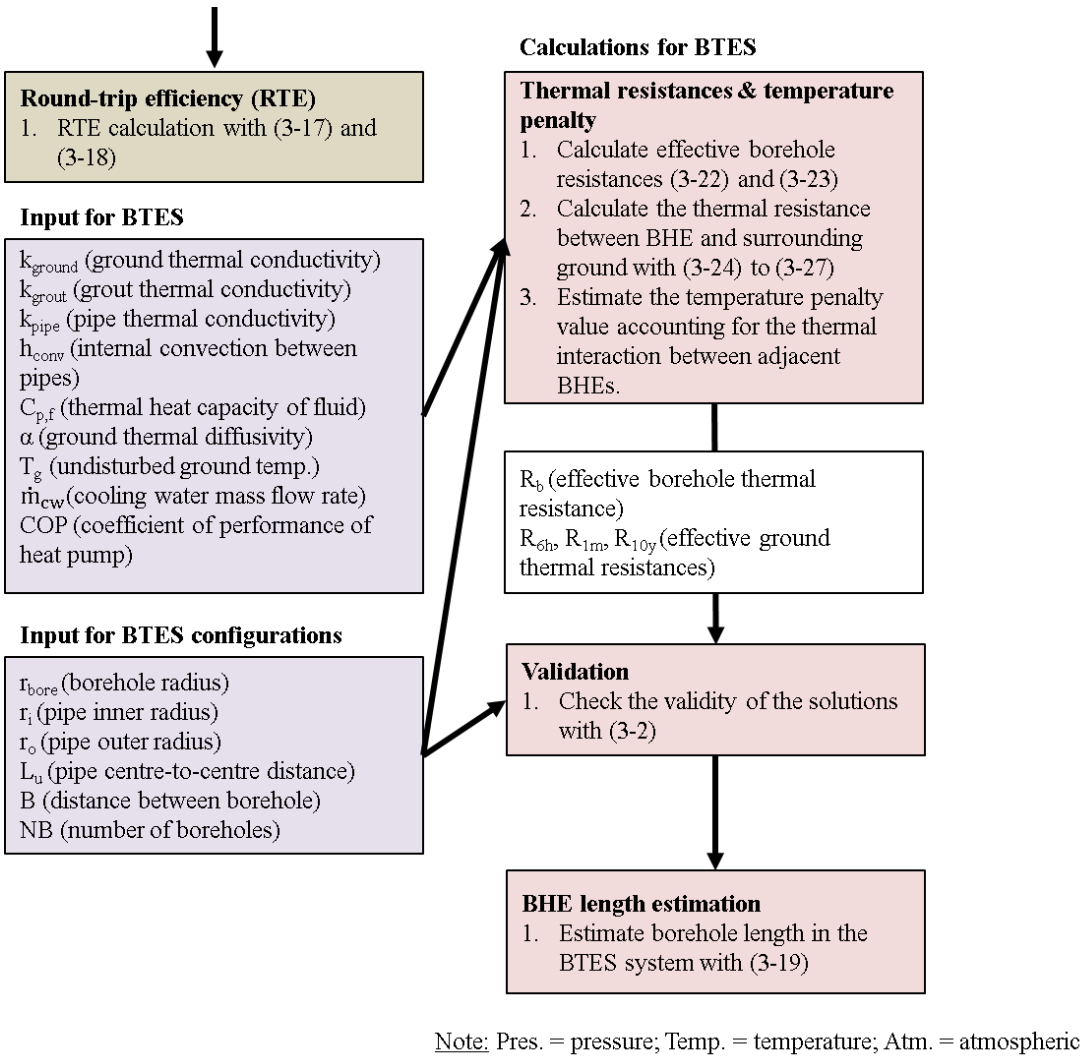

Note: Pres. = pressure; Temp. = temperature; Atm. = atmospheric

Figure 3-7b Global design flowchart of the integrated CAES-BTES system

Chapter 4: Parametric Study on the Integrated CAES-BTES System

4.1 Background of the Parametric Study

With the models introduced in Chapter 3, a parametric study is conducted to determine the key operating parameters and their effects on the overall performance of the integrated CAES-BTES system. The results discussed in this chapter demonstrate the technical feasibility of the integrated system. The hypothetical system with a power output of 1.5 MW is assumed to operate in a continuous daily cycle with 8 hours of discharge period, $t_{discharge}$. The scale considered for this study is suitable for a pilot project (Sustain X Inc., 2015) or a micro-grid power system.

The effects of the following parameters are studied for the CAES part of the integrated system:

- Inlet temperature for the 1st stage of expansion ($T_{e,1}^{in}$)
- Environment temperature (T_{env})
- Number of expansion stages (N_e)
- Number of compression stages (N_c)
- Storage temperature (T_s)
- Storage pressure (p_s)

For this study, the inlet pressure for the first stage of the expansion, $p_{e,1}^{in}$, is assumed to be equal to p_s. The environment pressure, p_{env}, is assumed to be constant at 100 kPa. The working fluid for the system is selected to be Therminol®-55, and its pre-defined thermodynamics properties are used in the calculation process (Eastman, 2020).

For the CAES part of the system, the following results are analyzed:

- Pressure at each stage of expansion ($p_{e,i}^{in}$ and $p_{e,i}^{out}$)
- Pressure at each stage of compression ($p_{c,i}^{in}$ and $p_{c,i}^{out}$)
- Air mass flow rate in the expansion and compression side of the system ($\dot{m}_e$ and $\dot{m}_c$)
- Heat transfer rate required for the expansion of air (Q_{req})
- Compression heat transfer rate (Q_{rel})
- Working fluid mass flow rate ($\dot{m}_{cw}$)
- Storage volume (V_s)

Operating conditions such as power consumed by a motor,P_c, discharge time per day, $t_{discharge}$, and generator power output, P_e, are predefined. In the parametric study, P_e and P_c are assumed to be 1.5 MW (Sustain X Inc., 2015).

The CAES model and the BTES model are linked with the two parameters, which are the amount of heat released from the compression side of the system, Q_{rel}, and $t_{discharge}$.

For the BTES, the following parameters are considered in the parametric study:

- Spacing between boreholes (B)
- Ground thermal conductivity and thermal diffusivity (k_{ground} and α_{ground})
- Grout thermal conductivity (k_{grout})

The 1-U pipe inserted for BHEs for the BTES is assumed to have thermal conductivity, k_{pipe}, of 0.45 W/m·K (VDI, 2001). The geometrical parameters of the BHEs are summarized in Table 4-1.

Table 4-1 1-U type borehole geometry

Parameter	Value (m)	Description
r_{bore}	0.054	Borehole radius
r_i	0.014	Pipe inner radius
r_o	0.017	Pipe outer radius
L_u	0.05	Distance between borehole

For the CAES, the round-trip cycle efficiencies for diabatic and adiabatic systems, $\eta_{RTE,d}$ and $\eta_{RTE,a}$, introduced with the equations (3-17) and (3-18), are selected as performance criteria, whereas for the BTES, the total length of the borehole, L_{total}, and the depth of each borehole, H, are considered. These

criteria for the BTES significantly affect the drilling cost, which accounts for most of the system's construction cost.

4.2 Results and Discussion for CAES

The results of the parametric study conducted with the CAES model are presented in this subchapter. For these results, the various ranges of the parameters are selected, as summarized in Table 4-2.

Table 4-2 Ranges of parameters considered for the CAES

Symbol	Unit	Minimum	Maximum	Increment	Base
$T_{e,1}^{in}$	K	373.15	873.15	20	623.15
T_{env}	K	283.15	323.15	2	303.15
N_e	-	1	6	1	3
N_c	-	1	6	1	3
T_s	K	293.15	873.15	20	373.15
p_s	bar	10	1000	20	500

For the parametric study, each parameter's effect on the system's performance is assessed separately. For the assessment of a single parameter, the other parameters are set to equal to the values shown in the "Base" column of Table 4-2.

4.2.1 Influence of Inlet Temperature for the 1st Expansion Stage

The first parameter considered in the study is $T_{e,1}^{in}$, for a range *between* 373.15 K and 873.15 K (100 °C to 600 °C). The upper bound for $T_{e,1}^{in}$ is selected similar to the maximum air temperature achieved within the existing Huntorf plant in Germany for protecting the machinery of the CAES system (Meng *et al.*, 2018). With the base parameters outlined in Table 4-2, Q_{rel} of 1.0 MW and $\dot{m}_c$ of 1.1 kg/s are determined for the compression side of the system, leading to the charging time, t_{charge}, to be 12 hours, and storage volume, V_s, to be 105 m^3.

The influence of $T_{e,1}^{in}$ on $\eta_{RTE,d}$ and $\eta_{RTE,a}$ on the CAES system are shown in Figure 4-1. As shown in the figure, it is clear that a greater difference between $T_{e,1}^{in}$ and T_s leads to a better RTE. The result can be interpreted with the Laws of Thermodynamics, as the increased temperature leads to greater enthalpy

difference at the inlet and outlet of the first expansion stage. Having a high inlet temperature means a greater expansion thermal energy requirement before the inlet. However, with increased inlet temperature for the expansion, it is possible to operate the expansion train with low mass flow rate, smaller storage volume and shorter charging time, which all contribute to an increase in RTE. As shown in Figure 4-1, the maximum $\eta_{RTE,d}$ and $\eta_{RTE,a}$ are determined to be 35% and 59%, respectively.

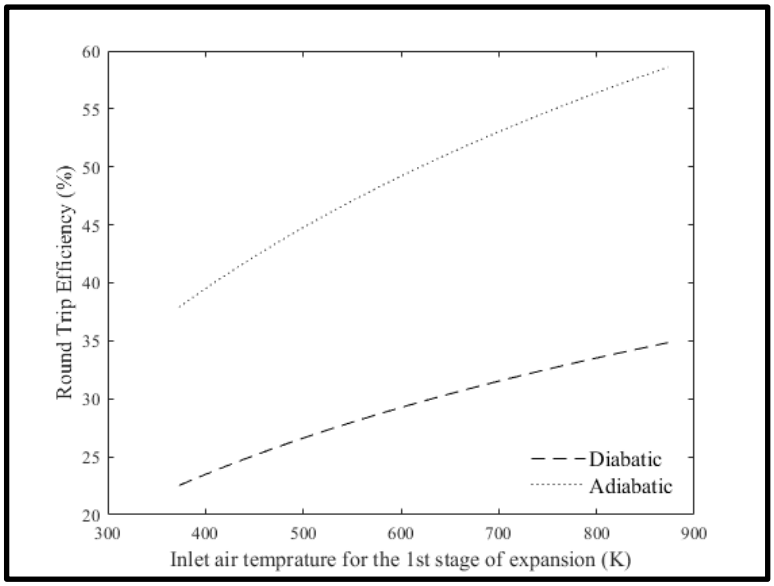

Figure 4-1 Influence of $T_{e,1}^{in}$ on Round Trip Efficiency (RTE) of the CAES system

Figure 4-2 presents the relationship between Q_{req} and $T_{e,1}^{in}$. The line on the plot labelled as "additional heat from external sources" is the difference between Q_{req} and Q_{rel}. This plot indicates that additional thermal energy must be added for the system at this scale to achieve the maximum $\eta_{RTE,a}$, shown in Figure 4-1. In order to avoid the need for the additional thermal energy for the expansion to design a fully adiabatic system, the ratio of the input and output power has to be adjusted appropriately.

According to a simple iterative calculation conducted with the model developed in this study, considering P_c approximately 1.5 to 2 times greater than P_e eliminated the demand for the additional thermal energy for expansion. Notably, the adjustment has resulted in a 5 – 20% increase in $\eta_{RTE,a}$, because of the shortened t_{charge} and increased Q_{rel}.

Figure 4-3 presents the influence of $T_{e,1}^{in}$ on $\dot{m}_e$ and V_s. As shown in the figure, a more significant difference between the inlet temperature and storage temperature results in lower $\dot{m}_e$. V_s is determined with $\dot{m}_e$ and pre-defined $t_{discharge}$ of 8 hours. With $\dot{m}_e$ shown in Figure 4-3 and the other operating

parameters considered in the analysis, an adequate expansion machine type can be selected. In this case, reciprocating multi-stage expanders may be the most suitable as they can accommodate the determined range of $\dot{m}_e$, and the expansion pressure ratio.

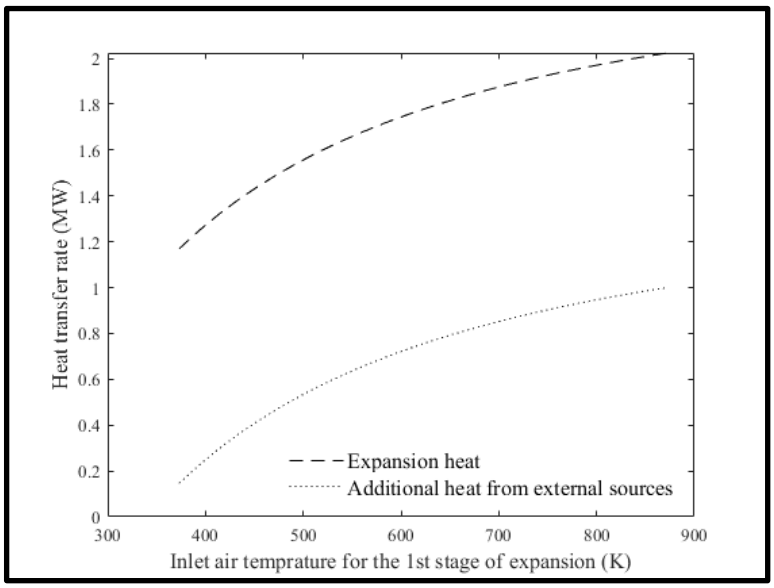

Figure 4-2 Influence of $T_{e,1}^{in}$ on expansion heat requirement of the CAES system

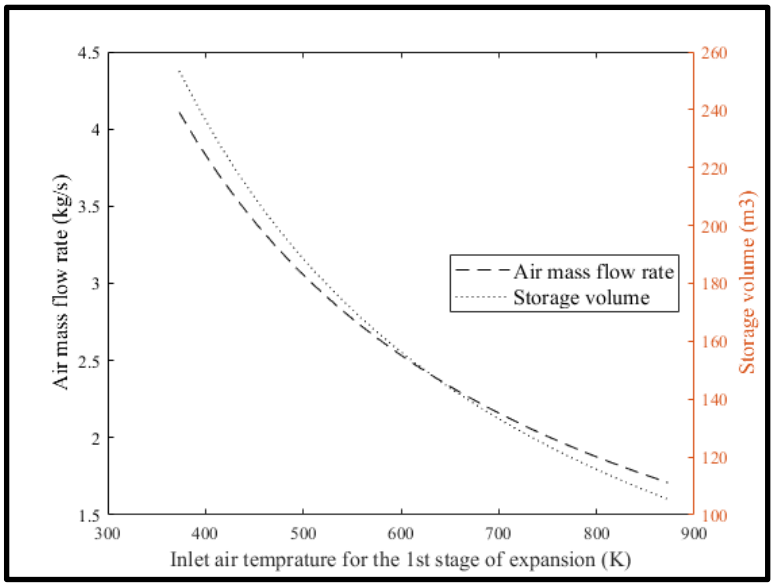

Figure 4-3 Influence of $T_{e,1}^{in}$ on air mass flow rate and storage volume on the expansion side of the CAES system

4.2.2 Influence of Environment Temperature

The second parameter considered is T_{env}. With the base parameters shown in Table 4-2, $\dot{m}_e$ is determined to be 2.4 kg/s, and Q_{req} is calculated as 1.8 MW on the expansion side of the system. V_s is calculated as 150.3 m^3. Figure 4-4 presents the impact of T_{env} on $\eta_{RTE,d}$ and $\eta_{RTE,a}$. As depicted in Figure 4-4, increasing T_{env} can lower $\eta_{RTE,d}$ and $\eta_{RTE,a}$. However, the degree of its impact is inconsequential, as the range of variation for this case is only 1 – 2%. $T_{env}{}'s$ Influence on Q_{rel} is also minimal, as shown in Figure 4-5.

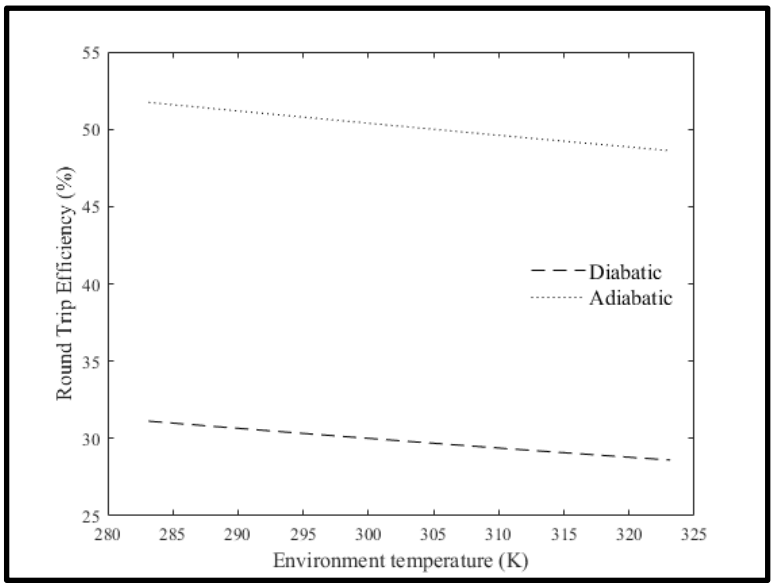

Figure 4-4 Influence of T_{env} on Round Trip Efficiency (RTE) of the CAES system

T_{env} has more noticeable impacts on $\dot{m}_c$ and $\dot{m}_{cw}$, as shown in Figure 4-6 and 4-7, respectively. The higher T_{env}, the longer heat exchange duration between the compressed air and the working fluid is required, as it is equal to the inlet temperature for the 1st stage of compression $T_{c,1}^{in}$. As a result of the increased T_{env}, $\dot{m}_c$ and $\dot{m}_{cw}$, are reduced, and t_{charge} is increased. Note that in Figure 4-7, a "cusp" can be observed from the line. The cusp signifies that after the 1st compression stage, the temperature of 320 °C is achieved by the compressed air that is at the boiling point of Therminol™. To accommodate this, 320 °C is considered as the fixed working fluid temperature for the scenarios, where T_{env} is less than about 290 K.

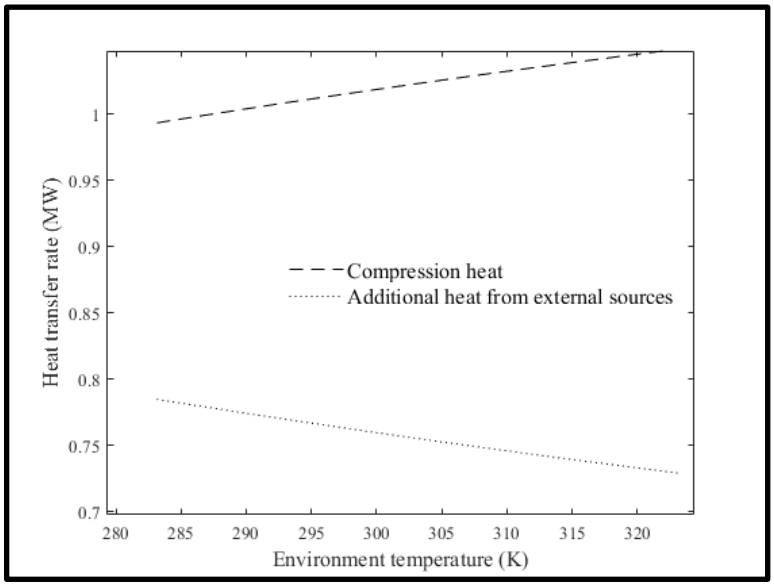

Figure 4-5 Influence of T_{env} on compression heat released of the CAES system

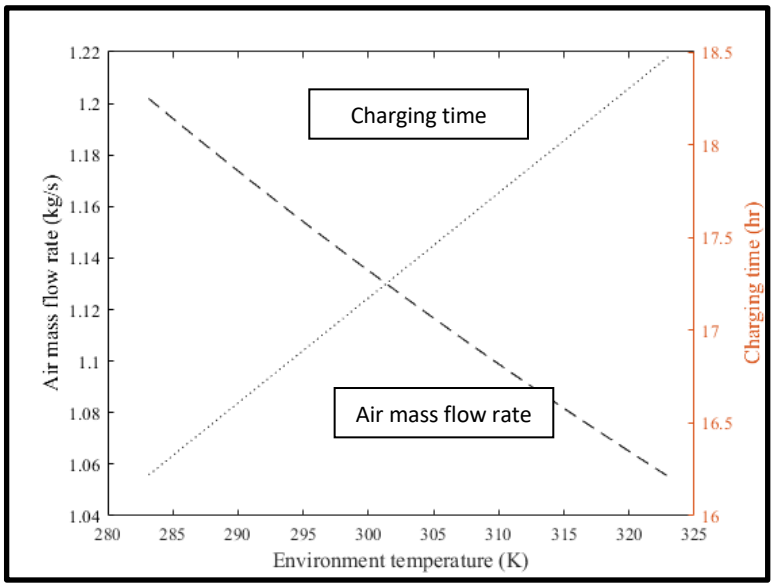

Figure 4-6 Influence of T_{env} on air mass flow rate on the compression side and charging time of the CAES system

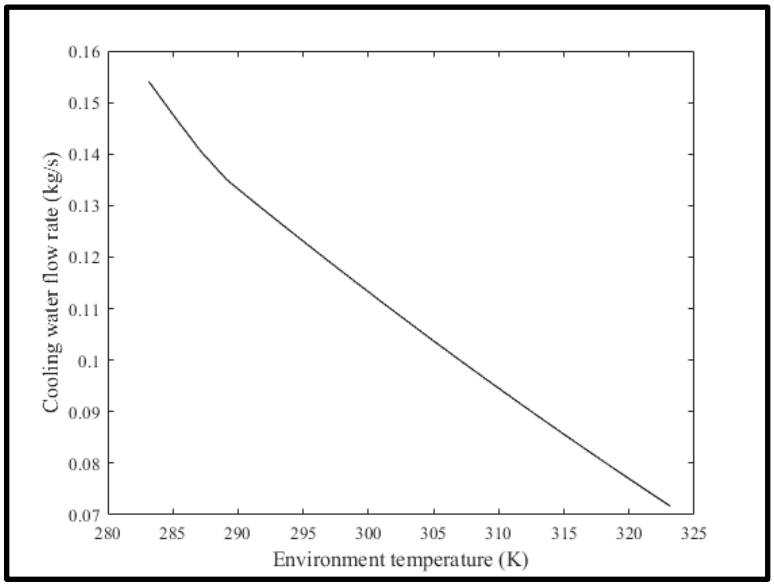

Figure 4-7 Influence of T_{env} on cooling water mass flow rate of the CAES system

4.2.3 Influence of Number of Compression and Expansion Stage

For the parametric study conducted for N_c, $\dot{m}_e$ of 2.4 kg/s, Q_{req} of 1.8 MW, and V_s of 150.3 m^3 are calculated with the base parameters from Table 4-2. Referring to Figure 4-8, increasing N_c from one to three has resulted in an increase of $\eta_{RTE,d}$ and $\eta_{RTE,a}$, by approximately 10% and 20%, respectively. However, $\eta_{RTE,d}$ and $\eta_{RTE,a}$ have improved by less than 5% when $N_c$is increased from three to six. This result is driven by a combination effect caused by the changes in Q_{rel} (Figure 4-9) and $\dot{m}_c$ (Figure 4-10). When more compression stages are considered, the pressure ratio for each stage can be reduced, resulting in a lower temperature rise for each stage. As a result, the amount of thermal energy required to be removed from the compressed air by the working fluid, and the duration of this heat exchange process can be reduced. Therefore, a system with more compression stages can utilize more energy to shorten t_{charge} by increasing both $\dot{m}_c$ and $\dot{m}_{cw}$ (Figure 4-11) to increase $\eta_{RTE,d}$ and $\eta_{RTE,a}$.

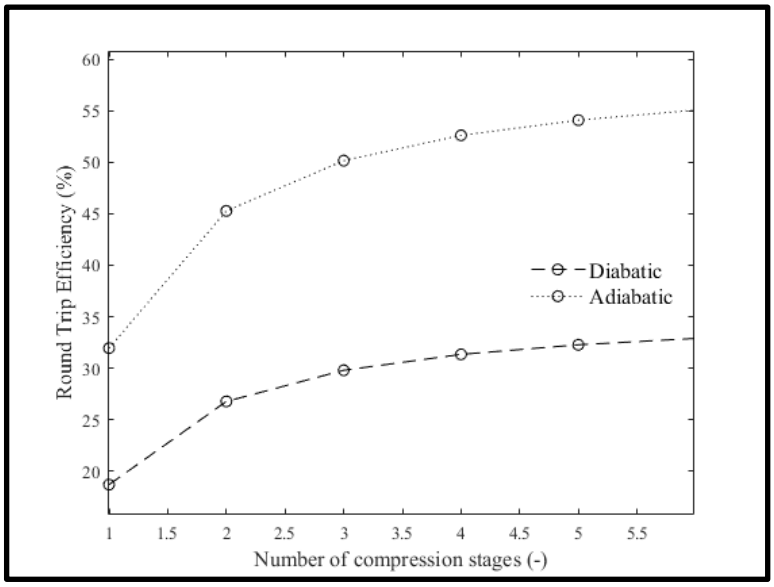

Figure 4-8 Influence of N_c on Round Trip Efficiency (RTE) of the CAES system

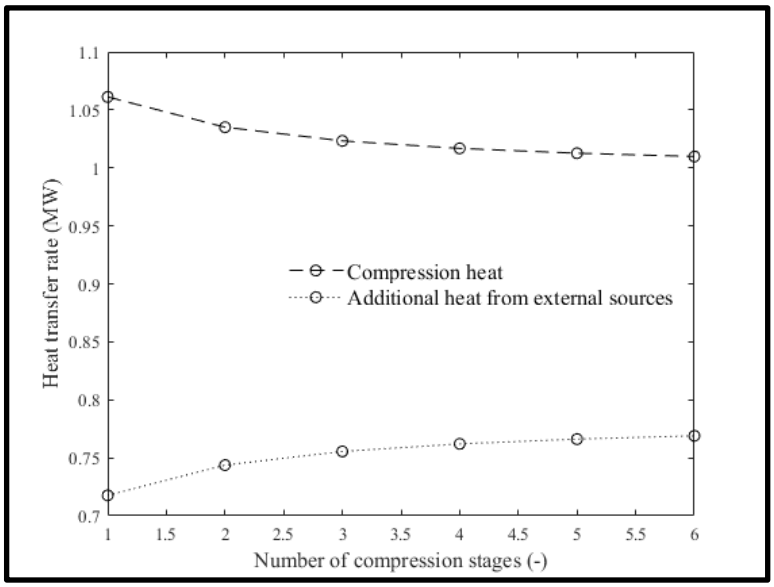

Figure 4-9 Influence of N_c on compression heat released in the CAES system

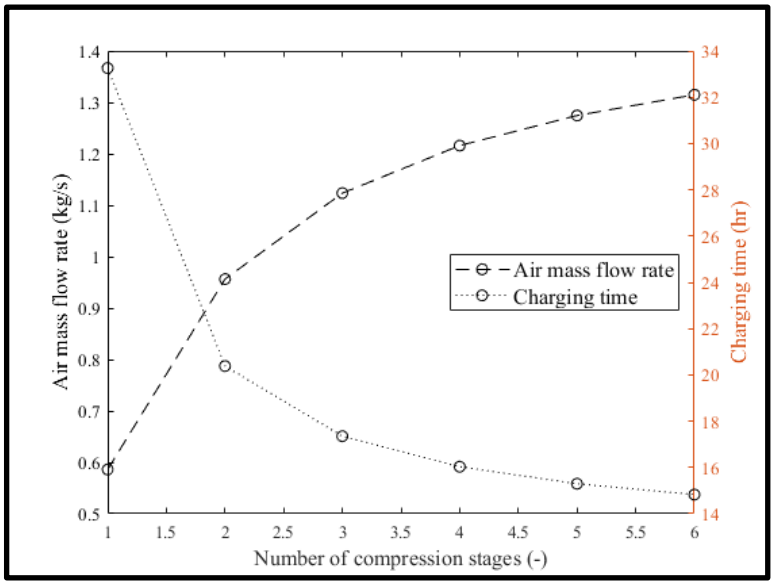

Figure 4-10 Influence of N_c on air mass flow rate on the compression side and charging time of the CAES system

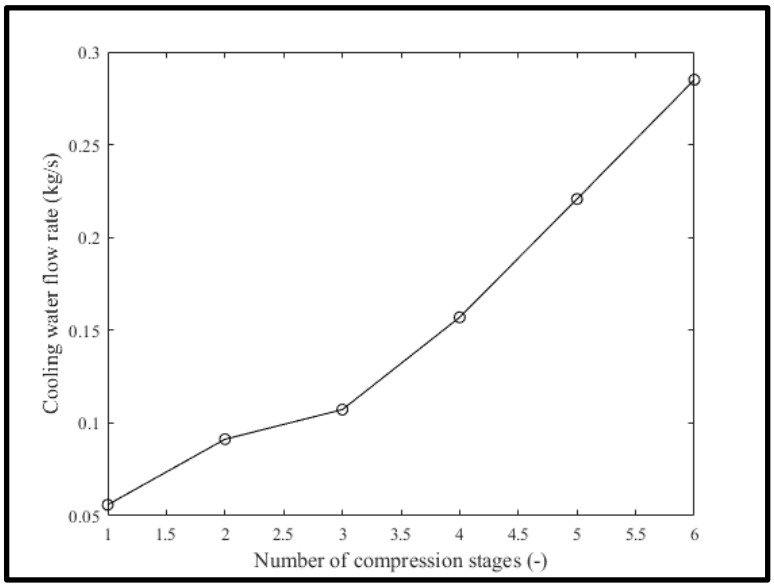

Figure 4-11 Influence of N_c on cooling water mass flow rate of the CAES system

$\dot{m}_c$ of 1.1 kg/s, $\dot{m}_{cw}$ of 0.1 kg/s, and Q_{rel} of 1.0 MW are calculated with the base parameters in Table 4-2 for the analysis on the influence of N_e. Having multiple expansion stages improves $\eta_{RTE,d}$ and $\eta_{RTE,a}$, due to the effects similar to that of having multiple compression stages. As shown in Figure 4-12, for a system with one stage of expansion, $\eta_{RTE,d}$ and $\eta_{RTE,a}$ are approximately 24% and 40%, respectively. However, when more than three expansion stages are considered, $\eta_{RTE,d}$ and $\eta_{RTE,a}$ are improved by 5%

and 13%. The effect of having N_e more than three presents an insignificant improvement on the efficiency, similar to the observation made for N_e.

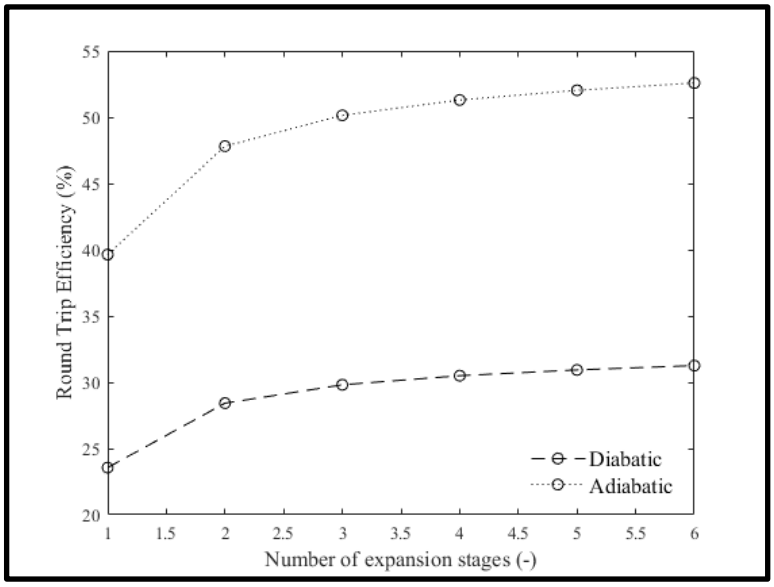

Figure 4-12 Influence of N_e on Round Trip Efficiency (RTE) of the CAES system

Influence of N_e on $Q_{req,}\dot{m}_e$ and V_s can be found in Figure 4-13 and Figure 4-14. These figures show that having multiple expansion stages requires higher Q_{req}, because of the increased number of interheaters in the system. Nevertheless, a high efficiency can still be achieved, as a system with more expansion stages can operate with lower $\dot{m}_e$ and reduced V_s requirement. Consequently, this can save energy input for the compression side of the system, which directly influences the round-trip efficiency.

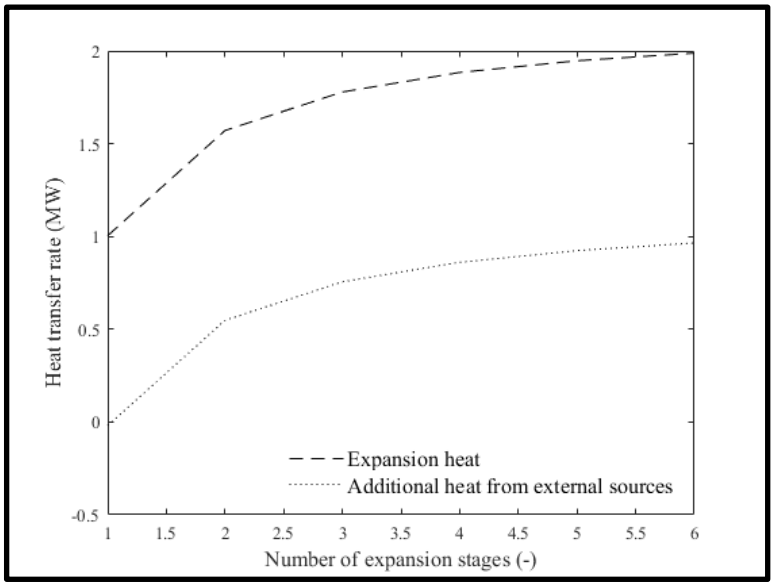

Figure 4-13 Influence of N_e required expansion heat of the CAES system

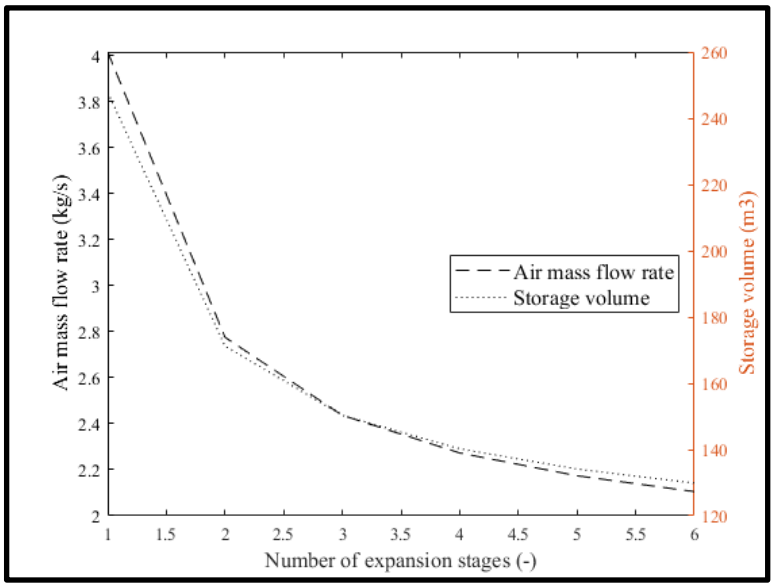

Figure 4-14 Influence of N_e on air mass flow rate and storage volume on the expansion side of the CAES system

4.2.4 Influence of Storage Temperature and Pressure

The last two parameters that are considered for the parametric study are T_s. and p_s. First, T_s is set to range from 20 ºC to 600 ºC (293.15 K to 873.15 K). With the base parameters shown in Table 4-2, $\dot{m}_c$ and $\dot{m}_e$ are calculated to be 1.1 kg/s and 2.4 kg/s, respectively.

As shown in Figure 4-15, T_s has a more significant influence on $\eta_{RTE,d}$ than on $\eta_{RTE,a}$. For dCAES, a high T_s minimizes the amount of heat of compression that has to be removed for the storage, as well as Q_{req}, as shown in Figure 4-16. However, for aCAES, it reduces the potential of utilizing the heat of compression. Therefore, increasing T_s does not have a significant effect on $\eta_{RTE,a}$.

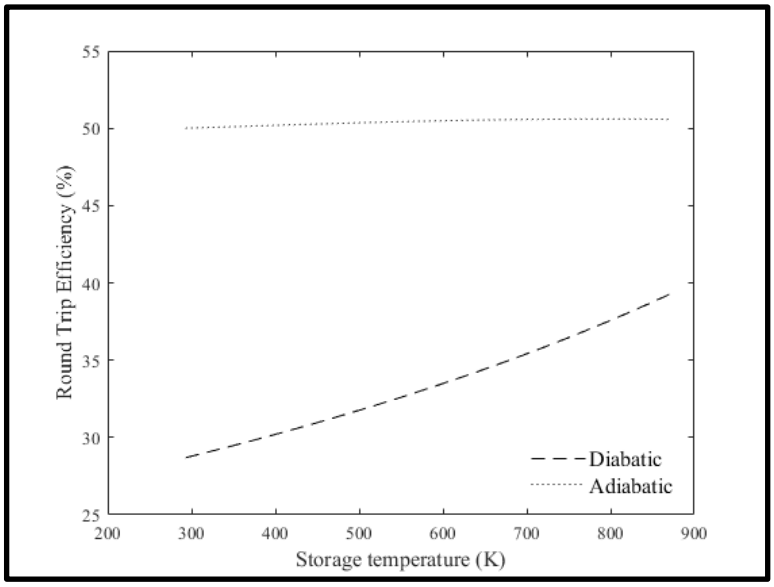

Figure 4-15 Influence of T_s on Round Trip Efficiency (RTE) of the CAES system

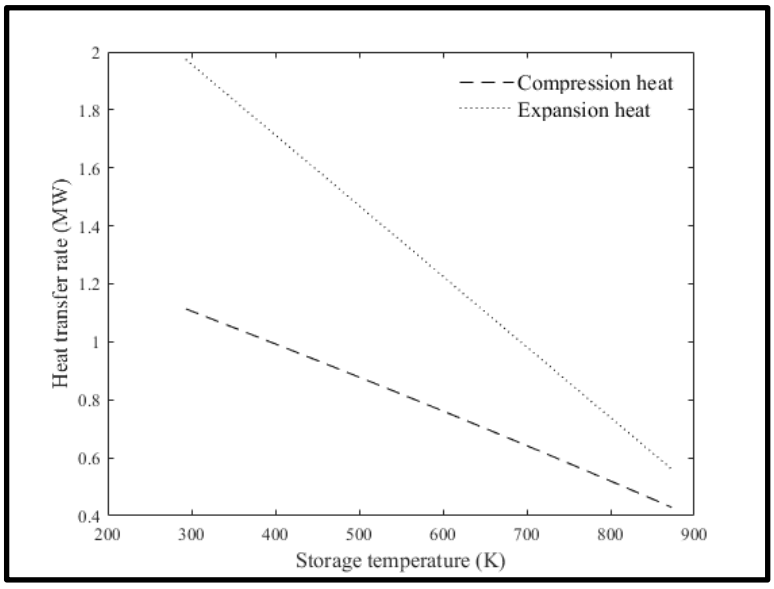

Figure 4-16 Influence of T_s on heat transfer rate of the CAES system

Despite the high potential efficiency, a dCAES system that operates with high air temperature is considered not feasible. Such a system requires either a large V_s or a high-pressure vessel that can withstand high temperature, as evident in Figure 4-17, which may not be cost-effective.

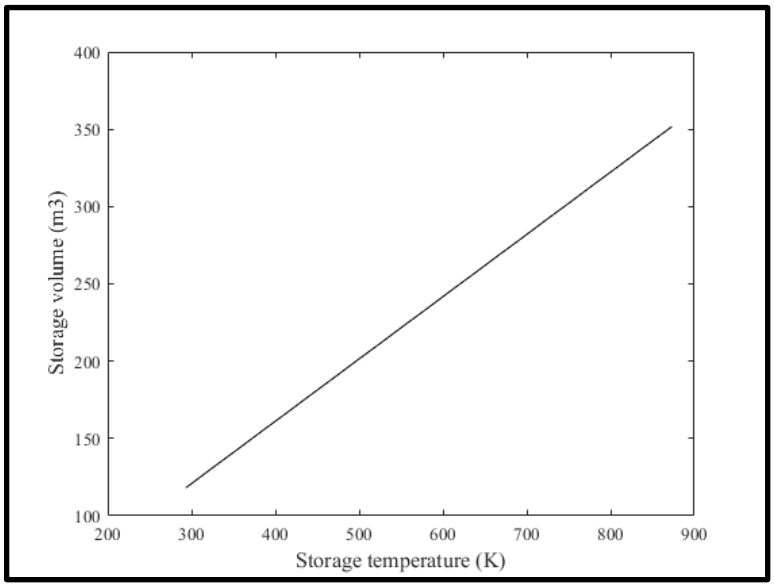

Figure 4-17 Influence of T_s on storage volume of the CAES system

As shown in Figure 4-18 and 4-19 p_s does not strongly affect the performance of CAES systems. However, p_s demonstrates a substantial influence on V_s, more than T_s. For instance, when p_s is set to be less than 100 bar (10 MPa), the system requires V_S greater than 1,000 m^3. As shown in Figure 4-20, when p_s is set to be greater than 100 bar, the required storage volume quickly becomes less than 800 m^3. At p_s of 1,000 bar (100 MPa), the required volume is significantly reduced to approximately 70 m^3.

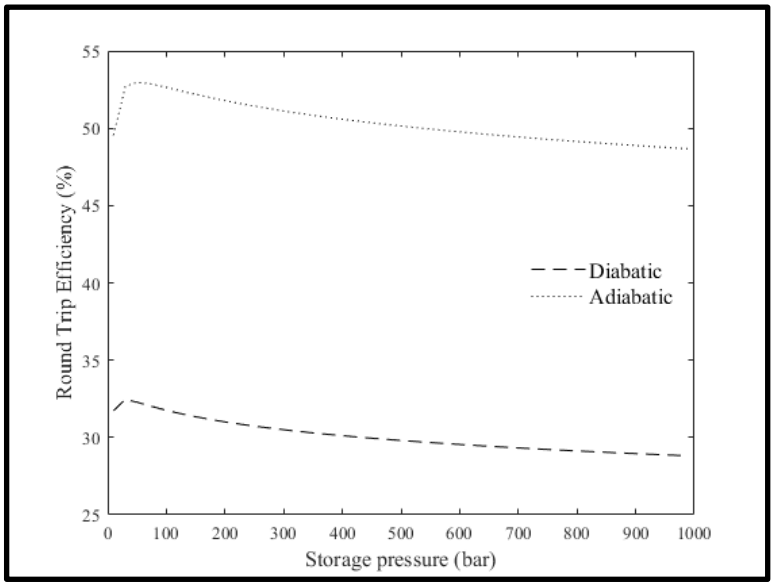

Figure 4-18 Influence of p_s on Round Trip Efficiency (RTE) of the CAES system

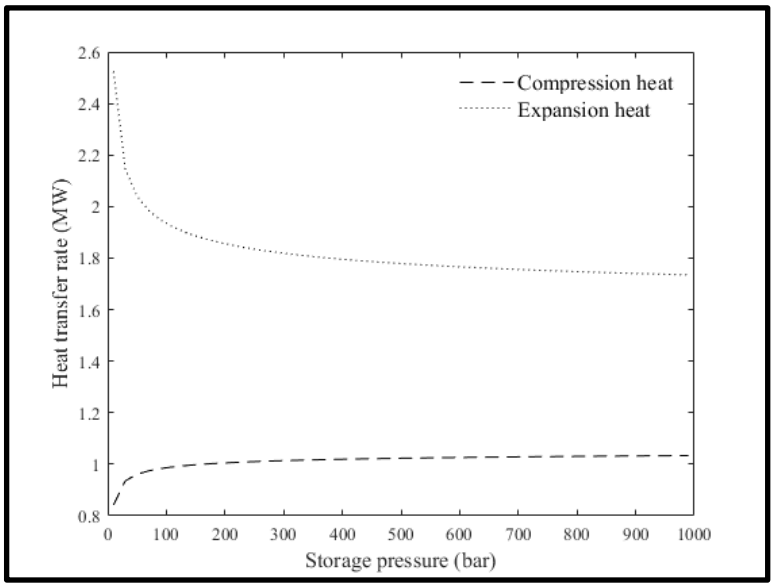

Figure 4-19 Influence of p_s on heat transfer rate of the CAES system

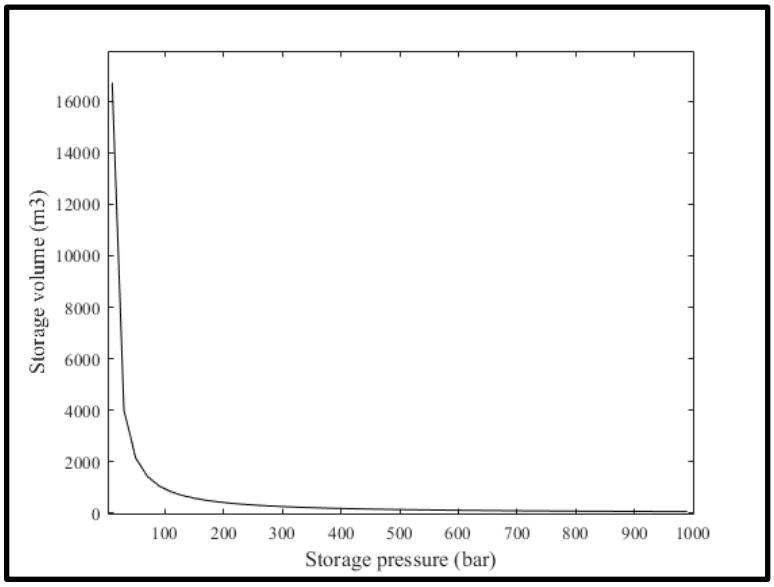

Figure 4-20 Influence of p_s on storage volume of the CAES system

4.3 Results and Discussion for BTES

For the analysis of the performance of the BTES, three types of parameters are considered, including the parameters related to the borefield configuration, borehole thermal properties, and the ground/rock thermal properties and the condition. Table 4-3 summarizes the ranges of the parameters considered in the study.

Table 4-3 Ranges of parameters considered for BTES

Symbol	Unit	Minimum	Maximum	Increment	Base
B	m	0.5	10	0.1	5
k_{ground}	W/m·K	0.5	8	0.5	3
α_{ground}	m^2/day	0.025	0.2	0.01	0.1
k_{grout}	W/m·K	0.2	2.5	0.1	1

Aside from the geometry of boreholes presented in Table 3-1, the parameters that are considered be constant are summarized in Table 4-4.

Table 4-4 Constant parameters considered for BTES

Parameter	Symbol	Unit	Value
Cooling water thermal heat capacity	$C_{p,f}$	J/kg·K	4000
Cooling water mass flow rate per kW	$m_{cw,kw}$	kg/s·kW	0.05
COP of heat pump	COP_{hp}	-	5
Thermal conductivity of pipe	k_{pipe}	W/m·K	0.45
Internal convection between pipes	h_{conv}	$W/m^2 \cdot K$	1000
Undisturbed ground temperature	T_g	^oC	20

Note that for the parametric study of the BTES system, q_y, q_m and q_h are assumed to be 1 MW, and the fluid inlet temperature, T_{in}, to be 80 ^oC.

4.3.1 Influence of Borehole Spacing

The first parameter that is considered for the BTES system is spacing between BHE, *B*. Figure 4-21 presents the relationship between *B* and the total length of pipes in a borefield, *L*. As shown in the figure, *L* requirement reduces with the greater B between BHEs. The main contributing factor this observation is the proportional relationship between B and the temperature penalty due to the thermal interactions between adjacent BHEs, T_P.

The influence of T_p on the system is more explicitly shown in Figure 4-22, which presents the influence of *B* on the number of boreholes required, *NB*, and borehole depth, *H*. For instance, for *B* at 3 m, about 140 boreholes at 60 m depth are required. However, when *B* is increased to 10 m, a smaller *NB* is required, but *H* for the BHEs has to be increased (i.e., $H = 200$ m, $NB = 40$) to operate the BTES at the same level of performance. The results are possible as longer BHEs can store more thermal energy in the storage medium, whereas shorter BHEs require more BHEs to store the same amount. However, the thermal front in the surrounding ground of the longer BHEs can propagate radially at a faster rate, so the undesired thermal interfaces between the BHEs are more probable. The risk is mitigated by increasing *B*. Therefore, to evaluate the best configurations of BTES further, additional other constraints such as surface area availability and financial budget must be considered.

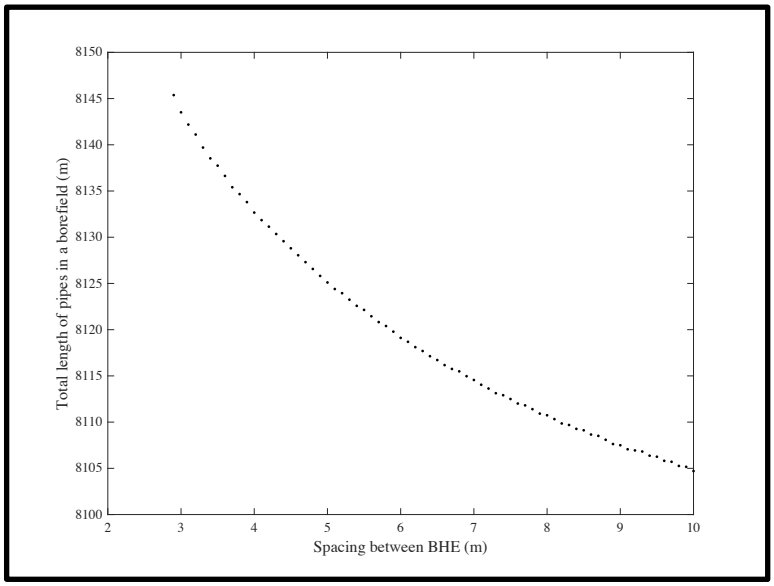

Figure 4-21 Influence of *B* on total length of pipes in a borefield of the BTES system

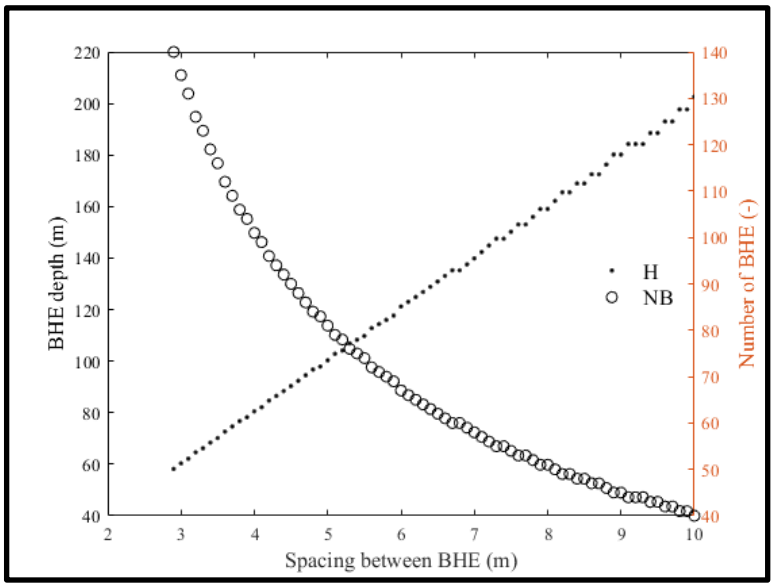

Figure 4-22 Influence of B on number and depth of boreholes of the BTES system

4.3.2 Influence of Ground Thermal Conductivity and Thermal Diffusivity

As shown in Figure 4-23, ground thermal conductivity, k_{ground}, has a critical influence on the overall performance of the BTES system, represented by L_{total}. For k_{ground} at 2 W/m·k, approximately 11,000 m of pipe is required, but for k_{ground} at 4 W/m·k, approximately 7,000 m of a pipe is required. A higher k_{ground} has enabled the model to design BTES system without increasing H and calculated the optimized H to be

approximately 100 m. Therefore, the plot shown in Figure 4-24 describing the relationship between k_{ground} and *NB* displays a similar trend as the plot in Figure 4-23.

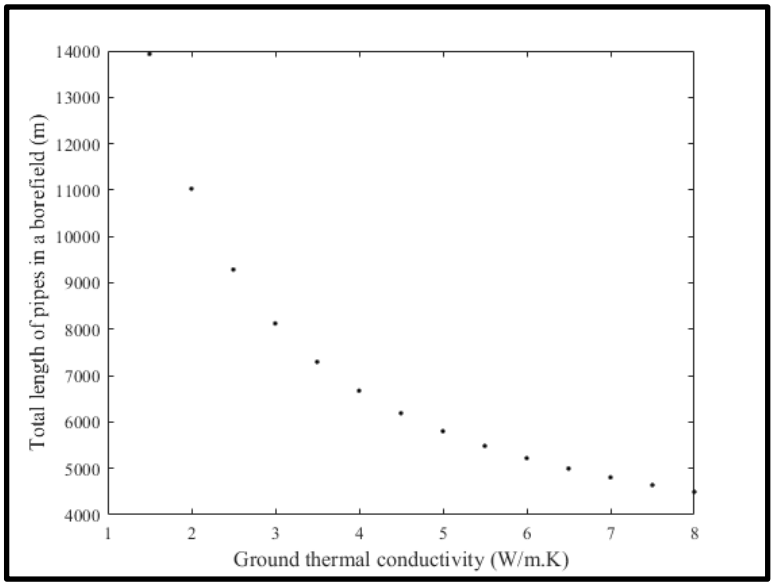

Figure 4-23 Influence of k_{ground} on total length of pipes in a borefield of the BTES system

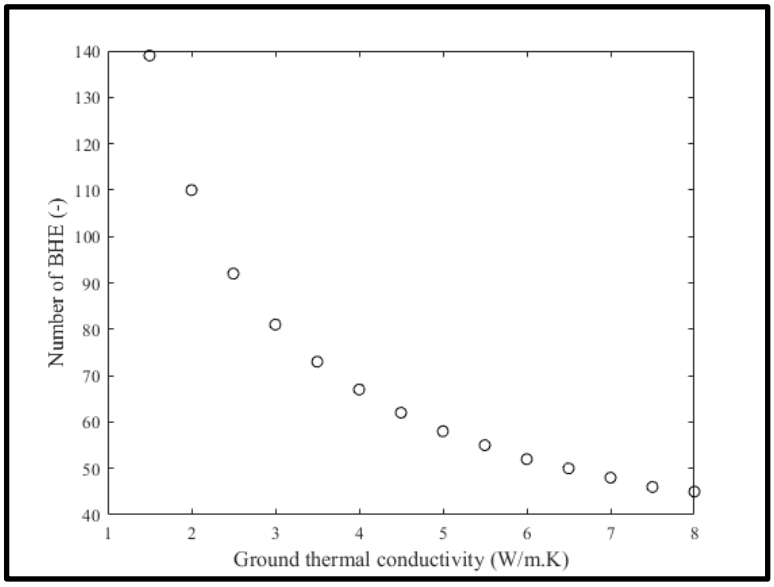

Figure 4-24 Influence of k_{ground} on number of boreholes in a borefield of the BTES system

The impact of the ground thermal diffusivity, $a_{ground,}$ on *L* is similar to that of k_{ground}, as shown in Figure 4-25. For ground with higher a_{ground}, a longer length of pipe is required for the BTES, as the thermal energy dissipates away to the far field quicker.

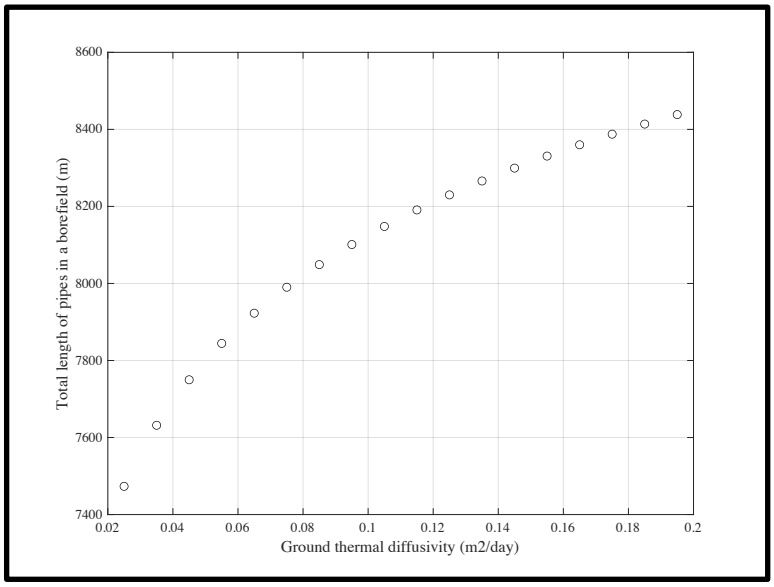

Figure 4-25 Influence of a_{ground} on total length of pipes in a borefield of the BTES system

4.3.3 Influence of Grout Thermal Conductivity

Another significant parameter to be considered is the grout thermal conductivity, k_{grout}. The influence of k_{grout} on L_{total} is presented in Figure 4-26. As shown in the figure, installation of BHEs with higher thermal conductivity cement is more effective in saving the overall cost of BTES system. Hence, greater k_{grout} is desired to enhance heat exchange process between the circulating fluid and the surrounding ground.

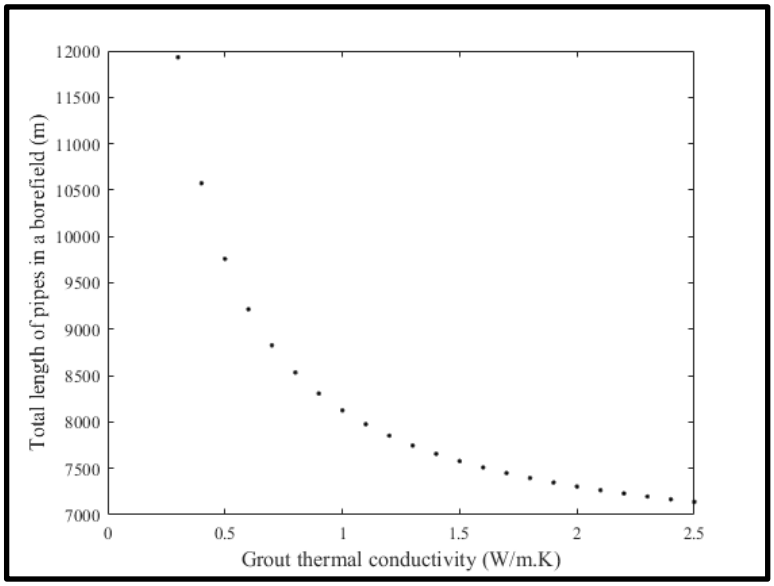

Figure 4-26 Influence of k_{grout} on total length of pipes in a borefield of the BTES system

4.4 Summary of the Parametric Study

In Chapter 4 of this thesis, the method and results of the parametric study were presented. The parametric study was conducted with the models introduced in Chapter 3 to determine the key operating parameters and evaluate the integrated CAES-BTES under different operating scenarios. For this study, a hypothetic integrated CAES-BTES system with an output power of 1.5 MW was assumed, and it undergoes a continuous daily cycle with 8 hours of discharge. The effects of the selected parameters on the performance of the CAES system were studied. The selected parameters included inlet temperature for the 1st stage of expansion, environment temperature, number of expansion stages, number of compression stages, storage temperature, and storage pressure. According to the parametric study results, the number of compression-expansion stages and the inlet temperature for the 1st stage of expansion greatly influence the round-trip efficiency of the integrated system. For instance, the round-trip efficiency increased up to 25% for having six compression-expansion stages compared to having a single stage. The statement is also true for the range of the inlet temperature for the 1st stage of expansion considered in this study, from 373.15 K to 873.15 K (100 ^{o}C to 600 ^{o}C). The study suggests that minimizing heat loss from the compression side of the system, adding more thermal energy for air expansion, and lowering air mass flow rate on the expansion side greatly influence the round-trip efficiency of the system. The storage pressure does not directly influence the round-trip efficiency, but it governs the storage volume requirement. Hence, it is strategic to operate the system with high storage pressure to reduce its construction cost.

For the BTES side of the integrated system, the spacing between boreholes, ground thermal conductivity and thermal diffusivity, and grout thermal conductivity are considered for the parametric study. As the results suggest, the higher thermal conductivities of a storage medium of BTES and grout material are desired conditions for the BTES. The study also presents that a storage medium with high thermal diffusivity is not desired as the thermal energy dissipates away to the far-field quicker.

Chapter 5: Levelized Cost of Storage (LCOS) and CAES-BTES System

5.1 Background on LCOS

As discussed in Chapter 1, various types of Energy Storage Systems (ESS) are available for integration with renewable power generation to overcome limitations associated with their intermittent nature. Each ESS system has its advantages and disadvantages, and its suitability varies based on the technical requirements, configuration, and scale of the power generation system. The economics of ESS often drives the decision on the ESS type for a particular power generation system. However, because of technical diversity and differences in application, the cost comparison among ESS technologies is challenging. For enabling a comprehensive comparison between the available technologies, a Levelized Cost of Storage (LCOS) is calculated for ESS technologies (Jülch, 2016).

The objective of the LCOS analysis is to quantify the discounted cost per unit of discharged electricity for specific storage technology and application (Schmidt *et al*., 2019). For determining the LCOS of a specific storage technology, the investment costs, production cost, and operation and maintenance (O&M) cost projected throughout the lifetime of the energy storage technology are considered (Lotfi *et al.,* 2016). The sum of the net present value of the aforementioned costs over the lifetime is divided by the total energy produced to calculate the LCOS.

Although the main concept of the LCOS analysis is to evaluate and compare the performance of various ESS technologies, it has several limitations. First, due to the lack of a common LCOS method (Schmidt *et al.,* 2019), the inputs to LCOS are decided by the estimator. This causes some discrepancies among the proposed LCOS studies, as they neglect or consider cost parameters, such as replacement and disposal costs, and performance-related parameters, such as capacity degradation (Schmidt *et al.,* 2019). The LCOS comparison results can vary by taking different input parameters as each parameter has different impacts on different storage technologies. For instance, relatively higher disposal and recycling costs can increase the LCOS of battery technologies more significantly than other types of ESS. The subjectivity of

the estimator can also cause discrepancies in projecting the future costs of ESS technologies (Schmidt *et al.,* 2019). The total costs of the ESS technologies are often projected to fall continuously due to technological development. However, there still exists uncertainty regarding the magnitude of the projected cost reduction, as calibrating a predictive model to past history is inappropriate if technological "breakthroughs" characterize the cost-time series. Another factor that is often overlooked in proposed LCOS methods is the indirect cost of ESS technologies, such as environmental impacts and curtailment effects (Hwang *et al.,* 2019). For applying and interpreting the LCOS of ESS, the limitations of the method should be deeply understood for better communications to take place.

5.2 Review of LCOS Method

The writer has selected the LCOS method proposed by Jülch (2016). With Jülch's method, the LCOS of the integrated CAES-BTES system is determined and compared with the diabatic and adiabatic CAES configurations to demonstrate its relative competitiveness and economic feasibility. Jülch's LCOS method is reviewed in this chapter.

Jülch (2016) has estimated LCOS for various ESS options, including PHS, CAES, battery technologies, and power-to-gas (PtG) systems, with the method outlined in her published work. The author suggests that this approach can provide a broader and comparable overview of the cost of ESS technologies compared to the profitability analysis focusing on a single ESS technology under specific conditions. The LCOS is expressed in the unit of the discounted cost of electricity per unit of discharged electricity. For each technology, the LCOS is studied based on the data collected from the literature. This study emphasizes the system configuration, and the detailed cost of each charging, discharging, and storage unit of each technology are analyzed. The LCOS is calculated with the equation shown below:

$$\mathrm{LCOS} = \frac{\mathrm{CAPEX} + \sum_{t=1}^{t=n} \frac{A_t}{(1+i)^t}}{\sum_{t=1}^{t=n} \frac{W_{out}}{(1+i)^t}} \tag{5-1}$$

where *CAPEX* is the capital expenditure, A_t is annual cost of the storage system at each point of time *t*, *n* is the lifetime of the storage, *i* is the discounted interest rate, and W_{out} is the energy output. A_t can be expressed as below:

$$\mathrm{A_t} = OPEX_t + CAPEX_{re,t} + c_{el} W_{in} - R_t \tag{5-2}$$

where $OPEX_t$ is the operation cost, $CAPEX_{re,t}$ is the reinvestments in storage system components, c is the cost of electricity supply, W_{in} is the annual electricity input, and R is the end of the storage life time recovery value. For batteries, the average energy output is considered, in order to accommodate their decreasing storage capacity over time.

For batteries, the net capacity, C_{net}, is considered, and it is calculated as below:

$$\mathrm{C_{net}} = C_r * DoD \tag{5-3}$$

where C_r is the rated capacity and DoD is the depth of discharge, which is defined as the percentage the storage option is typically discharged without harming the system's functionality.

The annual electricity output W_{out} is calculated by considering the power output of the discharging unit, P_{out} and the full load hours, FLH as below:

$$\mathrm{W_{out}} = P_{out} * FLH \tag{5-4}$$

where FLH can be determined with the following two expressions below:

$$\mathrm{cyc} = \frac{\mathrm{FLH}}{t_{out}} \tag{5-5}$$

$$\mathrm{t_{out}} = \frac{C_{net}}{P_{out} * \eta_{out}} \tag{5-6}$$

where t_{out} is the discharge time in a single cycle, and η_{out} is the efficiency of the output unit.

Lastly, the amount of input energy of the electricity, W_{in} can be determined with the equation below:

$$\frac{\mathrm{W_{in}}}{\eta_{in}} = W_{out} * \eta_{out} + W_{sd} \tag{5-7}$$

where W_{sd} is the amount of the energy that is self-discharged.

Based on equations (5-1) to (5-7), the LCOS for different ESS technologies are calculated. The input parameters used for the estimation are attached in Appendix B of this thesis. The detailed explanations and the sources of the data can be found in the original literature by Jülch (2016).

Long-term and short-term storage scenarios are presented in the study, where all ESS technologies are modelled with a power output capacity of 100 MW. In the long-term scenario, the discharge time is set to be 700 hours, and for the short-term scenario, the discharge time of 4 hours is considered. The discharge time is also referred to as an energy-to-power ratio. For instance, a system with 100 MW power output with 70 GWh of stored energy is equivalent to a system that can discharge for 700 hours at 100 MW power output.

For each scenario, two cases are further considered based on the technical readiness of each technology. The first case considers the technologies that were readily available in 2016, including PHS, diabatic CAES (dCAES), lead battery, Li-ion battery, and vanadium redox flow batteries (VRF). For the second case, the technologies that will be more promising by 2030, including adiabatic CAES (aCAES) and H_2 and CH_4 power-to-gas systems, are added in the analysis. The results of the analysis are shown in Figures 5-1 to 5-4. For these curves, the cost of electricity is not considered.

As shown in Figure 5-1, PSH is the most cost-efficient technology among the long-term storage options, assuming an appropriate landscape is available for its construction (a highly contentious issue in well-populated regions). However, H_2 and CH_4 power-to-gas systems have the potential to be cheaper options by 2030, as depicted in Figure 5-2. Compared to these systems, aCAES have approximately two to three times greater LCOS for one cycle or higher per year. For instance, the LCOS of the power-to-gas systems is about 0.26 – 0.55 €ct/kWh, where aCAES systems have LCOS of 2 – 4 €ct/kWh for one cycle per year operation. The other battery technologies have significantly high LCOS because of limited scalability. Jülch (2016) states that the CAPEX of battery technologies is solely dependent on fixed storage capacity. The other technologies are scalable based on the relationship between the power units (charging and discharging units) and storage capacity, as needed.

Referring to Figures 5-3 and 5-4, PHS has the lowest cost as short-term storage. At 365 cycles per year or 150 GWh of energy discharged per year, the LCOS of PHS is at 5 - 9 €ct/kWh. At the same scale, aCAES and dCAES systems have the LCOS of 7 – 11 €ct/kWh and 10 – 12 €ct/kWh. The battery technologies tend to have a greater LCOS than the mechanical ESS technologies, due to their high CAPEX and OPEX, relatively short lifetime, and low recovery value. However, with technological developments and

decreasing CAPEX, the LCOS of the battery technologies can be be expected to continue to drop slowly beyond 2030. The power-to-gas technologies have the greatest LCOS compared to mechanical ESS and battery technologies as short-term storage.

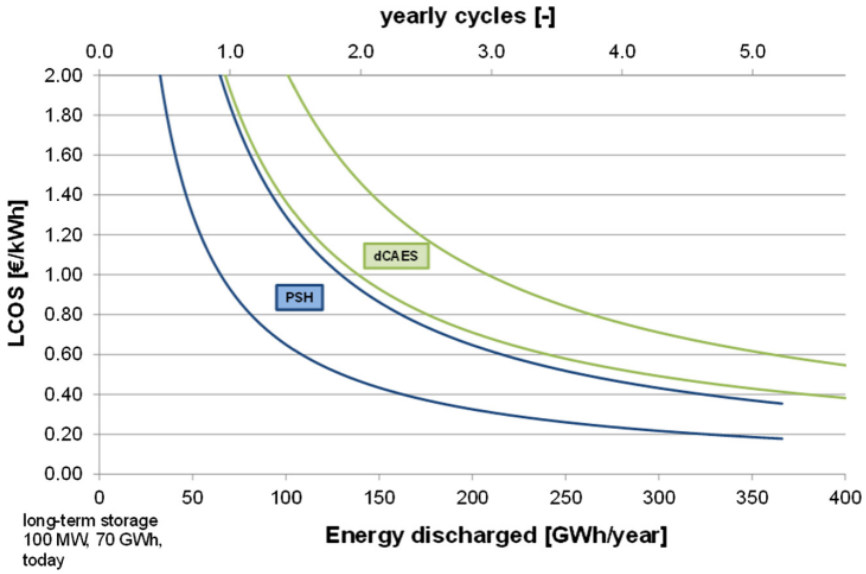

Figure 5-1 LCOS for long-term storage systems today depending on the yearly energy discharge, not including cost of electricity (Jülch, 2016)

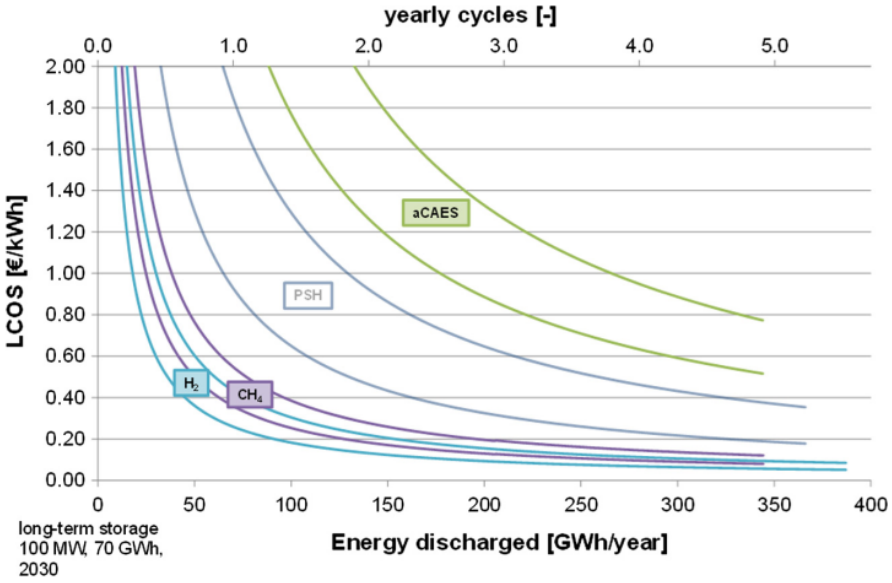

Figure 5-2 LCOS for long-term storage systems in 2030 depending on the yearly energy discharge, not including cost of electricity (Jülch, 2016)

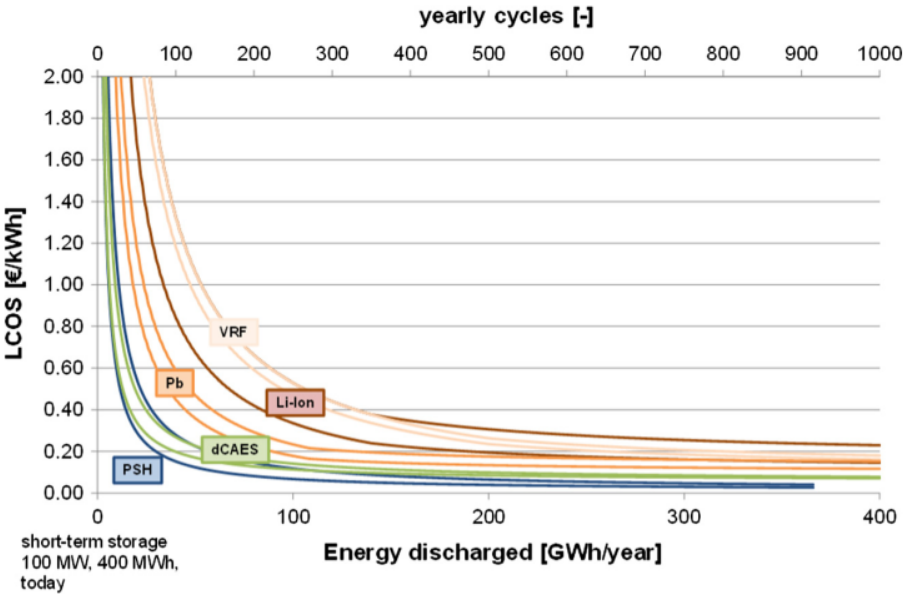

Figure 5-3 LCOS for short-term storage systems today depending on the yearly energy discharge, not including cost of electricity (Jülch, 2016)

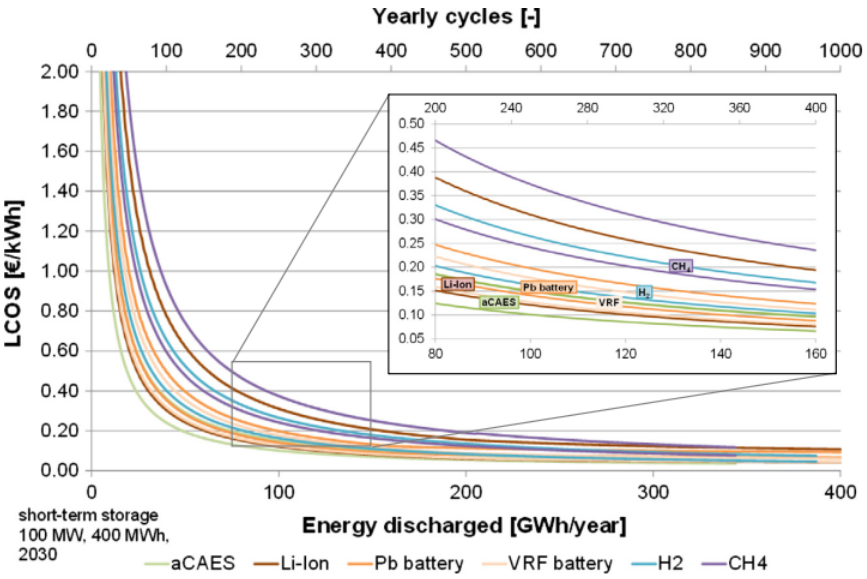

Figure 5-4 LCOS for short-term storage systems in 2030, depending on the yearly energy discharge, not including cost of electricity (Jülch, 2016)

Jülch (2016) also presents the cost breakdown of the LCOS estimated for each technology, assuming an electricity cost of 3 €ct/kWh. The study assumes one cycle per year for the long-term storage options and 365 cycles per year for the short-term storage options (i.e., one cycle per day). Figures 5-5 and 5-6

presents the cost components of the LCOS based on the assumptions for the long-term storage and short-term storage.

As shown in Figure 5-5, LCOS of PHS and CAES mainly originate from the storage unit. Hence, for the long-term application, where a large-scale storage medium is required for both PHS and CAES, the LCOS tends to be much higher than the power-to-gas system. Note that the salt cavern is considered as a storage unit for the CAES, which requires relatively expensive dissolution mining technology. For the PHS, the construction cost of the hydro dam influences the storage CAPEX. The battery technologies are not considered as a long-term storage option, due to their high CAPEX.

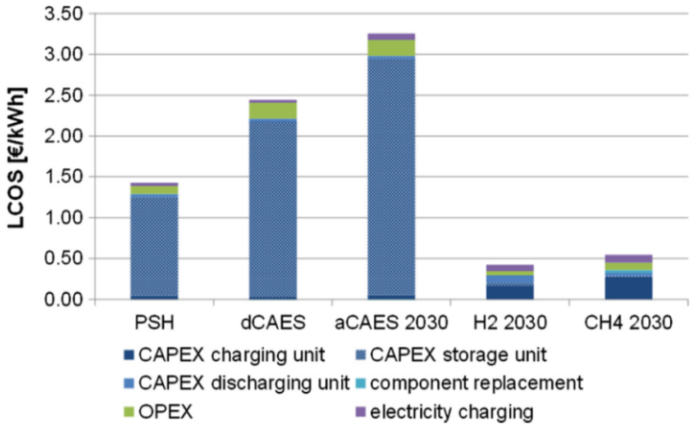

Figure 5-5 Cost components of the LCOS for the long-term storage at one cycle per year and an electricity price of 3 ct/kWh (Jülch, 2016)

Figure 5-6 compares all of the ESS technologies addressed in the study by Jülch (2016) as a short-term storage option. In this comparison, PSH, dCAES, and aCAES are the most cost-effective technologies as less storage volume is required. The battery technologies have greater LCOS compared to the three mechanical ESS technologies, because of the high cost associated with their storage unit. However, by 2030, they are expected to be at the level competitive to the mechanical ESS technologies. The projection is based on the expected improvements in their efficiency and technological developments. It is worthwhile noting that this is a projection, and if dCAES and aCAES technologies become more widely adopted, they also will experience improvements based on technical and manufacturing efficiencies.

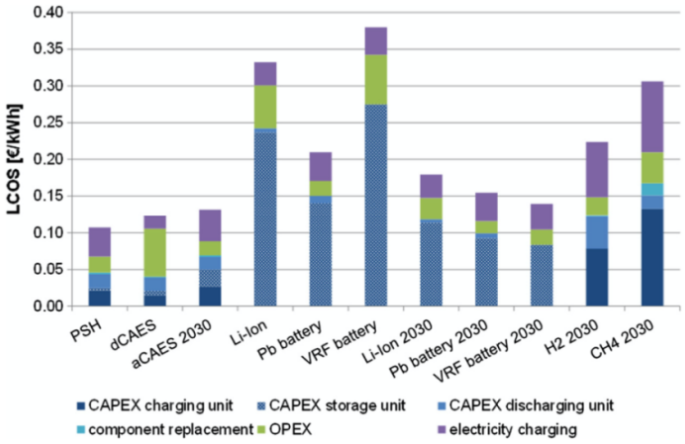

Figure 5-6 Cost components of the LCOS for the short-term storage at 365 cycles per year and an electricity price of 3 ct/kWh (Jülch, 2016)

Sensitivity analyses are conducted to determine the impact of the cost of electricity on the ESS technologies for the short-term application. As shown in Figure 5-7, dCAES is the least sensitive as it has a low dependency on electricity cost compared to the others, as it also relies on gas for power generation.

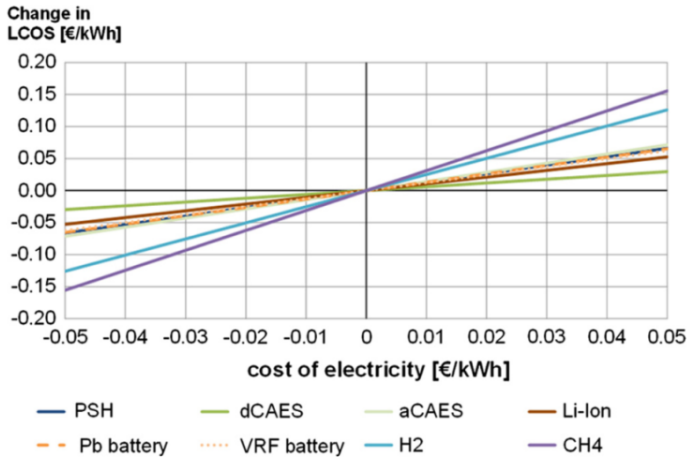

Figure 5-7 LCOS of the short-term storage system at 365 cycles per year and a varying electricity cost (Jülch, 2016)

5.3 LCOS of Integrated CAES-BTES System

The writer has employed the LCOS method proposed by Jülch (2016) to verify the integrated CAES-BTES system's financial feasibility. The result is compared with the LCOS of aCAES and dCAES under the same operational condition, as estimated by Jülch *et al.* (2015). The method of determining the LCOS

of CAES systems is presented in the conference paper published by Jülch *et al.* (2015). With the method from the literature, a simulation model is created with Microsoft Excel and Visual Basic. The results provided in the following subchapters are produced with the model.

5.3.1. Assumptions and Input Parameters for Comparative Analysis

For the comparative analyses, the CAES system is assumed to undergo the full cycle each time; that is, the storage is fully charged and fully discharged. The comparative analysis is conducted assuming all three systems considered, including integrated CAES-BTES, diabatic CAES (dCAES), and adiabatic CAES (aCAES). For the analysis, the net storage capacity of 1000 MWh with a rated storage capacity of 2500 MWh, and the depth of discharge (*DoD*) of 40% are assumed.

The technical parameters considered for the analysis are shown in Table 5-1. The model of the integrated CAES-BTES, introduced in Chapter 3, is utilized to produce the technical parameters for the comparative analysis. The input parameters are selected for the model similar to that of the aCAES (i.e., 240 MW of turbine power and 1 GWh of the net storage capacity). The model determines that a larger scale compressor is considered for the integrated CAES-BTES system relative to the aCAES system, to transfer adequate heat to the BTES system.

Table 5-1 Technical parameters for dCAES, aCAES, and integrated CAES-BTES system with 1GWh net storage capacity (modified from by Jülch *et al.*, 2015)

Input variable	Value		
	dCAES	aCAES	CAES-BTES
Compressor power [MW]	170	220	300
Turbine power [MW]	470	250	250
Rated storage capacity [MWh]	2500	2500	2500
Compressor efficiency (mechanical)	0.6	0.45	0.75
Compressor efficiency (thermal)	0	0.37	0.37
Combustion chamber efficiency	0.78	0	0
Turbine specific energy demand (b_{mech})	0.353	0.642	0.642
Turbine specific energy demand (b_{heat})	1.118	0.504	0.504
Depth of Discharge (*DoD*)	0.4	0.4	0.4
Self-discharge rate [1/hr]	0.00021	0.00021	0.00021
$t_{discharge}$ [hr]	6	6	6
t_{charge} [hr]	10	10	10
Net Storage Capacity [MWh]	1000	1000	1000

The specific CAPEX and OPEX input data are obtained from the original literature (Jülch *et al.,* 2015), except for the BTES. In the original literature, the specific CAPEX for the thermal energy storage considered for aCAES is assumed to be 25% of the total CAPEX of the CAES system. However, with the model developed for this paper, described in Chapters 3 and 4, the total BTES pipe length requirement can be calculated, which is the major contributor to the cost of a BTES system. The specific CAPEX for the BTES system, represented in € per metre of the pipe length, is obtained from Ghoreishi-Madiseh *et al.*, (2019). The cost unit is expressed in € in accordance to the original literature by Jülch *et al.* (2015). The specific CAPEX and OPEX of the integrated CAES-BTES system are assumed to be the same as the aCAES, as they share similar configurations in general. The economic parameters considered for the three systems are summarized in Table 5-2.

Table 5-2 Economic parameters for dCAES, aCAES, and integrated CAES-BTES system with 1GWh net storage capacity (modified from by Jülch *et al.*, 2015)

Input variable	Value		
	dCAES	**aCAES**	**CAES-BTES**
Specific CAPEX:			
Compressor [€/kW]	442	544	544
Storage capacity [€/kWh]	58	54	54
Turbine [€/kW]	393	399	399
Thermal storage (total) (25% of the CAPEX of all other components)		0.25	
BTES [€/m]			45
BTES length [m]			1324000
Specific OPEX:			
Energy based OPEX [€/kWh]	0.0031	0.0025	0.0025
Power based OPEX [€/kWa]	9	10	10
Startup cost [€/kW]	0.015	0.015	0.015
Natural gas cost [€/kWh]	0.0376	0	0
CO2 certificate cost [€/tCO2]	4.69		
Insurance cost (0.5% of CAPEX of all other components)	0.005	0.005	0.005

Lifetime input parameters are shown in Table 5-3. The system lifetime or the CAES financial time is assumed to be the same as the storage's lifetime, as it is less replaceable compared to the other components.

The financing input parameters are summarized in Table 5-4. The presented values are considered for a project in Germany (Jülch *et al.*, 2015). The calculated net interest rate taking all of the inputs into consideration is at 8.5%. Note that in Canada, the corporate tax is at 9% (Government of Canada, 2019).

Table 5-3 Life time parameters for dCAES, aCAES, and integrated CAES-BTES system with 1GWh net storage capacity (modified from by Jülch *et al.*, 2015)

Input variable	Value		
	dCAES	aCAES	CAES-BTES
Compressor [a]	25	25	25
Storage capacity [a]	30	30	30
Turbine [a]	35	35	35
Thermal storage [a]	-	30	30
CAES financial time [a]	30	30	30

Table 5-4 Financing parameters for dCAES, aCAES, and integrated CAES-BTES system with 1GWh net storage capacity (modified from by Jülch *et al.*, 2015)

Input variable	Value		
	dCAES	aCAES	CAES-BTES
Terms of financing:			
Interests on equity capital	0.135	0.135	0.135
Interests on debt capital	0.06	0.06	0.06
Share of debt capital	0.6	0.6	0.6
Corporation tax	0.15	0.15	0.15

5.3.2 Results and Discussion

For the initial LCOS comparison of the three CAES systems, the electricity cost is assumed to be 0. Figure 5-8 presents the comparison of the LCOS of the dCAES, aCAES, and CAES-BTES with varying yearly full load hours. As shown in Figure 5-8, dCAES has lower LCOS than the other two systems for the yearly full load hours of less than 1800 hours. The result is due to the lower upfront cost of the dCAES system compared to the others. The result also corresponds to the results presented in Jülch *et al.* (2015). After 1800 hours, aCAES and the integrated CAES-BTES have lower LCOS than dCAES. For instance, at yearly load hours of 2136 hours (equivalent for daily cycling), the LCOS of dCAES is 0.10 €/kWh, whereas the LCOS for aCAES and the integrated CAES-BTES system is 0.93 and 0.96 €/kWh. The LCOS of the integrated CAES-BTES system is marginally higher than the aCAES system. The greater CAPEX influences this for the compressor, which overshadows the cost reduction resulted from using the BTES system. The difference is less than 0.002 €/kWh for 2136 yearly full load hours.

A sensitivity analysis is conducted to assess the influence of electricity cost on the LCOS. The electricity cost is considered to range from -0.10 €/kWh to 0.10 €/kWh for the scenario of daily cycling. As shown in Figure 5-9, aCAES tends to have higher LCOS for the positive electricity price as it is more dependent on the price than dCAES. For dCAES, it is less dependent on the price as it relies more on natural gas for

power generation. The integrated CAES-BTES system has lower LCOS than dCAES under all electricity cost environment, and it demonstrates LCOS for positive electricity cost compared to aCAES. The result is influenced by higher compressor efficiency considered for the integrated CAES_BTES system, and the improved overall efficiency is due to the external utilization of the waste heat from the system. Note that the average hourly price in Ontario was about 0.024 CAD/kWh, which is equivalent to approximately 0.016 €/kWh (Statista, 2019).

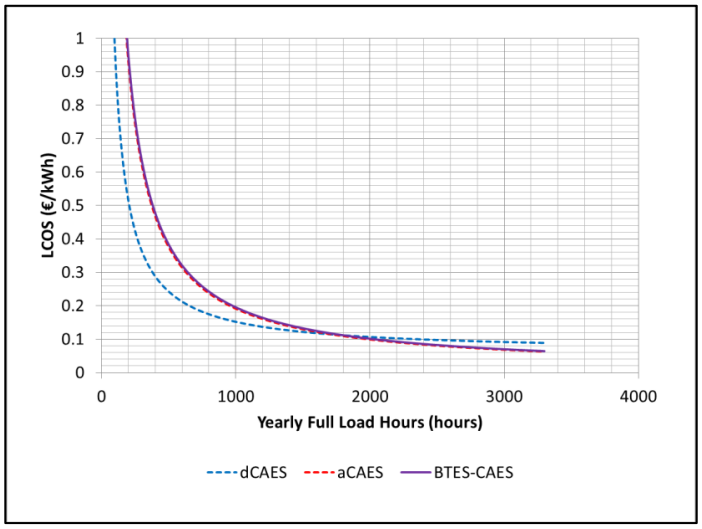

Figure 5-8 LCOS of dCAES, aCAES, and integrated CAES-BTES systems vs. yearly full load hours

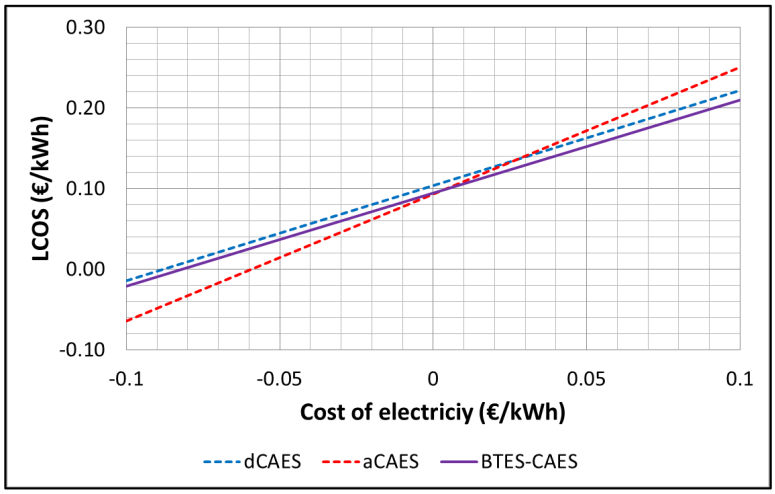

Figure 5-9 Effects of cost of electricity on LCOS

As addressed in Chapter 5.2, dCAES is a short-term ESS with the lowest LCOS claimed by Jülch (2016). As the integrated CAES-BTES system is cost-competitive to dCAES, it is valid to state that the integrated

CAES-BTES system has a notable opportunity to compete with the other short-term ESS technologies, even under the forecasted environment in 2030.

Aside from the economic advantage, the integrated CAES-BTES system has environmental advantages over other ESS technologies. Sternberg and Bardow (2015) have conducted a comparative environmental assessment on various ESS; their study, conducted based on the life cycle assessment (LCA) principle, compares the ESS that uses 1 MWh of surplus electricity. Based on this assumption, pumped hydro storage (PHS) and CAES have the lowest global warming impact, mainly from construction impacts of about 0.005 tCO_2-eq per MWh. Under the same assumption, battery technologies have presented the highest GW impact in the range of 0.02 to 0.08 tCO_2-eq per MWh.

The study assumes that appropriate geography is available for PHS. However, if it is not available, PHS's construction can be more costly and environmentally disruptive. The construction of the integrated CAES-BTES mainly takes place underground, hence it impacts the environment less than PHS while maintaining a low surface footprint. Dehghani-Sanij *et al.* (2019) also have outlined the environmental and health impacts of using batteries, which are often considered for various scales of energy storage facilities. If usages of batteries increase, more mining activities are inevitable, which can cause environmental pollutions. For instance, one study (Armand & Tarascon, 2008) suggests that Lithium-ion batteries produce approximately 70 kg CO_2 per kWh throughout their life cycle, including mining, transportation, manufacturing and disposal. The disposal and the recycling of batteries are also challenging due to their toxicity. As a mechanical ESS, the integrated CAES-BTES system does not possess environmental problems like the batteries. As the studies have demonstrated, the integrated CAES-BTES system can be an environmentally favoured option for decision-makers, in addition to its economic advantages.

Chapter 6: Conclusions

6.1 Conclusions

This study explored an integrated CAES-BTES system, which is a novel energy storage system (ESS), linking compressed air energy storage (CAES) and borehole thermal energy storage (BTES). The main objective of this study was to conduct a feasibility analysis of the integrated system. For the technical feasibility study, an energy model that simulates the proposed integrated CAES-BTES system was developed. The model simulates the operation of the integrated system, outputs thermodynamic conditions at each control point, and determines an appropriate sizing for the pre-defined energy demand. A design flow was also proposed based on the literature review and the energy model.

With the developed model, a parametric study was conducted. The parametric study demonstrated that for a system with 1.5 MW power output, diabatic and adiabatic round-trip efficiency of up to 40% and 60% were achievable, depending on the system's configuration. The most critical parameters for the performance of the CAES side of the system were determined to be the number of compression/expansion stages and the input temperature for the expander, as they dictate the thermal energy demand for the overall system. For the BTES system, the thermal properties of the storage medium and grout materials, such as thermal conductivity and diffusivity, showed a significant effect on the system's total length, which can directly influence the CAPEX of the system.

The levelized cost of energy storage (LCOS) study was conducted for the economic feasibility of the integrated CAES-BTES system. The LCOS was compared to conventional diabatic CAES (dCAES) and adiabatic CAES (aCAES) system, assuming a rated storage capacity of 2.5 GWh. The LCOS study results showed that the integrated system and aCAES system have similar LCOS when the electricity cost is assumed to be 0. For instance, both systems had lower LCOS than dCAES for full-year load hours greater than 1800 hours. A sensitivity analysis was also performed to determine the effects of the electricity cost. The sensitivity analysis demonstrated that the integrated system could result in lower LCOS than the other two systems if the electricity cost is 0.03€/kWh. The low economic and environmental costs of the integrated CAES-BTES make it a valid and feasible energy storage option for decision makers.

6.2 Limitations and Recommendations

The results presented in this thesis are produced with the assumptions incorporated in the methods and models, which are addressed throughout this thesis. These assumptions might limit the flexibility and accuracy required for a more detailed design process. The main limitations accounted in the thesis are listed below:

- The design of the integrated CAES-BTES system is solely conceptual. Specific components that are required for the operation of the system are not presented in this study.
- Energy loss at the throttle valve of the storage vessel is not considered in the simulation model. In reality, energy loss is inevitable at the valve.
- Inlet and outlet temperatures are assumed to be the same at the output for each compression and expansion stage, due to the absence of real operating conditions. These should be adjusted to maximize the efficiency of the real-world application.
- The BTES model considered in this thesis is valid for the sizing purpose, which is sufficient for this thesis. However, it does not adequately demonstrate the thermodynamics of the system.
- The input parameters used in the LCOS study are based on studies of European applications.

The following future works are recommended for the topic of this thesis:

- Detailed energy and exergy analysis for improved assessment of the proposed integrated CAES-BTES system.
- LCOS study of the integrated CAES-BTES system in the North American context.
- Determination of specific components required to construct the integrated system.
- The thermodynamics model provides improved fidelity and flexibility in studying the thermal interaction between the system and the environment.

References

Abd-el Fattah, E. S. F. (2005). Uncooled Compressed Air Storage for Balancing of Fluctuating Wind Energy. Papierflieger.

Allan, M., & Kavanaugh, S. (1999). Thermal Conductivity of Cementitious Grouts and Impact On Heat Exchanger Length Design for Ground Source Heat Pumps. HVAC&R Research, 5(2), 85-96. doi:10.1080/10789669.1999.10391226

Armand, M., & Tarascon, J. M. (2008). Building better batteries. nature, 451(7179), 652-657.

Bales, C., Gantenbein, P., Hauer, A., Henning, H. M., Jaenig, D., Kerskes, H., ... & Visscher, K. (2005). Thermal properties of materials for thermo-chemical storage of solar heat. A Report of IEA Solar Heating and Cooling programme-Task, 32.

Baljé, O. E. (1962). A Study on Design Criteria and Matching of Turbomachines: Part A—Similarity Relations and Design Criteria of Turbines. Journal of Engineering for Power, 84(1), 83–102. doi: 10.1115/1.3673386

Bär, K., Rühaak, W., Welsch, B., Schulte, D., Homuth, S., & Sass, I. (2015). Seasonal High Temperature Heat Storage with Medium Deep Borehole Heat Exchangers. Energy Procedia,76, 351-360. doi:10.1016/j.egypro.2015.07.841

Barbour, E., Mignard, D., Ding, Y., & Li, Y. (2015). Adiabatic compressed air energy storage with packed bed thermal energy storage. Applied energy, 155, 804-815.

Baudoin, A. (1988). Stockage intersaisonnier de chaleur dans le sol par batterie d'échangeurs baïonnette verticaux: modèle de prédimensionnement (Doctoral dissertation, Reims).

Bernier, M. A. (2006). Closed-loop ground-coupled heat pump systems. Ashrae Journal, 48(9), 12-25.

Bernier, M. A., Chahla, A., & Pinel, P. (2008). Long-term ground-temperature changes in geo-exchange systems. ASHRAE transactions, 114(2), 342-351.

BP. (2019). BP Energy Outlook 2019 Edition. London, United Kingdom. Retrieved on February 21, 2020, from https://www.bp.com/content/dam/bp/business-sites/en/global/corporate/pdfs/energy-economics/energy-outlook/bp-energy-outlook-2019.pdf

Bradshaw, D. T. (2000, July). Pumped hydroelectric storage (PHS) and compressed air energy storage (CAES). In 2000 Power Engineering Society Summer Meeting (Cat. No. 00CH37134) (Vol. 3, pp. 1551-1573). IEEE.

Brielmann, H., Griebler, C., Schmidt, S. I., Michel, R., & Lueders, T. (2009). Effects of thermal energy discharge on shallow groundwater ecosystems. FEMS Microbiology Ecology,68(3), 273-286. doi:10.1111/j.1574-6941.2009.00674.x

Brons, H., Griffioen, J., Appelo, C., & Zehnder, A. (1991). (Bio)geochemical reactions in aquifer material from a thermal energy storage site. Water Research,25(6), 729-736. doi:10.1016/0043-1354(91)90048-u

Brown, R. N. (2011). Compressors: Selection and Sizing. Gulf Professional Publishing.

Budt, M., Wolf, D., Span, R., & Yan, J. (2016). A review on compressed air energy storage: Basic principles, past milestones and recent developments. Applied Energy, 170, 250–268. doi: 10.1016/j.apenergy.2016.02.108

Cabeza, L. F. (2016). Advances in thermal energy storage systems: Methods and applications. Oxford: Woodhead Publishing.

Cao, S. (2010). State of the art thermal energy storage solutions for high performance buildings (Doctoral dissertation, MSc thesis. University of Jyväskylä, Norwegian University of Science and Technology (NTNU), NTNU/SINTEF Building and Infrastructure Laboratory).

Carnegie, R., Gotham, D., Nderitu, D., & Preckel, P. (2013). Utility Scale Energy Storage Systems: Benefits, Applications, and Technologies. State Utility Forecasting Group. Purdue University. West Lafayette, Indiana.

Carslaw, H. S. & Jaeger, J. C. (1959). Conduction of heat in solids. Clarendon P.

CleanTech Geomechanics (2019). CWCAS Advantages. Retrieved February 24, 2020, from https://cleantechgeo.com/

Couffin, P., & Perrin, M. (2004). Le stockage des énergies intermittentes. Clefs CEA, (50-51), 136-138.

Dehghani-Sanij, A. R., Tharumalingam, E., Dusseault, M. B., & Fraser, R. (2019). Study of energy storage systems and environmental challenges of batteries. Renewable and Sustainable Energy Reviews, 104, 192-208.

Dhaidan, N. S., & Khodadadi, J. M. (2017). Improved performance of latent heat energy storage systems utilizing high thermal conductivity fins: A review. Journal of Renewable and Sustainable Energy, 9(3), 034103.

Dincer, I. & Rosen, M.A. (2002). Thermal Energy Storage, Systems and Applications, John Wiley & Sons ltd.

Dynalene Inc. (n.d.). Heat Transfer Fluids. Retrieved March 4, 2020, from https://www.dynalene.com/heat-transfer-fluids/

Eastman (2020). Therminol®55 heat transfer fluid (technical brochure). Accessed on April 14, 2020, from: https://www.eastman.com/Literature_Center/T/TF8994.pdf#_ga=2.155889979.1059638335.1586894306-1911966440.1586894306

Eskilson, P. (1987). Thermal Analysis of Heat Extraction Boreholes, Ph.D. Thesis, University of Lund, Lund, Sweden.

Eskilson, P., & Claesson, J. (1988). Simulation model for thermally interacting heat extraction boreholes. Numerical heat transfer, 13(2), 149-165.

EU Commission SAVE Programme and Nordic Energy Research (2004). Pre-design guide for ground source cooling systems with thermal energy storage. COWI A/S, Denmark.

Florides G & Kalogirou S. (2007). Ground heat exchangers-a review of systems, models and applications. Renew Energy 32(15):2461–2478

Gao, L., Zhao, J., & Tang, Z. (2015). A Review on Borehole Seasonal Solar Thermal Energy Storage. Energy Procedia,70, 209-218. doi:10.1016/j.egypro.2015.02.117

Gas Processors Suppliers Association (GPSA) (2004). Section 13 – Compressors and Expanders. In Engineering Data Book. Tulsa, OK.

Geissbühler, L., Becattini, V., Zanganeh, G., Zavattoni, S., Barbato, M., Haselbacher, A., & Steinfeld, A. (2018). Pilot-scale demonstration of advanced adiabatic compressed air energy storage, Part 1: Plant description and tests with sensible thermal-energy storage. Journal of Energy Storage, 17, 129-139.

Ghoreishi-Madiseh, S. A., Fahrettin Kuyuk, A., Rodrigues de Brito, M. A., Baidya, D., Torabigoodarzi, Z., & Safari, A. (2019). Application of borehole thermal energy storage in waste heat recovery from diesel generators in remote cold climate locations. Energies, 12(4), 656.

Giramonti, A. J., Lessard, R. D., Blecher, W. A., & Smith, E. B. (1978). Conceptual design of compressed air energy storage electric power systems. Applied Energy, 4(4), 231-249.

Government of Canada. (2020). Corporation tax rates. Retrieved June 18, 2020, from https://www.canada.ca/en/revenue-agency/services/tax/businesses/topics/corporations/corporation-tax-rates.html

Griffioen, J., & Appelo, C. J. (1993). Nature and extent of carbonate precipitation during aquifer thermal energy storage. Applied Geochemistry,8(2), 161-176. doi:10.1016/0883-2927(93)90032-c

Guewouo, T., Luo, L., Tarlet, D., & Tazerout, M. (2019). Identification of optimal parameters for a small-scale compressed-air energy storage system using real coded genetic algorithm. *Energies*. https://doi.org/10.3390/en12030377

Guney, M. S., & Tepe, Y. (2017). Classification and assessment of energy storage systems. Renewable and Sustainable Energy Reviews, 75, 1187–1197. doi: 10.1016/j.rser.2016.11.102

He, W., & Wang, J. (2018). Optimal selection of air expansion machine in Compressed Air Energy Storage: A review. Renewable and Sustainable Energy Reviews, 87, 77-95.

Hellström, G. (1991). Ground heat storage: thermal analyses of duct storage systems. University of Lund, Sweden.

Holmberg, H., Acuña, J., Næss, E., & Sønju, O. K. (2016). Thermal evaluation of coaxial deep borehole heat exchangers. Renewable Energy,97, 65-76. doi:10.1016/j.renene.2016.05.048

Hwang, S. H., Kim, M. K., & Ryu, H. S. (2019). Real levelized cost of energy with indirect costs and market value of variable renewables: A study of the Korean power market. Energies, 12(13), 2459.

Ibrahim, H., Ilinca, A., & Perron, J. (2008). Energy storage systems—Characteristics and comparisons. Renewable and sustainable energy reviews, 12(5), 1221-1250.

Ibrahim, H., Younès, R., Ilinca, A., Dimitrova, M., & Perron, J. (2010). Study and design of a hybrid wind–diesel-compressed air energy storage system for remote areas. Applied Energy, 87(5), 1749-1762.

IEA (2012). IEA Online Data Services. Retrieved on February 26, 2020 from http://data.iea.org/ieastore/statslisting.asp

Ingersoll, L. R., & Plass, H. J. (1948). Theory of the ground pipe source for the heat pump. ASHRAE Transactions, 54, 339-348.

International Renewable Energy Agency (IRENA) (2017). Electricity Storage and Renewables: Costs and Markets to 2030. Abu Dhabi, United Arab Emirates. Retrieved on February 22, 2020, from https://www.irena.org/DocumentDownloads/Publications/IRENA_Electricity_Storage_Costs_2017.pdf

International Renewable Energy Agency (IRENA) (2019). Renewable power generation costs in 2018. Report, International Renewable Energy Agency, Abu Dhabi.

International Renewable Energy Agency (IRENA) (2019). Renewable Capacity Statistics 2019. Abu Dhabi, United Arab Emirates. Retrieved on February 22, 2020, from https://www.irena.org/publications/2019/Mar/Renewable-Capacity-Statistics-2019

Jaeger, J. C., & Carslaw, H. S. (1959). Conduction of heat in solids. Clarendon P.

Jannelli, E., Minutillo, M., Lavadera, A. L., & Falcucci, G. (2014). A small-scale CAES (compressed air energy storage) system for stand-alone renewable energy power plant for a radio base station: A sizing-design methodology. Energy, 78, 313-322.

Jülch ,V., Jürgensen, J., Hartmann, N., Thomsen, J., Schlegl, T. (2015). Levelized cost of storage method applied to compressed air energy storage. In: Proceedings SmartER Europe.

Jülch, V. (2016). Comparison of electricity storage options using levelized cost of storage (LCOS) method. Applied Energy, 183, 1594-1606. doi:10.1016/j.apenergy.2016.08.165

Kaldemeyer, C., Boysen, C., & Tuschy, I. (2016). Compressed Air Energy Storage in the German Energy System – Status Quo & Perspectives. Energy Procedia, 99, 298-313. doi:10.1016/j.egypro.2016.10.120

Kavanaugh, S. P., & Rafferty, K. (1997). Ground-source heat pumps: Design of geothermal systems for commercial and institutional buildings. Atlanta: American Society of Heating, Refrigerating and Air-Conditioning Engineers. Inc., Atlanta, GA.

Kerme, E. D., & Fung, A. S. (2020). Heat transfer simulation, analysis and performance study of single U-tube borehole heat exchanger. Renewable energy, 145, 1430-1448.

Lanahan, M., & Tabares-Velasco, P. C. (2017). Seasonal Thermal-Energy Storage: A Critical Review on BTES Systems, Modeling, and System Design for Higher System Efficiency. Energies,10(6), 743. doi:10.3390/en10060743

Lee, K. S. (2013). Underground thermal energy storage. London: Springer.

Lotfi, H., Majzoobi, A., Khodaei, A., Bahramirad, S., & Paaso, A. (2016). Levelized Cost of Energy Calculation for Energy Storage Systems. arXiv preprint arXiv:1610.07289.

Lottner, V., Schulz, M. E., & Hahne, E. (2000). Solar-assisted district heating plants: Status of the German programme Solarthermie-2000. Solar Energy, 69(6), 449-459.

Ghoreishi-Madiseh, S. A., Fahrettin Kuyuk, A., Rodrigues de Brito, M. A., Baidya, D., Torabigoodarzi, Z., & Safari, A. (2019). Application of borehole thermal energy storage in waste heat recovery from diesel generators in remote cold climate locations. Energies, 12(4), 656.

Malmberg, M., Mazzotti, W., Acuña, J., Lindståhl, H., & Lazzarotto, A. (2018). High temperature borehole thermal energy storage - A case study. Proceedings of the IGSHPA Research Track 2018. doi:10.22488/okstate.18.000036

Mangold, D., Miedaner, O., Tziggili, E. P., Schmidt, T., Unterberger, M., & Zeh, B. (2012). Technisch-wirtschaftliche Analyse und Weiterentwicklung der solaren Langzeit-Wärmespeicherung. Forschungsbericht zum BMU-Vorhaben N, 329607.

Mazloum, Y., Sayah, H., & Nemer, M. (2017). Exergy analysis and exergoeconomic optimization of a constant-pressure adiabatic compressed air energy storage system. Journal of Energy Storage, 14, 192–202. doi: 10.1016/j.est.2017.10.006

McBride, T., Bell, A., & Kepshire, D. (2013). ICAES innovation: foam-based heat exchange. SustainX, Seabrook.

Meng, H., Wang, M., Aneke, M., Luo, X., Olumayegun, O., & Liu, X. (2018). Technical performance analysis and economic evaluation of a compressed air energy storage system integrated with an organic Rankine cycle. Fuel, 211, 318-330.

Mesquita, L., McClenahan, D., Thornton, J., Carriere, J., & Wong, B. (2017). Drake landing solar community: 10 years of operation. In ISES Conference Proceedings (pp. 1-12).

Moran, M. J., Shapiro, H. N., Boettner, D. D., & Bailey, M. B. (2019). Fundamentals of engineering thermodynamics. Milton, Qld: Wiley.

Naresh, Y., Dhivya, A., Suganthi, K. S., & Rajan, K. S. (2012). High-temperature thermo-physical properties of novel CuO-therminol® 55 nanofluids. Nanoscience and Nanotechnology Letters, 4(12), 1209-1213.

Nordell, B. (2000). Large-scale thermal energy storage. In WinterCities' 2000: Energy and Environment 12/02/2000-16/02/2000

NRCan. (2017). Ground-Source Heat Pumps (Earth-Energy Systems). Retrieved from https://www.nrcan.gc.ca/energy/publications/efficiency/heating-heat-pump/6833

Oreskes, N. (2004). The Scientific Consensus on Climate Change. Science. v. 306, no. 5702, p. 1686 - 1686.

Pfleger, N., Bauer, T., Martin, C., Eck, M., & Wörner, A. (2015). Thermal energy storage–overview and specific insight into nitrate salts for sensible and latent heat storage. Beilstein journal of nanotechnology, 6(1), 1487-1497.

Philippe, M., Bernier, M., & Marchio, D. (2010). Sizing calculation spreadsheet: Vertical geothermal borefields. ASHRAE Journal, 52(7), 20–28.

Philippe, M., M. Bernier, D. Marchio. 2009. "Validity ranges of three analytical solutions to heat transfer in the vicinity of single boreholes." Geothermics 38:407 – 413.

Picard, D., & Helsen, L. (2014). A new hybrid model for borefield heat exchangers performance evaluation. In 2014 ASHRAE ANNUAL CONFERENCE (Vol. 120, No. 2, pp. 1-8). Ashrae; 1999.

Ramakrishnan, D., Bharti, R., Singh, K., & Nithya, M. (2013). Thermal inertia mapping and its application in mineral exploration: results from Mamandur polymetal prospect, India. Geophysical Journal International, 195(1), 357–368. doi: 10.1093/gji/ggt237

Reuss, M. (2015). The use of borehole thermal energy storage (BTES) systems. In Advances in Thermal Energy Storage Systems (pp. 117-147). Woodhead Publishing.

Rezaie, B., & Rosen, M. A. (2012). District heating and cooling: Review of technology and potential enhancements. Applied Energy, 93, 2-10. doi:10.1016/j.apenergy.2011.04.020

Safaei, H., & Aziz, M. J. (2017). Thermodynamic Analysis of Three Compressed Air Energy Storage Systems: Conventional, Adiabatic, and Hydrogen-Fueled. Energies, 10(7), 1020. doi: 10.3390/en10071020

Schmidt, O., Melchior, S., Hawkes, A., & Staffell, I. (2019). Projecting the future levelized cost of electricity storage technologies. Joule, 3(1), 81-100.

Skarphagen, H., Banks, D., Frengstad, B. S., & Gether, H. (2019). Design Considerations for Borehole Thermal Energy Storage (BTES): A Review with Emphasis on Convective Heat Transfer. Geofluids, 2019.

Socaciu, L. G. (2012). Seasonal thermal energy storage concepts. ACTA TECHNICA NAPOCENSIS-Series: APPLIED MATHEMATICS, MECHANICS, and ENGINEERING, 55(4).

Statista (2019). Average electricity price Ontario 2019. Retrieved June 18, 2020, from https://www.statista.com/statistics/483230/ontario-yearly-average-electricity-market-price/

Sternberg, A., & Bardow, A. (2015). Power-to-What?–Environmental assessment of energy storage systems. Energy & Environmental Science, 8(2), 389-400.

SustainX Inc. (2015). Technology Performance Report: SustainX Smart Grid Program. U.S. Department of Energy. Washington D.C., United States, DE-OE0000231.

The Federal Ministry for Economic Affairs and Energy (BMWi) (2015). The Energy of the Future: Fourth "Energy Transition" Monitoring Report - Summary. Berlin, Germany. Retrieved on February 22, 2020, from https://web.archive.org/web/20160920202129/https://www.bmwi.de/BMWi/Redaktion/PDF/V/vierter-monitoring-bericht-energie-der-zukunft-englische-kurzfassung%2Cproperty%3Dpdf%2Cbereich%3Dbmwi2012%2Csprache%3Dde%2Crwb%3Dtrue.pdf

Therminol. (n.d.). Therminol. Retrieved March 4, 2020, from https://www.therminol.com/product/71093433?pn=Therminol-55-Heat-Transfer-Fluid

VDI (2001). Thermische Nutzung des Untergrundes-Erdgekoppelte War-mepumpenalagen. VDI, 4640, 43.

Wagner, L. (2007). Overview of Energy Storage Methods. Dallas, Texas: Mora Associates. Retrieved on February 24, 2020 from http://www.moraassociates.com/reports/0712%20Energy%20storage.pdf

Wang, Z., Ting, D. S. K., Carriveau, R., Xiong, W., & Wang, Z. (2016). Design and thermodynamic analysis of a multi-level underwater compressed air energy storage system. Journal of Energy Storage, 5, 203-211.

Welsch, B. (2019). Technical, environmental and economic assessment of medium deep borehole thermal energy storage systems (Doctoral Thesis). Technische Universität Darmstadt, Darmstadt, Germany.

Xu, L., Torrens, J. I., Guo, F., Yang, X., & Hensen, J. L. (2018). Application of large underground seasonal thermal energy storage in district heating system: A model-based energy performance assessment of a pilot system in Chifeng, China. Applied Thermal Engineering, 137, 319-328.

Yan, Y., Zhang, C., Li, K., & Wang, Z. (2018). An integrated design for hybrid combined cooling, heating and power system with compressed air energy storage. Applied Energy, 210, 1151-1166.

Yang, H., Cui, P., & Fang, Z. (2010). Vertical-borehole ground-coupled heat pumps: A review of models and systems. Applied Energy, 87(1), 16–27. doi: 10.1016/j.apenergy.2009.04.038

Yavuzturk, C., Spitler, J. D., & Rees, S. J. (1999). A transient two-dimensional finite volume model for the simulation of vertical U-tube ground heat exchangers. ASHRAE transactions, 105(2), 465-474.

Zeng, H. Y., Diao, N. R., & Fang, Z. H. (2002). A finite line-source model for boreholes in geothermal heat exchangers. Heat Transfer—Asian Research: Co-sponsored by the Society of Chemical Engineers of Japan and the Heat Transfer Division of ASME, 31(7), 558-567.

Zizzo, R. (2009). Designing an optimal urban community mix for an aquifer thermal energy storage system(Doctoral dissertation, University of Toronto). Graduate Department of Civil Engineering.

Appendix A – Correlation Coefficients for Estimating the Effective Ground Thermal Resistances and the Temperature Penalty

Table A1 – Correlation coefficients for f_{6h} f_{1h} and f_{10y}

	f_{6h}	f_{1m}	f_{10y}
b_0	0.6619352	0.4132728	0.3057646
b_1	-4.815693	0.2912981	0.08987446
b_2	15.03571	0.07589286	-0.0915179
b_3	-0.0987942	0.1563978	-0.0387245
b_4	0.02917889	-0.2289355	0.1690853
b_5	0.1138498	-0.0049276	-0.0288168
b_6	0.00561093	-0.002695	-0.0028866
b_7	0.7796329	-0.638036	-0.1723169
b_8	-0.324388	0.2950815	0.03112034
b_9	-0.018241	0.149332	-0.1188438

Table A2 – Correlation coefficients c_i and d_i for the F function

i	b_i	c_i
0	7.8190E+00	1
1	-6.4270E+01	B/H
2	1.5387E+02	$(B/H)^2$
3	-8.4809E+01	$(B/H)^3$
4	3.4610E+00	$\ln(t/t_s)^2$
5	-9.4753E-01	$[\ln(t/t_s)]^2$
6	-6.0416E-02	$[\ln(t/t_s)]^3$
7	1.5631E+00	NB
8	-8.9416E-03	NB^2
9	1.9061E-05	NB^3
10	-2.2890E+00	A
11	1.0178E-01	A^2
12	6.5690E-03	A^3
13	-4.0918E+01	$(B/H)*\ln(t/t_s)$
14	1.5557E+01	$[(B/H)*\ln(t/t_s)]^2$
15	-1.9107E+01	(B/H)*NB
16	1.0529E-01	$(B/H)*NB^2$
17	2.5501E+01	(B/H)*A
18	-2.1177E+00	$(B/H)*A^2$
19	7.7529E+01	$(B/H)^2*\ln(t/t_s)$
20	-5.0454E+01	$(B/H)^2*[\ln(t/t_s)]^2$
21	7.6352E+01	$(B/H)^2*NB$
22	-5.3719E-01	$(B/H)^2*NB^2$
23	-1.3200E+02	$(B/H)^2*A$
24	1.2878E+01	$(B/H)^2*A^2$
25	1.2697E-01	$\ln(t/t_s)*NB$
26	-4.0284E-04	$\ln(t/t_s)*NB^2$
27	-7.2065E-02	$\ln(t/t_s)*A$
28	9.5184E-04	$\ln(t/t_s)*A^2$
29	-2.4167E-02	$[\ln(t/t_s)]^2*NB$
30	9.6811E-05	$[\ln(t/t_s)]^2*NB^2$
31	2.8317E-02	$[\ln(t/t_s)]^2*A$
32	-1.0905E-03	$[\ln(t/t_s)]^2*A^2$
33	1.2207E-01	NB*A
34	-7.1050E-03	$NB*A^2$
35	-1.1129E-03	NB^2*A
36	-4.5566E-04	NB^2*A^2

Appendix B – Input Technical and Financial Parameters for LCOS Study by Jülch (2016)

Note: The technical and financial parameters and their values are determined by Jülch (2016) from various literatures. The detailed explanations and the sources of the values can be found in her study. The full citation for Jülch (2016) is noted below:

Jülch, V. (2016). Comparison of electricity storage options using levelized cost of storage (LCOS) method. *Applied Energy, 183*, 1594-1606. doi:10.1016/j.apenergy.2016.08.165

Table B1 – Technical input data for PSH systems

Input variable	
Efficiency pump [%]	86
Efficiency turbine [%]	88
Self-discharge rate [%/d]	0.013
Component lifetimes:	
Pump [a]	35
Turbine [a]	35
Storage [a]	80

Table B2 – Technical input data for dCAES and aCAES

Input variable	dCAES	aCAES
Compressor efficiency (mechanical) [%]	60	45
Compressor efficiency (thermal) [%]	-	37
Combustion chamber efficiency [%]	87	-
Turbine specific mechanical energy demand (b_{mech})	0.353	0.64
Turbine specific heat energy demand (b_{heat})	1.12	0.504
Self-discharge rate [%/d]	0	0.75
Component lifetimes:		
Compressor [a]	25	25
Storage capacity [a]	40	40
Turbine [a]	35	35
Thermal Storage [a]	-	40

Table B3 – Input data for the LCOS calculation for large scale battery storage systems, today's values

	Li-ion	Pb	VRF
System efficiency (round trip) [%]	95	77	80
DoD [%]	80	50	100
Cycle durability at DoD	7000	2700	10000
Calendar life [a]	20	10	20
Self-discharge rate [%/month]	1	2	0.83

Table B4 – Input data for the LCOS calculation for large scale battery storage systems, future values

	Li-ion in 2030	Pb in 2030	VRF in 2030
System efficiency (round trip) [%]	95	78	85
DoD [%]	100	80	100
Cycle durability at DoD	10000	4000	10000
Calendar life [a]	20	10	20
Self-discharge rate [%/month]	1	2	0.83

Table B5 – Input data for the LCOS calculation for PtG systems

Input Variable	
Efficiencies:	
Electrolyzer [%]	70
Methanation unit [%]	80
H2 storage system [%]	97.8
CCGT [%]	58
Depth of discharge H2 storage system [%]	63
Self dischrage rate H2 storage system [%/d]	0.017
Electricity demand gas feed in [kWh/Nm^3 CH4]	0.1237
Electricity demand CO2 purification [kWh/kWh CH4]	0.025
Gas transmission losses [%]	0.0025
Component lifetimes:	
Electrolyzer stack [h]	95000
Electrolyzer system [a]	30
Methanation unit [a]	15
Gas feed in system [a]	15
CO2 purification plant [a]	25
H2 intermediate storage system [a]	15
H2 storage system [a]	30
CCGT [a]	25

Table B6 – Specific CAPEX, financial lifetime, typical input/output ratio and overall efficiency for the analyzed technologies

	PSH	dCAES	aCAES	Battery Li-ion		Battery Pb		Battery VRF		H2	CH4
Time scale	Today	Today	2030	Today	2030	Today	2030	Today	2030	2030	2030
Specific CAPEX:											
Charging unit [€/kW]	260…560	220…340	380…620	-	-	-	-	-	-	410…880	790…1360
Storage unit [€/kWh]	10…20	20…30	20…30	660…1050	230…610	240…320	190…270	930…1040	250…350	0.3…0.6	0.14
Other fixed cost [€]	-	-	230…360	-	-	-	-	-	-	-	264300
Discharging unit [€/kW]	220…460	230…380	25% of CAPEX	80	60…70	80	60…70	-	-	727	727
Thermal Storage	-	-	-								
Financial lifetime [a]	80	35	35	-	-	-	-	-	-	30	30
Tpyical i/o power ratio	0.95	0.92	0.92	1	1	1	1	1	1	2	2
Overall efficiency [%]	76	55	70	95	95	77	78	80	85	41	32

Table B7 – OPEX for the analyzed technologies

	PSH	dCAES	aCAES	Battery Li-ion		Battery Pb		Battery VRF		H2	CH4
Time scale	Today	Today	2030	Today	2030	Today	2030	Today	2030	2030	2030
Specific OPEX:											
Energy based [€ct/kWh]	0.05	0.33	0.26	-	-	-	-	-	-	0.3	0.3
Charging power based [% of CAPEX/a]	-	-	-	-	-	-	-	-	-	1.6	2.0; 1.5
Charging power based [€/kWa]	-	-	-	-	-	-	-	-	-	-	3.2
Discharging power based [€/kWa]	11	9	11	2	2	2	2	2	2	-	3.2
Discharging power based [% of CAPEX/a]	-	-	-	-	-	-	-	-	-	0.06	0.06
Startup cost [€/kW_start]	0.02	0.016	0.016	-	-	-	-	-	-	-	-
Electricity cost [€ct/kWh]	-	-	-	-	-	-	-	-	-	-	5
Natural gas cost [€ct/kWh]	-	3.5	-	-	-	-	-	-	-	-	-
CO2 Certificate cost [€/tCO2]	-	5	-	-	-	-	-	-	-	-	-